Titre: Title:	Partial Oxidation of Methane to Syngas Over Noble Metal Catalysts Supported by Fecralloy Fibre
Auteur: Author:	Zhenni Ma
Date:	2019
Type:	Mémoire ou thèse / Dissertation or Thesis
Référence: Citation:	Ma, Z. (2019). Partial Oxidation of Methane to Syngas Over Noble Metal Catalysts Supported by Fecralloy Fibre [Thèse de doctorat, Polytechnique Montréal]. PolyPublie. https://publications.polymtl.ca/3815/

POLYTECHNIQUE MONTRÉAL
affiliée à l'Université de Montréal

Partial oxidation of methane to syngas over noble metal catalysts supported by Fecralloy fibre

ZHENNI MA
Département de génie chimique

Thèse présentée en vue de l'obtention du diplôme de *Philosophiæ Doctor*
Génie chimique

Mars 2019

POLYTECHNIQUE MONTRÉAL
affiliée à l'Université de Montréal

Cette thèse intitulée :

Partial oxidation of methane to syngas over noble metal catalysts supported by Fecralloy fibre

présentée par **Zhenni MA**
en vue de l'obtention du diplôme de *Philosophiæ Doctor*
a été dûment acceptée par le jury d'examen constitué de :

Jason Robert TAVARES, président
Gregory PATIENCE, membre et directeur de recherche
Daria Camilla BOFFITO, membre et codirectrice de recherche
Oumarou SAVADOGO, membre
Jan KOPYSCINSKI, membre

DEDICATION

Dedicated to
My beloved parents
My lovely husband
My guardian angels
Thank you for your love and support...

ACKNOWLEDGMENTS

I would like to acknowledge all who in one way or another contributed to the completion of this thesis.

First and foremost, I wish to express my deep and sincere gratitude to my supervisor Prof. Gregory S. Patience for his solid support, motivation, caring and patience. His vast knowledge and caring encouragements guided me not only in scientific research, writing and presenting but also helped me overcome my weaknesses in communication. I will cherish this for the rest of my life. It was my deep honor to work as a PhD student under him.

Also I would like to thank my most beautiful co-supervisor Prof. Daria C. Boffito for her always timely help in my research and project. She is my true role model. I am blessed to have worked with her.

I would like to thank Prof. Patrice Perreault for his full support, immense knowledge and professionalism.

I would like to acknowledge Diego C. Pelegrin, Dr. Cristian Neagoe, Dr. Cristian Trevisanut and soon to be Dr Philippe Ouzilleau who have greatly contributed to the accomplishment of the work presented here.

I would like to thank my lovely old colleagues Samira, Marjan, Mehash, and Jaber and I will remember all the best time we have spent together.

My deep gratitude goes to all my colleagues Gianluca, Mohammad and technicians Sylvain and Yanik in Prof. Patience's group for sharing their knowledge and ideas, thank Yuxiang for his great help in translation of the abstract of this thesis to French, and to all my colleagues who helped me at various points during the Ph.D. thesis process.

I would also like to extend my thanks to my friends and colleagues at Polytechnique Montreal, Ling, Bing, and many more whose names I unintentionally forgot to mention, for their support in various aspects during this Ph.D thesis.

I would like to acknowledge the members of my committee for taking interest in my work, examining my thesis and providing insightful comments.

Finally, I would like to thank my family for their love, patience and continuous support during the past years.

RÉSUMÉ

Le torchage des rejets gazeux par l'industrie pétrolière émet une quantité importante de GES qui accélèrent le changement climatique en plus de nuire à l'environnement avec des polluants toxiques tels que des composés sulfurés et des métaux lourds. Le méthane est un vecteur énergétique précieux et sa conversion en combustibles liquides réduirait l'empreinte environnementale des pétrolières. Un procédé micro gaz-à-liquide (μGtL) pourrait réduire le brûlage de méthane par torchage et permettra de produire un carburant énergétiquement dense : le diesel.

Une opération unitaire intégrant simultanément la production de gaz de synthèse à haute pression et une étape Fischer-Tropsch peut réduire substantiellement les coûts d'exploitation liés à la synthèse de liquides GtL.

De plus, l'oxydation catalytique partielle (CPOX) pour la production des gaz de synthèse pourrait constituer une opportunité économique pour les microraffineries. En pratique, une pression supérieure à 2 MPa favorise la réaction de FT. Le défi consiste donc à opérer le procédé CPOX à cette pression tout en maintenant une sélectivité élevée. À ce jour, peu d'études ont été consacrées au CPOX du méthane à haute pression.

Le catalyseur CPOX doit résister à des contraintes de température et de pression élevées. De nombreux métaux et oxydes métalliques convertissent sélectivement le gaz naturel en CO et H_2. Ils sont cependant susceptibles au coking et doivent être régénérés périodiquement pour éviter la désactivation du catalyseur et l'encrassement des tuyauteries réacteur. Les métaux nobles démontrent une activité supérieure et une meilleure résistance à la formation du coke comparativement aux métaux non nobles. Les mailles en alliage ferrochrome (FeCr) sont des matériaux de support idéaux, car la pellicule protectrice de surface en alumine résiste à des températures supérieures à 1000 °C, et ce, sur des périodes allant jusqu'à 3000 h. Ils présentent également une excellente conductivité thermique et génèrent de faibles pertes de charge. Dans cette thèse, nous présentons pour la première fois l'oxydation partielle du méthane en gaz de synthèse dans un système hétérogène micro gaz-solide catalysé par métaux nobles sur support en mailles métalliques.

La première étape de ce projet consistait à concevoir un catalyseur approprié (composition, support, méthode de préparation et caractérisation du catalyseur). La seconde cherchait à étudier les conditions de réaction (température, pression, composition de l'alimentation et temps de contact) sur la sélectivité des produits souhaités. Pour mieux comprendre la réaction CPOX, nous introduisons le sujet de la formation du coke et de la régénération du catalyseur

en alliage FeCr. Une étude cinétique et l'analyse par spectrophotomètre de masse permettent de proposer un mécanisme de réaction pour l'activation du méthane.

Ainsi, nous avons préparé un catalyseur Pt/Rh (ratio massique Pt/Rh = 9) supporté sur alliage FeCr couvert en oxyde de magnésium (MgO) par synthèse auto-propagée à haute-température (SHS). Cette méthode génère des particules fines et une phase active uniformément dispersée et a donc été utilisée pour la majorité des essais dans ce projet. La réaction à été réalisée à 900 °C sous une pression entre 0.1 à 2 MPa avec un mélange de CH_4 et de O_2 à rapport massique 2 :1 sous flux horaire constant. Les résultats expérimentaux montrent que la conversion du méthane augmente avec la pression ainsi que la sélectivité en H_2 et en O_2. Inversement, en maintenant un temps de contact fixe, la conversion du méthane et la sélectivité de CO et H_2 s'avèrent optimaux à pression ambiante. L'étude thermodynamique du coke démontre un comportement métastable. Une augmentation du temps de contact devrait réduire la formation de coke.

Malgré une faible sélectivité, l'alliage FeCr vierge et oxydé mène tous deux à la conversion du méthane. Nos résultats par diffraction rayon X (XRD) démontrent que le dépôt direct de Pt/Rh engendre une surface plus amorphe sur l'alliage FeCr oxydé. À 900 °C et entre 0.1 MPa et 2 MPa, la production de syngas avec le catalyseur Pt/Rh supporté par alliage FeCr Pt/Rh était supérieur autres catalyseurs sur ce même support. La réaction début à 600 °C. À 900 °C, la conversion et la sélectivité se sont rapprochées des valeurs d'équilibre thermodynamique. Lors de nos tests, l'ajout de Pt a permis au catalyseur de résister à la formation du coke jusqu'à 65 min. La régénération rétablit la quasi-totalité de l'activité du catalyseur tout en laissant la surface intacte après plusieurs cycles de réaction-régénération.

Les matériaux CeO_2 ont une capacité de stockage d'oxygène. CeO_2 sur support en alliage FeCr exhibe une activité supérieure sous pression atmosphérique, mais restreinte à haute pression. Pt/CeO_2 supporté sur alliage FeCr était inerte entre 0.1 MPa et 2 MPa. Afin d'élucider le mécanisme de réaction, nous avons introduit séparément du méthane et de l'oxygène dans le système catalytique. Sans concurrence de réactions secondaire avec l'oxygène, le CeO_2 reste réactif pour l'activation méthane. Un courant d'oxygène alimenté à 21 % a généré le CO avec grande pureté. En séparant le méthane de l'oxygène, la réaction d'activation du méthane par le catalyseur peut examiner à nouveau. Nos données supportent un modèle cinétique de premier ordre avec une énergie d'activation de 46 kJ/mole. De plus, il démontre que la non-dissociation du méthane adsorbé est une étape limitante. À haute pression, trois cycles oxydation et de réduction (alimentation à 21 % en O_2 et 30 % en CH_4 respectivement) ont indiqués que la réaction se produit de manière directe.

ABSTRACT

Gas flaring accelerates climate change with greenhouse gases also harms the environment with other pollutants such as H_2S, carbon sulphides, NOx and heavy metals. Methane is a valuable energy vector, and converting the associated gas from thousands of wells to liquid fuels would reduce the environmental footprint of oil field operations. Micro Gas-to-Liquids technology (μGtL) can potentially reduce the natural gas that is flared throughout the world while producing valuable diesel.

Integrating a high pressure syngas step with Fischer-Tropsch (FT) in a single vessel reduces investment and operating costs to synthesize GtL liquids. Methane catalytic partial oxidation (CPOX) to produce syngas for FT is an economic opportunity for micro refineries. FT reaction favours at least 20 bar. Therefore the challenge is to operate CPOX at pressure of 20 bar and pursue high selectivity. To date, only a few studies have focused on high pressure catalytic partial oxidation of methane.

CPOX catalyst must resist high temperature and high pressure stresses. Many metals and metal oxides selectively convert natural gas to CO and H_2 while forming coke. Coke must be removed intermittently, otherwise it deactivates the catalyst and blocks the reactor and process lines. Noble metals presented higher activity in CPOX reaction and higher resistance to coke formation than non-noble metals. FeCralloy knitted fibres are ideal materials for supports because the surface protective alumina scale resists temperature over 1000 °C over 3000 h of operation. Also, FeCralloy has excellent heat conductivity and low pressure drop.

We approach this subject by employing a micro gas – solid heterogeneous system for CPOX at pressure up to 2 MPa in the presence of the noble metal catalyst supported on metal fibres for the first time.

Designing a suitable catalyst (composition, support, preparation method, and characterization) is the first step of this project. Investigating the reaction conditions (temperature, pressure, feed composition, and contact time) on the selectivity of desired products is the second step. To further understand the CPOX reaction, we discussed coke formation on FeCralloy catalysts and catalyst regeneration. We modelled experimental data of methane reduction and oxidation separately.

We prepared Pt/Rh (Pt/Rh = 9) catalyst supported on MgO over FeCralloy woven fibre by solution combustion synthesis. This method generated fine particles within a uniformly dispersed active phase and it was therefore employed in most of our work. At 900 °C, from

0.1 - 2 MPa, and with a 2:1 feed composition of CH_4 to O_2, keeping a constant weight hourly space velocity, methane conversion and selectivity of H_2 and CO increased with pressure. However, keeping a constant contact time, methane conversion and selectivity of H_2 and CO favoured lower pressure. Thermodynamic calculations demonstrated that the coke is metastable. Increasing contact time should reduce coke formation.

The virgin FeCralloy and the oxidized FeCralloy were reactive in converting methane as well, although the selectivity was poor. According to XRD analysis, direct deposition of Pt/Rh on the FeCralloy fibres prompted a more amorphous surface of the oxidized FeCralloy. Selectivity to syngas with Pt/Rh FeCralloy catalysts was superior to other FeCralloy catalysts at 900 °C and at 0.1 MPa and 2 MPa. Methane conversion and CO and H_2 selectivity were sensitive to temperature. At temperature of 900 °C, methane conversion and H_2 and CO selectivity were close to the thermodynamic equilibrium value. Adding Pt resisted coke formation at high pressure in 65 min tests. Upon regeneration, Pt/Rh FeCralloy catalyst recovered its entire activity, and the catalyst surface remained intact after multiple reaction regeneration cycles.

CeO_2 materials have an oxygen storage capacity. CeO_2 supported on FeCralloy catalyst revealed superior activity in converting methane to syngas under atmosphere pressure, but high pressure restrained its activity. Pt/CeO_2 FeCralloy was inert at both 0.1 MPa and 2 MPa. To understand its mechanism, we fed methane and oxygen separately into the catalytic system. Without competing oxygen reactions, CeO_2 based FeCralloy were quite reactive in activating methane. Feeding 21 % oxygen stream to CeO_2 FeCralloy catalysts generated CO with high purity. Separately feeding methane and oxygen into the catalytic system provided an alternative view to understand the methane activation on the catalyst surface. A first–order kinetic model characterizes the activation of methane on the catalyst surface with an activation energy of 46 kJ/mol. A hybrid Eley–Rideal model accurately described the oxidation reaction. During oxidation, there is a competition between catalyst oxidation and gaseous oxides formation. Three oxidation (feeding 21 % oxygen) – reduction(feeding 30 % methane) cycles at high pressure additionally validated the models. The formation of CO and H_2 is under direct mechanism.

TABLE OF CONTENTS

LIST OF TABLES

LIST OF FIGURES

LIST OF SYMBOLS AND ABBREVIATIONS

GtL	Gas-to-Liquids
μGtL	Micro Gas-to-Liquids technology
FT	Fischer-Tropsch
CPOX	catalytic partial oxidation
SMR	Steam Methane Reforming
POX	Partial Oxidation
ATR	Auto-Thermal Reforming
MRU	Micro-Refinery Unit
SCS	Solution Combustion Synthesis
GGFR	Global Gas Flaring Reduction
BCM	billion cubic meters
EIA	U.S. Energy Information Administration
SEM	Scanning electron microscopy
EDS	Energy Dispersive Spectroscopy
WHSV	Weight hourly space velovity
TOF	Turnover frequency
L_a	Diameter of crystallites composing the coke
n	number of tanks in the n–CSTR in series model
Pe	Peclet number of axial dispersion
r	reaction rate, μmol g^{-1} s^{-1}
E_a	activation energy, kJ mol^{-1}
k_0	reduction reaction rate constant, μmol g^{-1} s^{-1}
k_i	oxidation reaction rate constant, i = 1,2,3, $cm^3 mol^{-1} s^{-1}$
C_i	selectivity to compound, molm^{-3} (if i is solid, mole O_2 per m^3 CeO_2)
R_i^2	coefficient of determination
S_i	selectivity to compound i
t_m	mean residence time, s
U_g	gas linear velocity, m s^{-1}
X	conversion, %
P_i	partial pressure
F_i	molar flow rate of reactants, mol s^{-1}
ϕ	objective function for modeling
τ	contact time

CHAPTER 1 INTRODUCTION

1.1 Background and problem identification

Syngas, also called synthesis gas, consists of a mixture of hydrogen and carbon monoxide. It is a crucial intermediate to produce synthetic hydrocarbon fuels via the Fischer-Tropsch technology, and to produce hydrogen or methanol. We can produce syngas from natural gas, including tight gas, shale gas, coal bed methane or wasted associated gas — flare gas.

At high pressures, typical in most oil reservoirs, associated gas is dissolved in crude oil. When the crude is pumped to the surface, it vaporizes out of solution. The main content of this associated gas is CH_4 (81 %). Gas flaring is the easiest and most economical way to discard associated gas. As CH_4 has a greenhouse effect 20 times (which increases with time : around 60 within 20 years) higher than that of CO_2 [8], venting it from the well-head to the atmosphere is worse than flaring with respect to the environmental impact. Remote oil field locations also make it difficult to build pipelines or electricity transmission lines to utilize associated gas.

Flaring associated gas produces mainly H_2O and CO_2, but also CO along with a variety of air pollutants, such as NOx, SO_2 and toxic heavy metals. The air pollution associated with flaring and venting of natural gas puts the health of local communities and extraction site workers at risk [9]. The World Bank launched the Global Gas Flaring Reduction partnership in 2002 as part of the World Summit on Sustainable Development. They estimated that every year petroleum companies flare as much as $35 billion worth of natural gas.

Venting and flaring gas is not a option, the transportation of natural gas is also limited because of expensive costs in pipelines and infrastructure. Gas-to-Liquids (GtL) technologies present an attractive alternative : transforming the associated natural gas into added-value liquid products and meantime reducing greenhouse gas emissions, brings both economical and environmental benefits. Gas-to-Liquids (GtL) technologies generate various GtL products, such as high quality naphtha, jet fuels, diesel, lubes and waxes, which can be transported by the existing pipelines and infrastructure [10]. The Fischer-Tropsch (FT) technology, a dominating process in GtL, relies on the production of syngas (H_2/CO ratio of 2).

The first problem is that converting methane to Fischer-Tropsch liquid products calls for multi-stage process. Conventional processes to convert methane to syngas - steam reforming, CO_2 reforming and auto-thermal reforming - are suitable for large scale industry. Some companies have been looking for smaller scale and simpler process to reduce the large capital

cost [11]. Considering the amount of associated nature gas is relatively small and not steady, we need to find a solution suitable for micro scale industrial process.

In this project, we aim to create a mobile and scalable Micro-Refinery Unit (MRU) deployable at the well-head to convert associated gas into high value liquid fuels, and reduce greenhouse gas emissions. This unit would combine two processes in a single reactor : catalytic partial oxidation and Fischer-Tropsch (favors 2 MPa).

Catalytic partial oxidation of methane is a mild exothermic reaction which saves external energy. It produces H_2 and CO at a ratio of 2, suitable for Fisher–Tropsch process. Converting methane to syngas under high pressure is in high demand for the further FT process.

The second problem is that high pressure inhibits CPOX reaction and promotes coke formation, a suitable CPOX catalyst candidate for working at extreme conditions and resist coking is necessary.

Although Ni based catalysts are good candidates for industrious purpose due to their cheap cost, a major problem is the irreversible deactivation by coke formation and Ni sintering.

Compared to Ni catalysts, noble catalysts (Pt or Rh) are more expensive but with much less loading, they show better activity and stability and resistance to coke formation which extends their lifetime. Also the choice of the support, promoters and preparation techniques can greatly affect the catalyst activity and stability and further coke formation.

FeCralloy fibres can work at temperature over 1050 °C for 3000 h. Its knitted structure allows high gas flow output. Based on these, CPOX over new catalysts supported on FeCralloy fibres will be an interesting and promising topic.

1.2 Objectives

The main objective of the present study is to develop a high pressure catalytic methane partial oxidation process to produce syngas suitable for the Fischer-Tropsch reaction, over noble metal catalyst supported on FeCralloy fibres.

The first specific objective is catalyst design. A suitable catalyst under optimum operation conditions can maximize the conversion of methane and the selectivity of syngas. Preparing effective and novel catalysts is the first issue of this work.

Different combinations and composition of metals, supports and promoters affect catalyst properties, especially on activity and the thermal stability. The preparation methods also affects the catalyst structure and thus its performance.

In this section, we will study the influence of the above mentioned factors on product selec-

tivity to determine an appropriate catalyst.

The second specific objective is process design. Beside the catalyst nature, reaction conditions also influence methane conversion and syngas selectivity in CPOX. Reaction conditions refer to reactor type, choice of catalyst and pre-treatment, external conditions, like temperature, pressure, methane and oxygen (air) ratio, gas flow rates regards to contact time, and the feeding order of methane and oxygen.

We further focus the study of CPOX reaction under atmosphere pressure and 2 MPa, and optimize the reaction condition to maximize the methane conversion and syngas selectivity and limit coke formation.

The third specific objective is to study the catalyst deactivation and regenerative ability. To prolong the lifetime of catalysts, we would identify the impact of temperature and pressure on coke build–up, characterize the coked catalyst to identify the coke type and investigate the regenerative ability of the catalysts.

The fourth specific objective is to study the reaction kinetics. A better understanding of the relationship between reactive species on the catalyst surface is necessary. The last series of experiments consist of data aimed to kinetic modelling. Developing suitable models for methane reduction and oxidation are necessary.

CHAPTER 2 LITERATURE REVIEW

The world's energy consumption is growing fast especially in Asia and China has become the world's second largest consumer of oil after the USA [12]. Fossil fuels still dominate the world energy production. The proved oil reserves concentrate in the middle East and Russia [12]. Apart from middle east, the rest big fraction of the reserves presents as oil sand (tar sand) and other non-conventional sources [13]. The cost of exploration and production steadily increases. At the present world production rate, the proved oil reserves will deplete within 40 years [12]. Therefore there is a strong need for alternative fuels and a flexible energy network, such as liquefied petroleum gas (LPG), natural gas, methanol, dimethylether (DME), ethanol, biodiesel, synfuels and hydrogen [12].

All oil production produces associated natural gas. As many oil fields are far from the market-place and often off-shore, we call this gas "remote gas" or "stranded gas" [14]. Oil producers sometimes reinject the associated gas to reinforce the oil recovery. However a significant fraction (5 % of the total natural gas production) is flared [15], due to economical issues and technical limitations.

GtL converts natural gas into liquid fuels either via direct conversion or via syngas as an intermediary (indirect GtL). Indirect GtL has high carbon efficiency. Synthesis gas (syngas) is the key intermediate step in the indirect route of GtL. Syngas is a mixture of hydrogen, carbon monoxide and carbon dioxide. It may contain nitrogen for ammonia synthesis [12]. Syngas creates flexibility for the chemical industry and for the manufacture of synthetic fuels (synfuels) thus is important in energy conversion [16]. Almost any carbon source, natural gas, oil products, coal and biomass, can produce syngas. Recent trends in syngas application concentrate on the conversion of cheap remote natural gas into liquid fuels (GtL). Oil is the most versatile fossil fuel with high energy density and is easy to ship with the existing pipelines and infrastructure.

Industry and academy are looking for : 1) scaling up to large scale GtL plants (more than $500\,000 \mathrm{Nm}^3{}_{syngas}\mathrm{h}^{-1}$), or, 2) scaling down to small, compact syngas units, for example fuel cells ($5 - 100 \mathrm{Nm}^3{}_{syngas}\mathrm{h}^{-1}$) [12].

Syngas production may be responsible for 60 % of the total investment of a large-scale natural gas conversion plant [12]. Therefore, we need to optimize syngas production processes.

2.1 Syngas production processes

Conventional processes to produce syngas from methane include : Steam Methane Reforming (SMR), Dry Reforming (DRM), Partial Oxidation (POX), and Auto-Thermal Reforming (ATR).

2.1.1 Steam Methane Reforming (SMR) and Dry Reforming (DRM)

Among all the syngas production methods, the steam reforming process is a mature technology [17]. It is the most widely used technique in industry for large scale production. In SMR, methane reacts with steam to produce hydrogen and carbon monoxide at a H_2/CO ratio of 3.

$$CH_4 + H_2O = CO + 3H_2 \qquad \Delta H = 206\,\mathrm{kJ\,mol^{-1}} \tag{2.1}$$

The process operates between 430 °C and 1000 °C and pressure between 1.5 MPa to 3 MPa. SMR is highly endothermic and its catalyst is normally Ni on a stable support due to their cheap cost [18]. A typical SMR process includes tubular and packed reactors with heat recovery to preheat the feed gas or to increase steam in waste heat boilers [10]. It is an energy intensive process. The large capital cost makes it uneconomical for small scale units ; also its high H_2/CO ratio need separation for follow up Fischer-Tropsch process.

Another appealing reforming process is carbon dioxide reforming (dry reforming, DRM). It is also a strong endothermic reaction with higher enthalpy than SMR :

$$CH_4 + CO_2 = 2CO + 2H_2 \qquad \Delta H = 247\,\mathrm{kJ\,mol^{-1}} \tag{2.2}$$

CO_2 reforming is suitable for treating CO_2 rich associated gas and its H_2/CO ratio of 1 is ideal for carbonylation reactions but not for Fischer-Tropsch process.

2.1.2 Auto Thermal Reforming (ATR)

In Auto Thermal Reforming process, oxygen and steam react with methane to produce syngas [18]. ATR is a hybrid of homogeneous partial oxidation and steam reforming. The exothermic oxidation provides the energy to sustain the endothermic steam methane reforming reaction, so the maximum reaction temperature decreases and the oxygen consumption is lower.

ATR reactor consists of a burner, a combustion chamber, and a fixed catalyst bed placed in a compact refractory lined vessel [19]. The process operates between 900 °C to 1150 °C with

pressure between 1 to 8 MPa. Typically, O/C is between 0.5 – 0.6 with O_2 as oxidant [20] and the temperature of the flame core exceeds 2000 °C. One advantage of ATR is the controllable H_2/CO ratio based on the downstream need. The adiabatic heat balance determines the exit temperature ; the thermodynamic equilibrium at that temperature determines the product gas ratio [12]. The ATR reactor is more compact than a SMR reformer, however, larger than a POX unit. The catalyst should withstand high temperature without excessive sintering and contain no volatile components at extreme conditions. Industry often employs nickel on magnesium alumina spinel catalysts.

2.1.3 Partial oxidation (POX)

In partial oxidation reaction, methane reacts with a substoichometric amount of oxygen to produce hydrogen and carbon monoxide at a 2 : 1 ratio. It is a mildly exothermic reaction.

$$CH_4 + \frac{1}{2}O_2 = CO + 2H_2 \qquad \Delta H = -36\,\mathrm{kJ\,mol^{-1}} \tag{2.3}$$

Homogeneous POX

Homogeneous partial oxidation operated at high temperature (1200 °C to 1500 °C) without catalysts [18]. Non catalytic POX needs high temperature to ensure complete conversion and to reduce coke formation. A separate soot scrubber system in the downstream should be installed to remove the coke.

High temperature POX may have fewer CH_4 and CO_2 in the outlet than ATR [12]. However, higher reaction temperature calls for burning additional fuel. The POX reactor is less efficient than a steam reformer due to the less efficient heat recycle [12].

Catalytic partial oxidation (CPOX)

A catalyst would significantly reduce the operating temperature of the POX reaction, which is economically attractive [21].

Catalytic partial oxidation of methane with oxygen produces syngas at high space velocity over solid catalysts below 1000 °C. In 1929 Liander, who was interested in the ammonia process, first suggested CPOX that occurred above 850 °C [21]. Unlike the intensive development of SMR, CPOX remained almost unexplored until 1990 [4]. Pioneer work of Hickman and Schmidt demonstrated that CPOX reaction with Rh catalyst can achieve almost fully conversion of methane directly to H_2 and CO at reaction times as short as 1 ms [22, 23, 24].

What's more, following the initial employment of Pt-10% Rh [22, 25], researchers have studied various metallic gauze catalysts. Methane conversion and CO selectivity are low on Pt gauze operating between 200 °C to 900 °C [4]. Adding Rh to the Pt (Pt/Rh = 9) increased the conversion to 30 % [26]. Surface oxides of Pd, Pt and Pt-Ir form and degrade catalytic activity more than Pt-10%Rh [4, 26, 27, 28, 29]. CO selectivity was 95 % at 1000 °C and 0.1 MPa in a 15 mm quartz reactor operating with a CH_4/O_2 ratio of 2 [27]. Pd and Ni metals on stainless steel gauzes and FeCralloy woven metal fibres convert almost 100 % of the methane at 90 % CO selectivity with little coke (0.1 %) [30, 31].

In summary, advantages of CPOX are as following :

1) it is mildly exothermic, which makes it convenient for industrial processes from an energy management perspective ;

2) The H_2/CO molar ratio of 2 is ideal for the Fischer-Tropsch reaction, and it avoids the process to remove excess hydrogen as SMR ;

3) the CO_2 content can be quite low, suitable for direct further process ;

4) it avoids the large capital cost in superheated steam ;

5) it allows higher gas hourly space velocities and thus the capital cost and production scale to achieve large capacity are lower.

2.2 Catalysts of methane catalytic partial oxidation

The CPOX catalysts enhance reaction rate and allow high gas velocities while approaching thermodynamic equilibrium. The choice of catalyst is a crucial component of the CPOX reaction. Therefore, the investigation of their composition, structure, and preparation methods is essential for better understanding catalyst performance.

2.2.1 Metals and their activation

The group VIII metals are active in methane activation. Therefore CPOX catalysts divide into two main groups : non-noble metals (Ni, Co and Fe, etc.) and noble metals (Pt, Pd, Rh Ru, and Ir, etc.).

The low price of Ni ($0.013/g) based catalysts makes them the most widespread used catalysts in steam reforming. However, methane cokes on Ni more rapidly than noble metals and surface carbon species, such as carbide species and filaments, form on the surface and may alter the catalyst structure [32]. More importantly Ni sinters at high temperature, resulting in a Ni particle growth and a loss of surface area and activity [12]. Co presents a lower activity than

Ni, as it easily become oxides under the process conditions [33]. Iron is active in SMR when under strong reducing conditions in the hot part of a shaft furnace [12].

The noble metals catalysts show better performance in terms of stability and reactivity [34], and resist to coke formation because carbon does not dissolve in those elements [35]. Although they are more expensive (for example Pt \$28/g), they operate at high space velocity in CPOX thus decreasing the metal loading and the total cost. Among all the noble metals, Rh and Pt are the most active and stable CPOX catalyst [18]. Pt showed lower activity and H_2 yield than Rh [23, 36, 37], , but its price is lower. CPOX reaction rate increases with pressure when maintaining the constant gas hourly space velocity over Pt, but the rate is less prominent for Rh [18]. Rh and Ru showed 10 times higher turnover frequency (TOF) values than Ni, Pt, or Pd [38, 39]. One study [40] declared Pt to be the most active metal.

Pre-reduction of the catalysts is to have stable metallic state, and the reduced catalysts will be oxidized again when exposed to an oxidative atmosphere [12]. The reduction of pure nickel oxide by hydrogen starts at temperature between 200 °C – 250 °C. Supported catalysts require higher reduction temperature due to the interaction with support [12]. The addition of small amounts of Pt, Pd or Cu to the catalyst may enhance the activation rate, probably by providing more active sites for the dissociation of hydrogen [33].

Industrial catalyst are activated by various reducing agents, such as hydrogen, steam, hydrocarbons, etc, [33]. Hydrogen or carbon from thermal cracking of hydrocarbons could act as an initiator for the reduction process [12]. In SMR, when metallic nickel is available, sufficient hydrogen forms to reduce the catalysts quickly [12].

The ignition temperature of the activation depends on the reactivity of the source material and the state of the catalyst [16]. Activation starts in the hot part of the reactor and the activation zone moves backwards to colder inlet [15]. The mechanism may involve H_2 back diffusion from activated catalysts to the neighboring inactivated ones. In lab-scale systems for SMR process, operating at different conditions, additional H_2 should be present in the feed gases to prevent catalyst from oxidation [12].

2.2.2 Non-metal catalysts

Sulphur poisons VIII group metals. Problems in desulphurizing heavy feedstocks lead to investigate non-metallic catalyst, although their reaction rates are often lower than transition metals [12]. In SMR and CPOX, molybdenum carbide and tungsten carbide reflected high activity [41, 42]. In syngas atmosphere, carbides are stable only at elevated pressures (9 bar) or high concentration of CO, and convert into oxides at ambient pressure [12]. Molybdenum

carbide is hardly stable in a plug-flow reactor [42], because it easily becomes oxidized from the inlet.

Others attempted ceria as catalysts for reforming processes, especially in high temperature fuel cells. CeO_2 has an activity of two orders lower than Ni [43].

2.2.3 Supports

CPOX reaction occurs on the catalyst surface, so the exposed surface area determines the catalyst performance. Stabilization of the metal catalyst by distributing it on the support maximize its surface area. The industrial catalyst exposed to severe conditions, for example in a tubular reformer involving steam partial pressure close to 30 bar and temperature above 800 °C [12]. The support should be able to withstand these conditions without losing strength. Furthermore, it should not contain volatile components.

There has been a widely trend towards ceramic-based catalysts. Al_2O_3, MgO, SiO_2, etc. are not easy reducible ones oxides [44]. They also involved in reactions as followed :

$$SiO_2 + 2H_2 \leftrightarrow SiH_4(gas) + 2H_2O \tag{2.4}$$

$$SiO_2 + 2H_2O \leftrightarrow Si(OH)_4(gas) \tag{2.5}$$

$$Al_2O_3 + H_2O \leftrightarrow 2AlO(OH) \tag{2.6}$$

$$Al_2O_3 + 2KOH \leftrightarrow 2KAlO_2 + H_2O \tag{2.7}$$

$$MgO + H_2O \leftrightarrow Mg(OH)_2 \tag{2.8}$$

Silica is volatile (Eq 1.5) at high temperature in high pressure steam (for example, at 600–900 K and 1–100 atm steam pressure, $Si(OH)_4 is the most likely silicon-containing gaseous species$), unless combining it with alkali. Silica would slowly escape from the catalyst (or brickwork) and deposit on the heat exchangers and catalytic reactors downstream of the reformer [12].

At high temperature, MgO supported catalysts are sensitive to steam at low temperature because of hydration (Eq 1.8). The reaction may result in breakdown of the catalyst due to an expansion of the molecular volume. At pressure typical of tubular reformer, hydration cannot take place at temperature above 350 °C [12]. In industrial circumstance, hydration is a problem only when the magnesia-based catalyst expose to liquid water or close to the condensation temperature [45]. Magnesia reacted with alumina to magnesium aluminium spinel ($MgAl_2O_4$) eliminates hydration, because spinel support is robust and withstand high reaction temperature [12].

The most common support is Al_2O_3, including α-, θ-, δ-, and γ-Al_2O_3 phases. For Ni based catalysts, the activity for different support is : Ni/γ-Al_2O_3 < Ni/δ-Al_2O_3 < Ni/θ-Al_2O_3 $\approx$ Ni/α-Al_2O_3 [46]. α phase alumina is the most stable phase. γ-alumina has high surface area, is suitable catalyst support for low temperature adiabatic reforming. But after reaction at 850 °C for 4 h, Al_2O_3 of γ phase turns to α phase [46].

CeO_2, TiO_2, ZrO_2, etc. are relatively easy reducible oxides [44]. Rh catalyst supported on reducible oxide deactivated fast, possibly due to the decrease of active catalyst sites which replaced by suboxide [44].

The surface PH affects the catalyst activity and coke formation. Normally, the acid sites on catalyst surface promote the coke formation, as strong acid sites have significant effects on coke formation reactions such as cyclization and hydrogen transfer reaction and these sites are preferentially deactivated by coke [46]. Mehr [47] found that catalysts supported with MgO reduced coking and were more stable, because of the basic state of MgO. Among the irreducible oxides, Rh catalyst with MgO support shows the highest catalytic activity with stability [44].

The oxygen storage capacity of support also affects the catalyst activity. The lattice oxygen of CeO_2 could react with carbon to form CO and thus accelerate the methane conversion [48]. Cerium oxides (CeO_2, Ce_2O_3) found out to improve noble metal stability and the oxygen adsorption rates [49].

The support is either a powder or a pre-shaped solid. The conventional granule catalysts have problems like high pressure drop, uneven metal dispersion, large temperature gradient of catalyst bed, etc. Structured catalysts like monolith and gauze (fibers) combining mechanical strength and thermal resistance, can overcome those problems.

Monolith catalyst have 3 main parts, support body (ceramic or metallic), washcoat (oxides, such as Al_2O_3) and active species (noble metals). The surface area of monolith support is usually low, therefore, preparing a washcoat with high surface area is necessary.

Metal gauze acts as active component and also support. Gauze catalysts can achieve extremely high space velocities (12 000 000 h^{-1}), allowing greater throughput for an industrial scale. Initial gauze catalysts in CPOX are pure Pt and Rh metal gauzes [22, 25]. FeCralloy metal woven fibre is also an suitable support for preparing CPOX catalyst, however, there is few study on it [30, 31, 50]. Table 2.1 summarizes the experimental conditions and performance of gauze catalysts in CPOX reaction.

2.2.4 Promoters

Three types of promoters often participate in CPOX reaction : rare earth (Ce, La, etc.) oxides, alkaline earth metal (Mg, Ca, Ba, etc.) oxides and precious metal elements.

Adding promoters improves catalyst activity and stability [46]. Wang [51] found that the effect of promoters on Ni/α-Al_2O_3 catalyst is more significant than on Ni/γ-Al_2O_3 catalyst. A low loading of Ce serves a well dispersion, but high loading forms bulk CeO_2 and decreases the catalytic activity. Promoters also show resistance to carbon deposition by increasing surface carbon gasification, or inhibiting carbon solubility [18].

However, loading large amount of promoters may decrease the active sites and then decrease the activity [51, 52, 53]. Alkali as a promoter to eliminate carbon formation may escape slowly from the catalyst. High temperature increases the alkali loss while adding acidic components could restrain it [12]. The volatized alkali may deposit in colder parts of the reactor system and hydroxyl ions strongly promote stress corrosion in stainless steel [33]. Moreover, alkali reacts with some catalyst support materials (γ-alumina), causing a decrease in mechanical strength [12].

Table 2.1 Gauze catalysts in CPOX reaction. $\star$ only volume flow rate availble.

Catalysts	Temperature °C	Pressure MPa	τ s	CH_4/O_2 ratio	X_{CH_4}	S_{CO}	S_{H_2}
Pt [54]	500-800	0.1	0.14-0.0002	2	31	7	low
Pt [26]	200-900	0.1	0.00021-0.00042	2	20.9	89.9	10.7
Pt [27] Pt/10%Ir Pt/5%Rh Pt/10%Rh	700-1100	0.1	0.00021-0.00033	2	25	95	28
Pt/10%Rh [26]	200-1050	0.1	0.00015-0.0005	2	33	96.3	33.9
Pt [55]	670-920	0.1	0.02–0.2	2.5	5	50	–
Pt [56]	800-1100	0.1	–	–	25	97	96
Rh [57]	1000-1200	0.1-3	0.024-0.00036	–	97	97	89
Steel gauze [30]	950	0.1	$\star$ 70 mL min^{-1}	2.5	32.5	19.6	–
Pd/steel gauze	950				90-97	3-97	–
FeCrAl foil	900				38.5	49.5	–
Pd/FeCrAl foil	920				99.2	88.6	–

2.2.5 Catalyst preparation methods

The common CPOX catalyst preparation methods include :

1) Impregnation

The metal precursors dissolves in an aqueous or organic solution and contact a porous support. Capillary action dominates the adsorption process. By drying and calcining to drive off the volatile components we can obtain the catalyst.

2) Co-precipitation

One or more metals are precipitated together with the mixture of the precursors and support. It is a one step reaction and can reach high metal loading up to 80 %. The drawback is the particle agglomeration and uneven composition.

Methods such as sol-gel or electrochemical methods are limited in industrial process due to the high cost. In our study we also consider other preparation methods.

3) In situ spray-pyrolysis

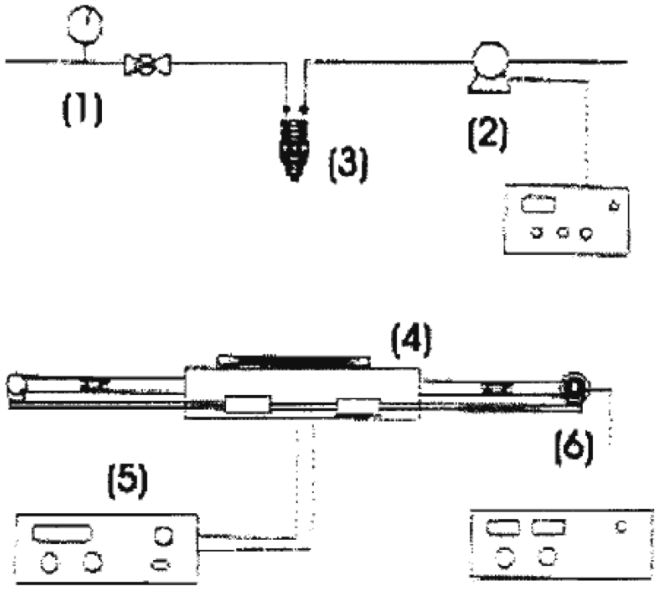

Figure 2.1 A typical in-situ spray pyrolysis system [2] : (1) Compressed air supply ; (2) Syringe pump and controller ; (3) Spray nozzle ; (4) Substrate holder ; (5) Temperature controller ; (6) Step motor and controller.

In situ spray pyrolysis [2] is a versatile technique to produce materials with various composition, size and morphology. One typical spray pyrolysis apparatus consists compressed air supply to atomize the precursor solution through a nozzle (Figure 2.1). Spray pyrolysis is

suitable for industrial applications, as it allows widely solution recipes ; moderate operation temperature ; easy controlling film thickness, and no local overheating.

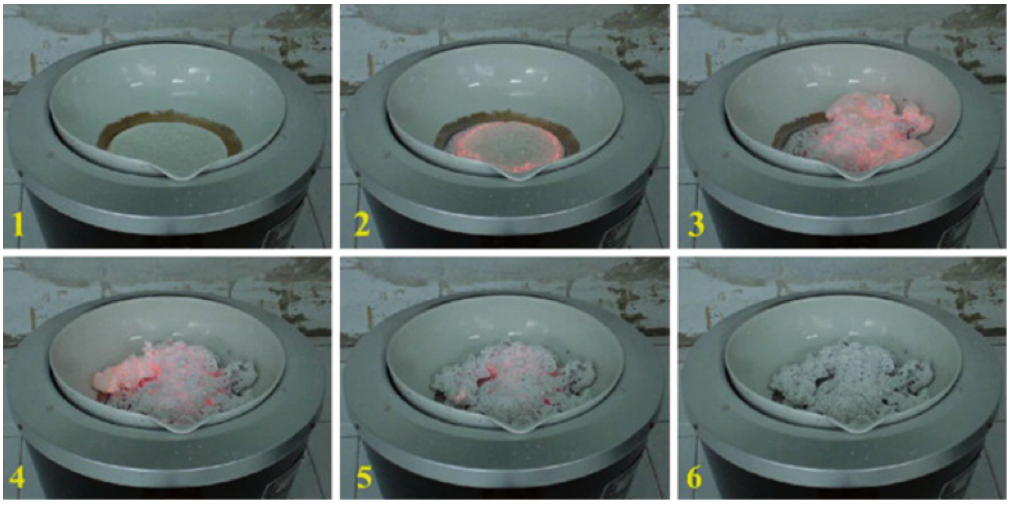

Figure 2.2 A SCS example : the evolution of combustion reaction. When heated the solution containing $Ca(NO_3)_2$, $Al(NO_3)_3$ and β-alanine below 1000 °C, we observed a smoldering flame and fine particles formed [3].

4) Solution combustion synthesis

The principle of solution combustion synthesis (SCS) method [3] is that once initiate one reaction by heating, an exothermic reaction can self-sustain the temperature for combustion and to produce homogeneous powder product (Figure 2.2). By preparing the combination of metal salts (nitrates, sulfates and carbonates) as oxidants in an aqueous solution with a fuel (glycine, urea and other soluble carbohydrates) as reducing reagents, the reaction occurs when reaching the ignition temperature. The powder can be a single phase pyrolysed product with/without subsequent heat treatment.

SCS is a relatively simple, cheap and fast process ; it can be adapted to coat nanocrystalline metal oxides, such as Al_2O_3, and zero-valent metal onto monoliths, honeycombs and gauzes. Prepared by SCS, Ru/Al_2O_3 loaded on monolith catalyst for oxy-steam reforming of methane [58], and palladium on zirconiastabilised lanthanum manganese oxide perovskite on FeCralloy gauzes for natural gas combustion [50] are quite active.

2.2.6 The effect of different reaction conditions

The CPOX system consists multiple reactions besides SMR (Eq 1.1), DRM (Eq 1.2) and POX (Eq 1.3) [4] :

$$CH_4 + 2O_2 \rightarrow CO_2 + 2H_2O \tag{2.9}$$

$$H_2 + \frac{1}{2}O_2 \rightarrow H_2O \tag{2.10}$$

$$CO + \frac{1}{2}O_2 \rightarrow CO_2 \tag{2.11}$$

$$CH_4 \rightleftharpoons C + 2H_2 \tag{2.12}$$

$$CO + H_2 \rightleftharpoons C + H_2O \tag{2.13}$$

$$CO + H_2O \rightleftharpoons CO_2 + H_2 \tag{2.14}$$

$$2CO \rightleftharpoons CO_2 + C \tag{2.15}$$

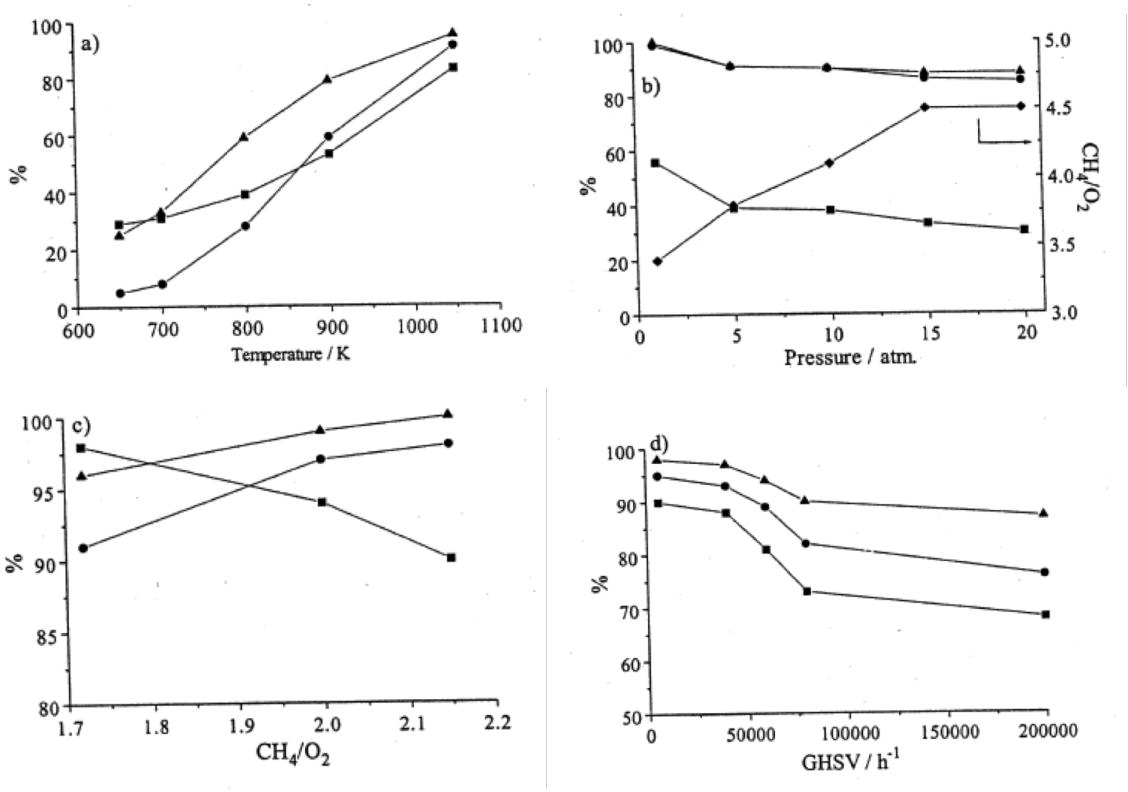

Figure 2.3 Effect of reaction conditions on CPOX over Ru catalyst [4] : (a) Temperature; (b) Pressure; (c) CH_4/O_2 ratio; (d) Gas hourly space velocity. (Square : X_{CH_4}, Sphere : S_{CO}, Triangle : S_{H_2})

Effect of temperature

At temperatures lower than 450 K, CPOX cannot occur [21]. For temperatures between 500 K and 1120 K, thermodynamics equilibrium calculations [4] can predict the POX products. It suggests that higher temperature increases methane conversion and CO and H_2 selectivity (Figure 2.3 (a)).

Effect of pressure

Increasing the pressure decreases both the methane conversion and CO and H_2 selectivity, predicted by the thermodynamics [4]. Otherwise, at increasing pressures, higher temperatures are necessary to obtain high conversion, and high selectivity to H_2 and CO. Elevated pressure inhibits the reforming reactions since they result in gas expansion, while hardly affecting the complete oxidation of methane. Therefore more CO_2 and H_2O form with increasing pressure. The experimental results of CPOX are very close to the thermodynamic predictions (Figure 2.3 (b)).

Effect of CH_4/O_2 ratio

The effect of the CH_4/O_2 ratio on the product distribution from the CPOX reaction is shown in Figure 2.3 (c). A CH_4/O_2 ratio of 2 is ideal for CPOX. A ratio higher than 2 brings excess methane and lower the methane conversion, but increases H_2 and CO selectivities as stoichiometry is unfavor the total combustion reaction. A ratio below 2 with more oxygen generates more CO_2 and H_2O. Feeding CH_4/O_2 at a ratio of 0.5 yields complete combustion products (CO_2 and H_2O) [4].

Effect of gas flow rate

At space velocities lower than 40 000 h^{-1}, CPOX can reach thermodynamic equilibrium. At higher space velocities, kinetics become limiting the CPOX and may not reach equilibrium (Figure 2.3 (d)).

2.3 Catalyst deactivation

Catalyst deactivation, the loss of catalytic activity and/or selectivity with time, is tricky but inevitable in industrial practice [1]. The expenses of process shut-down and replacement of the catalyst is frustrating. The life time of the catalysts vary from seconds to years. For example, chemical cracking catalysts deactivate in seconds but the catalyst for ammonia synthesis may

function over 5 years. Although it is inevitable, we could postpone its deactivation by better catalyst design and a well-management system.

2.3.1 Deactivation mechanism

The presence of contaminants in the reaction atmosphere, blockage or fouling of the catalyst active sites, or coke all lead to the deactivation of the catalyst [1]. The causes of catalyst deactivation are thermal, mechanical and chemical. Table 2.2 summarized the mechanisms of solid catalyst deactivation.

Table 2.2 Mechanism of catalyst deactivation [1]

Mechanism	Type	Phenomenon
poisoning	chemical	chemisorption on active sites blocking active sites
fouling	mechanical	physical desorption on surface and pores
thermal degradation	thermal	loss of specific surface area and active phase-support reaction
vapour formation	chemical	volatile compounds formation
vapour-solid and solid-solid reactions	chemical	inert phase by reaction among gas–phase, support or promoter
attrition/crushing	mechanical	loss of catalytic material loss of internal surface area

2.3.2 Poisoning

Poisoning [59], a strong chemisorption of impurities or even reactants or products, blocks the adsorption sites and changes the electronic and geometric structure of the catalyst surface [60]. Based on their chemical structure, catalyst poisons classified as [1] :

• Groups VA and VIA : N, P, As, Sb, O, S, Se, Te.

• Group VIIA : F, Cl, Br, I.

• Toxic heavy metals and ions : As, Pb, Hg, Bi, Sn, Zn, Cd, Cu, Fe.

• Molecules that adsorb with multiple bonds : CO, NO, HCN, benzene, acetylene, unsaturated hydrocarbons.

Table 2.3 presents examples of common poisons for some catalytic reactions over specific catalysts.

Table 2.3 Common poisons for specific catalytic reactions over selected catalysts [1]

Catalyst	Reaction	Poisons
SiO_2-Al_2O_3, zeolites	Cracking	Organic bases, hydrocarbons heavy metals
Ni, Pt, Pa	De-/hydrogenation SMR	Compounds of S, P, As, Zn, Hg, halides, Pb, NH_3, C_2H_2
Fe, Ru	Ammonia synthesis	O_2, H_2O, CO, S, C_2H_2, H_2O
Co, Fe	FT synthesis	H_2S, COS, As, NH_3, metal carbonyls
Noble metals on zeolites	Hydrocracking	NH_3, S, Se, Te, P
Ag	C_2H_4 oxidation	C_2H_2
Vanadium oxide	Oxidation/selective catalytic reduction	As/Fe, K, Na from fly ash
Pt, Pa	CO xidation	Pb, P, Zn, SO2, Fe
Co and Mo sulfides	Hydrotreating of residuum	Asphaltenes, N compounds, Ni, V

2.3.3 Fouling, coking and carbon deposition

Different from poisoning, fouling is the physical (mechanical) deposition of species from the fluid phase on the catalyst surface and blocks active sites or pores [1]. For example, the deposition of coke and carbon in porous catalysts [61]. Regarding the origin of the carbon and coke, their definition differs : carbon forms from CO disproportionation while coke is from by decomposition and/or condensation of hydrocarbons [62].

The chemical structures of coke or carbon vary with reaction type, catalyst type, and reaction conditions [1]. Menon [62] classified the catalytic reactions accompanied by carbon or coke formation to coke-sensitive and coke-insensitive reactions. In the former reactions, such as catalytic cracking, catalysts lose activity as the deposited coke is unreactive. In the latter reaction, such as FT reaction and catalytic reforming, coke is reactive to a gasifying agent (H_2, etc) The structure and location of the coke and also its formation mechanism affect catalyst activity. Carbon and Coke formed on supported metal catalysts may

1) block reactants to reach active sites by monolayer chemisorption or multilayer physisorption ;

(2) completely encapsulate thus deactivate metals ;

(3) plug micro- and meso- pores and decrease effective surface area.

(4) in extreme cases, strong carbon filaments build up in pores and break down catalysts and clog reactor voids [1].

Fortunately, some forms of poisoning and many forms of fouling are reversible and regenera-

tion of these systems are feasible [12].

2.3.4 Thermal degradation and sintering

Thermal deactivation refers to the loss of catalytic surface area due to crystalline growth, loss of support porosity and conversion of catalytic phases to non-catalytic phases [1]. The first two processes are sintering which typically occurs at reaction temperatures higher than 500 °C ; the third refers to solid–solid reaction. The rate of sintering depends on temperature, atmosphere, metal type, metal dispersion promoters, support surface area, texture, and the porosity [63]. Depending on the type of the reaction, the activity of the catalyst differs with increasing metal crystallite size [64]. The principal mechanisms of metal crystallite growth are (1) crystallite migration ; (2) atomic migration and (3) vapour transport [1]. In some cases, it is not single mechanism and could be a couple of several or all mechanisms. Thermal degradation is generally slow and irreversible. Therefore regeneration of a sintered catalyst is not feasible [12].

2.3.5 Gas-vapour/solid and solid state reactions

Other chemical routes are [64] :

(1) gas-vapour phase reacts with the catalyst surface to produce inactive bulk and surface phases and volatile compounds and chemical-assisted sintering (due to adsorbate interactions, different from thermal sintering). For example, Fe and Ru are active phases in ammonia synthesis while their oxides are inerts.

(2) catalytic solid-support or solid-promoter reactions, however, it is difficult to keep track of its degree as diffusion and solid-state reaction are affected by surface reactions. For example, The presence of gas-phase oxygen or steam may enhance the diffusion rate of Al_2O_3 to the surface to form an aluminate.

(3) solid-state transformations of the catalytic phases during reaction.

2.3.6 Mechanical failure of catalysts

Mechanical failure includes : (1) crushing in fixed bed ; (2) attrition in slurry or fluidized bed reactors and (3) erosion in any reactor [64]. Attrition leads to a reduction of particle size, rounding or smoothing of particles and washcoat loss. A rise in pressure drop indicates fouling and the plugging of the lines by accumulation of the worn catalysts.

2.3.7 Catalyst deactivation and regeneration in syngas production

Catalyst deactivation in syngas production

The most probable mechanism for the deactivation of catalysts in laboratorial scale syngas production is coke formation. There are three types of coke [33] whisker-like, encapsulating film, and pyrolytic carbon. Table 2.4 summarizes carbon species formed in syngas routes, especially in SMR with Ni catalysts [1, 12].

Table 2.4 Routes to carbon

Carbon type	Reaction	Phenomena	Critical parameters
Whisker carbon	Eq. 1.12, 1.13, 1.15, 2.16	Break-up catalyst Pressure drop rise	$> 450\,^{\circ}C$, low H_2O/C ratio olefins or aromatic feed
Encapsulated films	Eq. 2.17	Blocking Ni surface progressive deactivation	$< 500\,^{\circ}C$, low H_2O/C ratio low H_2/C_nH_m, aromatic feed
Pyrolytic coke	Eq. 2.18	Encapsulation of catalyst desposits on tube wall	$> 600\,^{\circ}C$, long residence time high pressure, acidic catalyst

Reactions relate to carbon formation (besides Eq 1.12, 1.13 and 1.15) [12] :

$$C_nH_m \rightarrow nC + 0.5mH_2 \tag{2.16}$$

$$C_nH_m \rightarrow olefins \rightarrow coke \tag{2.17}$$

$$C_nH_m \rightarrow (CH_2)_n \rightarrow encapsulated\ \ coke \tag{2.18}$$

Whisker carbon typically grows as carbon fiber (nanotube) from the dissociation of hydrocarbons or CO on the catalyst surface [33]. Its strength is high enough to destroy the pores of catalyst particle. Damaged catalyst and accumulated carbon lead to maldistribution of the feed and hot spots or hot tubes, further partially or totally clog the reactor [33]. Low temperature encapsulated coke blocks the catalyst surface by a film of polymerized carbonaceous compounds. Thermal pyrolysis in steam crackers leads to pyrolytic coke which encapsulates the catalyst or deposits on the tube wall.

The type and crystallite size of metal, promoter and support all affect the coke formation rate. For example, supported Co, Fe, and Ni catalysts actively produce filamentous carbon above $350\,^{\circ}C$; the order of coke formation rate for these non-noble metals is Fe > Co > Ni [65]. Noble metals like Pt, Ru, and Rh, with equal or much higher activity than Ni, generate little coke. According to Claridge et al [5], the relative rate of carbon deposition is in the order Ni > Pd > Rh > Ru > Pt, Ir. The rate of carbon formation on precious metals

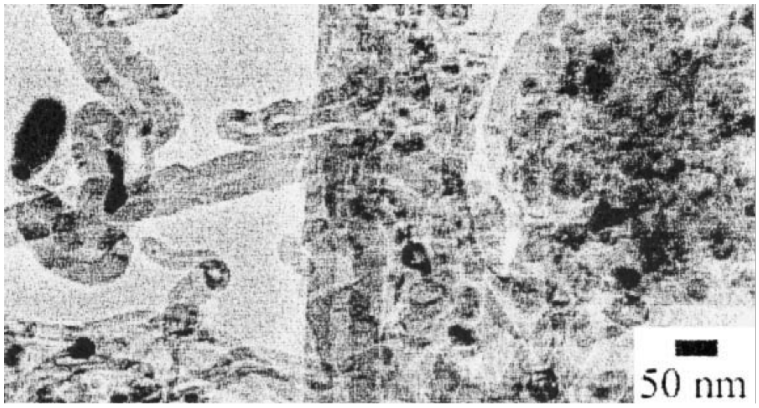

Figure 2.4 Two types of carbon formed on Ni based catalysts [5] : i) encapsulated carbon, which envelops the nickel particles resulting in deactivation, and ii) whisker carbon, which grows from the face of the nickel particles and does not alter the rate of synthesis gas formation, but is likely to eventually result in reactor clogging.

is much less than on Ni [39], also because Ni particles dissolve carbon [66]. Ni catalysts supported on Al_2O_3 and promoted by alkaline earth oxides are popular in SMR process. Carbon infiltrates Ni particle and develops to filaments from the back of Ni particle, which gets squeezed down the support surface and loses, especially at high temperature and low steam/CH_4 ratio [67, 65]. At different condition with other metals, filaments may grow from the top of the metal particles or penetrate into the metal and create bulk carbides [67]. In Nobel metals, the mobility and/or solubility of carbon is weak, thus the nucleation process is difficult. Therefore adding noble metals resist carbon formation.

Sintering is another issue in deactivating catalysts in syngas routes. For most tubular reformers, the operation temperature is above the Tammann temperature of nickel ($T_{tammann} = \frac{1}{2}\ T_{melt} = 581\,°C$, Ni solid has 70 % of its viberation freedom and its diffusion into lattice becomes possible), thus is exposed to sintering[12]. Sintering is a complex phenomenon and may occur below the Tammann temperature as well. Sintering of Ni catalyst leads to the growth of nickel particles and a decrease of surface area and activity. Besides catalyst composition and structure and support, operation temperature and chemical atmosphere that contacting the catalyst determine the extent of sintering. At low temperature, metal particles migrate over the support, collide and finally coalesce ; while at high temperature, particle coarsening (Ostwald ripening) is dominant [12]. The presence of water greatly accelerates sintering.

Group VIII metals are vulnerable to the presence of sulphur, therefore pre-treatment of the raw feed stream is necessary [12].

Catalyst regeneration in syngas production

Rapid accumulation of whisker carbon forms dust or irreversibly breaks down the catalyst, while slow build-up even with high amount of carbon may not damage the catalyst structure [12]. Fresh whisker carbon are quite reactive for gasification (reverse reaction of Eq 1.15). In practice, at temperature of 600 °C – 700 °C, a steam/hydrogen ratio of 10 removes fresh carbon [45]. The reactivity of aging whisker coke and encapsulated coke layer are lower, thus oxygen (air) stream is more effective to remove these coke. The rate of the regeneration, for example for cracking catalysts, depends on the surface area of the coke and it swiftly becomes diffusion–limiting [12]. The vigorous exothermic oxidation leads to the risk of overheating the catalyst. Adding a few percent of air to the steam flow at temperature over 450 °C easily erases the coke [61, 33]. If whisker carbon already damages the catalyst, a high pressure drop will remain after regeneration. It is futile to remove the pyrolytic coke by steam [68], and it is difficult even with air. Regeneration the catalysts by frequent "on–line decoking" with steam is more feasible rather than "off–line decoking" with steam and air [69]. High temperature hydrogen stream theoretically can eliminate encapsulated coke, however, it is not practical to set it up in industry [70].

2.4 CPOX reactors

Reactors in catalytic partial oxidation of methane include fixed bed reactor, fluidized bed reactor, monolithic reactor and membrane reactor.

2.4.1 Fixed bed reactor

Fixed bed reactor is easy to operate. Massive work reports CPOX reaction with fixed bed quartz reactor at ambient pressure with temperature from 1073 – 1273 K [46] : reactor diameter ranges from 1 – 10 mm, particle size varies from 20 – 60 mesh ; the choice of catalyst is usually Ni supported Al_2O_3 catalysts ; at contact time of 0.25 s, methane conversion, selectivity of H_2 and CO reach to $>$ 85 %, 75–85 % and 75–95 %, respectively. As CPOX reaction is exothermic and fast, the sintering and loss of catalyst active phases are problematic due to hot spots [71].

Li [71] designed a dual–catalyst fixed bed system. Instead of filling single type of catalyst, he loaded Pt or metal oxides catalysts and Ni reforming catalysts based on indirect mechanism. H_2 selectivity was higher than single fixed bed system with Pt or Rh catalyst. Pan [72] designed a two-step CPOX process with two fixed beds in series : the ratio of CH_4/O_2 at the first step was 8 :1 with low operation temperature of 620 K ; and at the second step the ratio

was 8 :3. This design prevented temperature runaway, and the feed stream stayed out of the explosive limits, and received high H_2 and CO selectivity (97 % and 98 % respectively).

2.4.2 Fluidized bed reactor

Fluidized bed has uniform particle mixing and temperature gradient which eliminates hot spot and inhibits coke formation, thus is suitable to exothermic reactions [73]. However the drawbacks include increased reactor size and pumping powers, particle entrainment, particle entrainment, erosion of internal components and pressure loss risks [73].

Jing [74] operated CPOX in fluidized bed for 10 without coke formation and Ji operated 100 h without coke formation and active phase loss. Schmidt [75] fed methane and air into an adiabatic fluidized bed reactor at 1123 K. Methane conversion was over 90 % with Rh and Ni catalysts with CO selectivity of 95 %, however, Pt catalyst presented poor activity and selectivity and produced more water. The activity of Pt and Rh maintained stably in 10 h, while Ni deactivated due to the lost of active phases. Santos [76] reported isothermal distribution in fluidized bed reactor and methane conversion close to thermodynamic equilibrium with 0.6 % coke.

2.4.3 Monolithic reactor

Monolithic reactor fills with structured catalysts (honeycombs, foams, or interconnected fibers) and contains interconnected or separated channels (straight, wavy or crimped) [77]. They have numerous advantages such as low pressure drop under high fluid output, high specific external surface area, limiting internal diffusion, low axial dispersion and back mixing, alleviating fouling and clogging, etc [77]. Therefore, the lifetime of catalyst is extended and the scale–up to industrial size is more achievable [77]. Low heat transfer of ceramic monolith supports have problems in temperature control [77].

Korchnak [78] first employed monolithic reactor in catalytic partial oxidation of methane to produce a hydrogen rich gas. Torniainen received high methane conversion and syngas selectivity over 90 % at contact time of 10 ms, ambient pressure, 1273 K, with Pt, Ph and Ni catalysts supported on Al_2O_3 foam monolith [79]. Kikas found that countercurrent autothermal Pt/Rh monolithic reactor increased hydrogen selectivity by 5 % and decreased ignition temperature by 200 K [80]. Schwiedernoch preheated the feed stream to ignition temperature and sent it to the monolithic reactor at room temperature and ambient pressure, and found initially methane completely oxidized to H_2O and CO_2 then the selectivity of syngas increased with increasing temperature of the catalyst bed [81]. Schmidt deposited

Ni, Rh, Pt, Ir, Pd, Fe, Co, Re, Ru on ceramics monolith [23, 79]. Rh and Ni monolith catalysts showed high activity and selectivity, however, Ni was easy to deactivate even on monolith supports. Li found that in Ni monolithic reactor, adding steam increased hydrogen selectivity but decreased methane conversion and CO selectivity, and adding CO_2 increased CO selectivity however lowered methane conversion and H_2 selectivity [74].

2.4.4 Membrane reactor

In a membrane reactor, catalytic reaction and separation process occur simultaneously. There are two types of membrane reactor : hydrogen permeable and oxygen permeable membrane reactors. A hydrogen permeable membrane promotes hydrogen to selectively penetrate and thus produce pure hydrogen [82]. In a oxygen permeable membrane reactor, oxygen, in–situ separated from air, transports through the membrane as oxygen ion (O^{2-}) and reacts with methane over a selective catalyst [83]. The key for the scale-up of membrane reactors is to increase the oxygen permeability of membrane and its stability under reducing atmosphere.

2.5 CPOX mechanism

Much debate on the CPOX mechanism divides into three main ideas,

i) the direct mechanism,

ii) the combustion–reforming mechanism,

iii) a mechanism in between.

The combustion–reforming mechanism proposed that first methane undergoes complete oxidation to CO_2 and H_2O (Eq 1.9) and then the unconverted methane react with steam and CO_2 to produce CO and H_2 through steam reforming (Eq 1.1) and CO_2 reforming (Eq 1.2) [18].

The direct mechanism assumes that H_2 and CO are primary reaction products formed by POX (Eq 1.3) in the presence of gas phase O_2. The equation below, including the competitive formation of H_2O and CO_2 describes the direct mechanism [7] :

$$CH_4 + (2 - \frac{x}{2} - \frac{y}{2})O_2 \rightarrow xH_2 + yCO + (1-y)CO_2 + (2-x)H_2O \qquad (2.19)$$

where $0 \leqslant x \leqslant 2$, $0 \leqslant y \leqslant 1$.

Both mechanisms can occur over noble metal and non-noble metal catalysts. The reaction conditions modify the reaction routes. Catalysts with different active components follows different reaction mechanism. Even the same catalyst can undergo direct and indirect mechanisms simultaneously - a mixed mechanism.

There are two approaches in studying the mechanism of CPOX [7]. One is operate under high temperature and at ambient or elevated pressure to be close to industrial condition and compare the data from the reactor outlet with numerical simulations in order to propose a reaction mechanism [23, 84, 85, 86, 87]. The other is to conduct under isothermal low pressure or diluted conditions which is different from industrial application, for example TAP tests in vacuum [88, 89], isothermal reactor [90, 91], and spectroscopic analysis[92]. Depending on different experimental condition and effluent products, Mallens [89], Weng [92] supported the direct mechanism, Tavazzi [87], Wang [88], Slaa [90] and Souza [91] advocated the indirect mechanism and Deutschmann [93, 94] endorsed a mechanism in between.

Schmidt's group [6, 7] developed a capillary sampling method with a spatial resolution of 300 µm, to measure the temperature and species profiles along the centerline of the catalyst bed. From Figure 2.5, clearly there are two stages in Rh supported CPO catalyst bed : 0 to 2 mm, a short oxidation zone, and 2 mm to 10 mm, a longer endothermic reforming zone. The temperature of the inlet of the bed is almost 200 °C higher than the outlet. The oxygen consumed fast in the oxidation zone, resulting in a sharp temperature increase. The temperature decreased along the catalyst bed, mainly due to the endothermic steam reforming reaction proceeds. H_2 and CO formed in both zones, and the mechanism illustrated in Figure 2.6. For Pt supported catalysts, the oxidation zone is longer than Rh and they produce less syngas due to their lower steam reforming activity.

2.6 Summary of the literature review

CPOX is an inexpensive alternative technology to produce syngas (CO and H_2). Some downstream processes operate at high pressure, such as chemical synthesis via Fischer-Tropsch reaction (2 MPa), H_2 production via PSA (Pressure-Swing Adsorption) and Membrane Gas Generation Technologies (1-2 MPa), and flame and flameless combustion (0.5-1.5 MPa) [12]. Therefore operating CPOX under high pressure is an opportunity to make the reactor more compact by combining CPOX and the other process in a single vessel.

Operation under pressure would strongly benefit :

1) the intensification of the process and the minimization of the reactor volume ;

2) integration with downstream processes, avoid the energy loss related with compressing hot

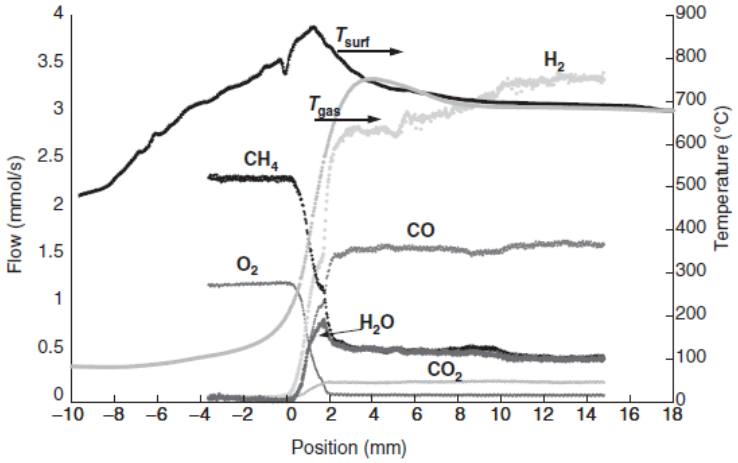

Figure 2.5 Temperature and concentration profile of a Rh supported CPOX catalyst bed [6, 7]. 0 mm indicates the start of the catalyst, whereas 10 mm is the end. Before and after this range are heat shields made by two blank monoliths.

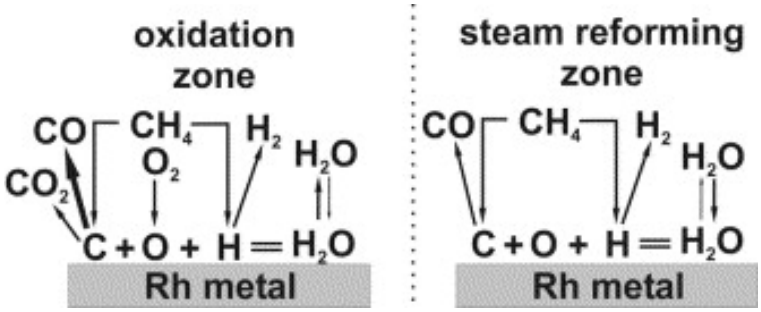

Figure 2.6 CO and H_2 are the primary products in CPOX over Rh catalyst and form in both reaction zones through direct and indirect mechanisms [6, 7].

and high hydrogen content gases.

However, as CPOX is a gas expansion reaction, higher pressure disfavors CPOX thermodynamically. There are a few studies on high pressure CPOX [94, 95, 96, 97, 98]. Lyubovsky et al [94] demonstrated CPOX with microlith based catalysts at pressures up to 0.8 MPa. The product composition profiles indicated high initial selectivity to CO (> 85 %) and low initial selectivity to H_2 (mostly H_2O). Burke et al [95] carried out CPOX with Rh/γ-Al_2O_3 foam monolith catalyst at pressures up to 1.5 MPa. Methane conversions reached 54 % with O_2 conversion of 86 % and selectivity of CO and H_2 of 89 % and 65%, respectively. Larsen et al [96] tested CPOX with Rh and Pt coated foams from 0.1 to 1.1 MPa total pressure. Fichtner et al [98] tested micro structured honeycomb catalysts at operating pressure up to 1.2 MPa with oxygen and up to 2.0 MPa with air at a catalyst temperature of 1100 °C. The methane conversion rate drops from 90 % at 0.15 MPa to 77 % at 2 MPa. H_2 and CO selectivity declined to 83 % and 76 % respectively. Basini et al [97] demonstrated the possibility to operate CPOX at 2 MPa in a bench-scale reactor with CH_4 conversion over equilibirum prediction, CO selectivity close to equilibrium and low H_2 selectivity. However, Basini admits there may be experimental uncertainties that cause this surprising observation. He successfully sustained the reactions without deactivation for 500 h at 1.5 MPa with selectivity of CO over 90 % and H_2 over 85 %.

We were the first to carry on CPOX at pressure up to 2 MPa in a laboratory micro reactor, and produce suitable syngas (H_2/CO ratior of 2) for further process. We were also the first to use noble catalysts supported on FeCralloy knitted fibres (thickness of 2 mm). FeCralloy has high thermal conductivity, this may help distribute the excess heat through the catalyst bed, reducing the presence of local hot spots. Also it offers the benefit of a reduced pressure drop over the bed, which allows higher linear gas velocities and increase the overall throughput, which is important when scaling up the process.

CHAPTER 3 COHERENCE OF THE ARTICLES

A brief description of the chapters and the link in between are as follows :

Chapter 1 : the first chapter highlights the situation of wasted associate natural gas and the potential of producing value–added fuels while reducing greenhouse gas emissions. It briefly discusses the problems involved in converting methane (the major gas in associated natural gas) to liquid fuels. We proposed that a high pressure catalytic partial oxidation of methane would meet the requirements to combine downstream process (Fischer–Tropsch reaction). The main goal will focus on developing suitable catalysts which are active at high temperature and high pressure.

Chapter 2 : this chapter reviews the status of the syngas production routes and compares each process, leading to a conclusion that high pressure catalytic partial oxidation is suitable for the small scale industry. The second part of the chapter focuses on the catalysts for syngas production. Factors concerning to a suitable catalyst and the deactivation and regeneration of the catalyst are discussed. We introduce the common reactors applied in syngas production based on the nature of the catalyst and operation conditions. Finally, we review three mechanisms which argue the formation of CO and H_2 is direct or indirect.

Chapter 3 : a brief description of all the chapters and the main links.

Chapter 4 : the first article gives a comprehensive introduction of the micro refinery unit (MRU), including the background, the choice of the technology and the concept of its design. A dual stage test demonstrated its possibility. Calculations on greenhouse gas reduction approved its environmental benefit. The challenges were also illustrated. This paper entitled "A micro–refinery to reduce associated natural gas flaring", has been published on "Sustainable Cities and Society" in 2016.

Chapter 5 & 6 & 7 : This section is the scientific contribution of this thesis in the form of three original journal articles.

In order to find a better catalyst, we prepared several catalyst supported on FeCralloy fibres. Based on the type of the catalyst (metal) : we employed virgin FeCralloy and oxidized FeCralloy (Chapter 6), Pt/MgO, Pt/Rh (9 :1, 1 %, Chapter 6), CeO_2 and Pt/CeO_2 (Chapter 7) as catalysts and tested their activity. Based on they type of the supports, we coated MgO (Chapter 5), and applied virgin and oxidized FeCralloy (Chapter 6 & 7) and CeO_2 (Chapter 7, according to its high reactivity, we consider it as a catalyst more than a support). Based on the type of preparation method, we deposited the active phases by solution combustion

synthesis (Chapter 5 & 6 & 7), which is more effective than spray pyrolysis (Appendix A).

In order to understand the catalytic performance of the catalysts, we ran a full temperature profile from 400 °C to 900 °C at ambient pressure (Chapter 6 & 7), and compared the catalytic results at ambient pressure and 2 MPa at the optimal temperature of 900 °C (Chapter 5 & 6 & 7). We discussed the effect of space time (regarding to weight or volume of the reactants) on conversion and selectivity from 0.1 MPa, 0.5 MPa, 1 MPa to 2 MPa (Chapter 5). We evaluated the effect of CH_4/O_2 ratio (1.5 – 2.5) on products development at 2 MPa (Chapter 6). Inspired by chemical looping process, we separately fed methane and oxygen to the catalytic system (Chapter 7).

To study the coke formation, we compared the formed coke with thermodynamic equilibrium value calculated by FactSage under different pressure (0.1 MPa – 2 MPa, Chapter 5) and under different temperature (400 °C to 900 °C, Chapter 6). By using scanning electron microscope, we accessed the catalyst surface and observed the type of coke was whisker–like (Chapter 6 & 7). The regenerative ability of the catalyst is discussed in Chapter 6.

In Chapter 7, methane and oxygen were quite competitive in adsorbing on the surface. Cycling oxygen and methane feeds generated high purity hydrogen and CO. By separate feeding methane and oxygen to CeO_2 based catalysts, we were able to understand the surface reactions on the catalyst surface. CO and H_2 form directly from methane rather than via CO_2 reforming.

The paper in Chapter 5 entitled "Partial Oxidation of Methane to Syngas over Pt/Rh/MgO Catalyst Supported on FeCralloy Woven Fibre" has been published on Canadian Journal of Chemical Engineering in 2016. The paper in Chapter 6 entitled "FeCralloy partially oxidizes methane selectively" has already passed peer review and been submitted to "Catalysis Today". The paper in Chapter 7 entitled "Catalytic partial oxidation of methane with CeO_2 based FeCralloy catalysts" will be submitted to "Applied Energy".

Chapter 8 : general methodology including material, catalyst preparation, experimental preparation.

Chapter 9 : general discussion of the work and summary of the results.

Chapter 10 summary of the project, discuss the hurdles and the limitation, and provides recommendation for future work.

CHAPTER 4 METHODOLOGICAL ASPECTS

4.1 Materials

The materials for the CPOX process are categorized in three groups (table 4.1) :

1) the raw materials for catalyst synthesis

To define the best catalytic system and maximize the selectivity of the desired products (CO and H_2), we prepared several Pt catalysts supported on FeCralloy knitted fibres (and we compared them with commercial Pt and Pt/Rh gauzes (Appendix A)).

2) feed gases injected into the reactor ;

3) mixed gases to correct the accuracy of MS and GC.

Table 4.1 Materials for catalyst synthesis, feeds, and calibration.

	Material	Company
Catalysis synthesis	FeCralloy® woven fibre	ERATEC
	$Al(NO_3)_3{\cdot}9H_2O$	Sigma Aldrich
	$Ce(NH_4)_2(NO_3)_6$	Sigma Aldrich
	$PtH_2Cl_6{\cdot}6H_2O$	Sigma Aldrich
	$Mg(NO_3)_2{\cdot}6H_2O$	Sigma Aldrich
	$CO(NH_2)_2$	Sigma Aldrich
	$(Pt(NH_3)_4(NO_3)_2$	Sigma Aldrich
	$RhCl_3$	Sigma Aldrich
	Pt gauze (52 mesh)	Sigma Aldrich
	Pt/Rh gauze (52 mesh, 90 :10 wt %)	Alfa Aesar
Feed	CH_4	Liquid Air
	30 % O_2 (Ar as balance)	Liquid Air
	Ar	Liquid Air
Calibration	CO_2 10% CH_4 10% CO 25% Ar 5% H_2 balance	Liquid Air
	CO_2 15% CH_4 15% CO 15% H_2 20% Ar balance	Liquid Air
	CO_2 2% CH_4 5% CO 5% Ar 10% H_2 balance	Liquid Air
	CO_2 6% CH_4 20% CO 30% H_2 10% Ar balance	Liquid Air

4.2 Catalyst preparation

The metallic support (from Eratec) is a FaCralloy knitted fibre, with a mass fraction of 20 % chromium, 5 % aluminum, yttrium > 0.1 %, 0.3 % silicon, 0.08 % manganese, 0.03 % copper, 0.03 % carbon and the balance is iron. The diameter of the fibre is 50 µm.

All the reagents were certified high purity chemicals by Sigma Aldrich and were used without further purification.

4.2.1 Coating by solution combustion synthesis

We cut the woven fibres to 10 mm×10 mm squares. They were then washed in a water/acetone solution (1 :1) in an ultrasonic bath for 30 min to remove surface contaminants. A muffle furnace dried the samples at 120 °C for 1 h and calcined at 1000 °C for 3 h at a heating and cooling rate of 5 °C min^{-1}. Virgin FeCralloy then transformed to oxidized FeCralloy with a protective layer of α-Al_2O_3, which prevents the bulk of FeCralloy (Fe and Cr) from being oxidized.

We deposited an extra support or active phases, Pt, by adding dropwise an aqueous solution containing soluble precusors (preferablly nitrates) and urea ($CO(NH_2)_2$) as the organic fuel, to the FeCralloy squares. We calculated the mass of the reagents according to Vita et al. [58]. The stoichiometric ratio between oxidizing (O : total valences of oxidizers, i.e. nitrates) and reducing species (F : total valences of fuel, i.e. urea) was 1. We placed the mixture (FeCralloy adsorbed precusor solution) in the furnace or heating bowl at 600 °C for 2 min. This procedure was repeated multiple times and took 10 mL solution in total to reach the expected mass on the oxidized FeCralloy. Finally, the catalyst calcined at 1000 °C in static air for 4 h.

4.3 Catalyst characterization

4.3.1 X-ray difraction (XRD)

XRD is one of the most common techniques to analyze the crystalline structure of materials. A Philips X-Pert MPD diffractometer consists of an X-ray source, a sample holder and a detector. A Cu Kα radiation at 50 kV and 40 mA measured the diffraction of the crystalline phases of the samples. The scanning rate was 0.02 ° s^{-1} with 2θ varying from 20° to 90°. We attributed the peaks according to the PCPFWIN database and calculated the crystallite size with the Scherrer equation (particle shape factor = 0.9). For FeCralloy catalysts, silica substrate is suggested to avoid the noise signal of stainless steel base of the instrument.

4.3.2 Scanning electron microscopy (SEM)

We performed scanning electron microscopy (JSM-7600A) with an EDS (Energy Dispersive Spectroscopy) detector to assess the surface morphology and the existence and the mass ratio

of different element [99].

4.3.3 Nitrogen adsorption/desorption (BET)

The surface area and textural properties of catalysts are important parameters to determine the dispersion of the active metals involved in heterogeneous reactions. To determine the surface area and total pore volume, we used the BET method with an Autosorb-01 N_2 porosimeter.

4.3.4 Thermogravimetric analysis (TGA)

The thermal decomposition of the fresh catalyst and the approximation of coke formation on the surface of the used catalyst can be determined using a TGA instrument. The TGA employed in this project was a Q5000IR from a TA instrument, which has the capability to heat up the sample with a low heating rate ($5\,^{\circ}\mathrm{C\,min^{-1}}$) up to high temperatures ($1100\,^{\circ}\mathrm{C}$). The temperature and the sample weight are continuously recorded. A nitrogen flow is required continuously to keep the reaction medium free of the reactant gas.

4.4 Experimental description

4.4.1 Experimental setup

The reactor for methane partial oxidation was a 300 mm – 600 mm long quartz reactor, 8mm ID, and stainless steel as exterior casing (ID of 12 mm) (Fig. 4.1). We cut circular disks of the FeCralloy catalyst to fit snugly inside the reactor and placed them at the middle of of the reactor. We placed 1 cm glasswool under the catalysts to keep it from moving. We also supported the catalyst and glasswool with sand. We can refer to it as a gauze reactor. As FeCrallloy catalysts are not moving during reactions, we can employ the fixed bed model to describe the kinetics behavior.

An electrical furnace heated the reactor to the reaction temperature. Bronkhorst mass flow controllers (MFC, in the range of 0 to $1\,\mathrm{L\,min^{-1}}$) dosed the gas flow to the reactor and maintained the O_2 in Ar at 21 %. A spring-loaded back-pressure valve maintained a constant reactor pressure (0.1 MPa to 2 MPa). A type-K thermocouple monitored the temperature at the top of the catalyst bed (effluent side). The feed gas without preheating entered the quartz tube. The feed gas manifold included CH_4, 30 % O_2 in Ar and Ar. The feeding direction in this setup is flexible, so we either fed the gas from the top to the bottom or the opposite direction. We heated up the exit line to avoid water vapor cooling down and blocking the

line, and connected a quench preventing condensables from entering GC or MS. The first 4 way valve directed the feed gas to either the reactor or the second 4 way valve. The second valve directed the effluent gas to the vent or to the analytical instrument of MS or GC. Non-condensible gases are either analyzed online by MS or offline by GC. Before starting the experiment, we purge with argon as an inert gas until it reached the desired temperature.

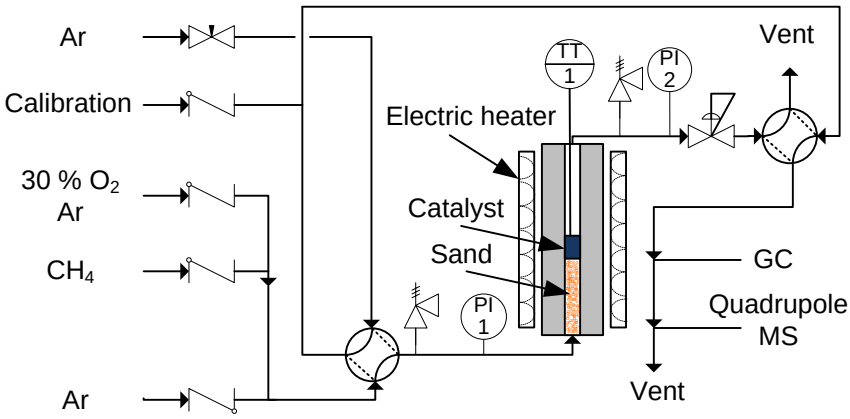

Figure 4.1 Typical setup.

4.4.2 Mass Spectroscopy (MS)

A quadrupole mass-spectrometer (Hiden HPR-20/QIC) monitored effluent gas concentration on-line at a frequency of 2 Hz. We corrected the CO signal by subtracting the contribution of CO_2. We calibrated the MS every one or two weeks with 4 calibration gas bottles containing the mixtures of Ar, CO, CO_2, CH_4 and H_2 (Table 4.1).

4.4.3 Gas Chromatograph (GC)

A gas chromatograph (Agilent 7890B) with two TCD detectors and one FID dector sampled the effluent gas every 7 min to measure the gas composition and verify the MS signal. The columns in the GC were a capillary POLT Q column (30 m × 0.53 mm × 40 µm) and a Molsieve column (30 m × 0.53 mm × 30 µm). The oven temperature was constant at 50 °C. We calibrated the residence time and concentration of each gas with 4 calibration gas bottles (Table 4.1) every one or two months.

4.4.4 Experimental procedure

To start the experiments, we used the setup shown in Figure 4.1, after calibrating all the MFCs. The catalyst bed consisted of 2–4 catalyst disks stacked on top of each other with a total bed height of 3–8 mm. We placed disks in the centre of the reactor without reduction pretreatment.

After injecting the Ar to check for leakages, we heated the reactor to the reaction temprature at a rate of 5 °C min^{-1} under Ar atmosphere. When the temperature reached the set point, we injected feed gases. We changed pressure, gas flow rate for each screening (usually 65 min) catalytic test. We repeated each test 2–3 times (except the long test of 255 min). We monitored the gas signal by MS online and by GC at a interval of 10 min. We fed 50–100 mL min^{-1} 30 % O_2 in Ar to remove the coke and regenerate the catalyst between tests.

4.4.5 Qualification of the products

The conversion of methane (X_{CH_4}) and selectivity towards CO (S_{CO}), H_2 (S_{H_2}), CO_2 (S_{CO_2}) and the coke based on the inlet CH_4 (S_{C}) were calculated as follows :

$$X_{\text{CH}_4}(\%) = \frac{q^{in}_{\text{CH}_4} - q^{out}_{\text{CH}_4}}{q^{in}_{CH4}} \times 100 \tag{4.1}$$

$$S_{\text{CO}}(\%) = \frac{q^{out}_{CO}}{q^{in}_{\text{CH}_4} - q^{out}_{\text{CH}_4}} \times 100 \tag{4.2}$$

$$S_{\text{H}_2}(\%) = \frac{q^{out}_{H2}}{(q^{in}_{\text{CH}_4} - q^{out}_{\text{CH}_4}) \times 2} \times 100 \tag{4.3}$$

$$S_{\text{CO}_2}(\%) = \frac{q^{out}_{CO2}}{q^{in}_{\text{CH}_4} - q^{out}_{\text{CH}_4}} \times 100 \tag{4.4}$$

$$S_{\text{C}}(\%) = \frac{q^{in}_{\text{CH}_4} - q^{out}_{\text{CH}_4} - q^{out}_{\text{CO}_2} - -q^{out}_{\text{CO}}}{q^{in}_{CH4}} \times 100 \tag{4.5}$$

Where : $q^{in}_{\text{CH}_4}$ and $q^{out}_{\text{CH}_4}$ are the molar flow rates of methane at the reactor entrance and exit, respectively ; q^{out}_{CO}, $q^{out}_{\text{H}_2}$ and $q^{out}_{\text{CO}_2}$ are the molar flow rates of CO, H_2 and CO_2 at the reactor exit.

CHAPTER 5 ARTICLE 1 - A MICRO-REFINERY TO REDUCE ASSOCIATED NATURAL GAS FLARING

Zhenni Ma, Cristian Trevisanut, Cristian Neagoe, Daria C. Boffito, Seyed Mahdi Jazayeri, Chand Jagpal, Gregory S. Patience

Published : Sustainable Cities and Society, 27, 2016, 116 - 121

5.1 Abstract

Gas flaring accelerates climate change with greenhouse gases but also harms the environment with other pollutants such as H_2S, carbon sulfides, NOx and metals. Methane is a valuable energy vector and converting the associated gas from thousands of wells to liquid fuels would reduce the environmental footprint of oil field operations. Micro Gas-to-Liquids technology (μGtL) reduces flared natural gas and emissions while producing valuable diesel. Integrating a high pressure syngas step with Fischer-Tropsch (FT) in a single vessel reduces investment and operating costs, which is now an insurmountable hurdle that face producers exploiting wells far from gas pipeline infrastructure. We have demonstrated that coupling these two technologies produces C_{7+} liquid. Furthermore, the high pressure POX reactor can convert 96% of the methane while producing a H_2/CO ratio of 2, which is ideal for FT, at 900°C. With a capacity of 100 $MCFd^{-1}$, one micro-refinery unit can reduce CO_2 emissions by 1.2 $ktyr^{-1}$.

5.2 Introduction

At high pressures, typical of most oil reservoirs, associated gas is dissolved in the crude oil. When the crude is pumped to the surface, the associated gas comes out of solution. This associated gas (also known as solution gas) consists of a mixture of methane (CH_4), ethane, propane, butane, and pentanes. It also contains a number of compounds including water vapor, hydrogen sulfide (H_2S), carbon dioxide (CO_2), helium, nitrogen, and volatile organic compounds. CH_4 has a greenhouse effect 20 times higher than CO_2 (Alberta Energy Regulator in 2013). Consequently, venting it from the well-head to the atmosphere is worse than flaring the gas with respect to the environmental impact. Safety concerns, financial barriers for alternative technologies, low domestic gas prices, lack of incentives or market make flaring the easiest and most economical way to deal with it. Further, high capital costs prohibit building gas gathering infrastructure or power conversion and transmission lines.

Figure 5.1 Global flaring (with permission http ://skytruth.org/mapping-global-flaring) on February 19, 2015. Picture points to black box indicates gas flaring in North Dakota's Bakken Shale is as bright as city lights of Minneapolis or Chicago (Wogan 2013)

The Global Gas Flaring Reduction (GGFR) estimates that 140 billion cubic meters (BCM) of gas were flared annually, which emits more than 300 million tons of CO_2 to the atmosphere. Flaring associated gas produces mainly H_2O and CO_2, but also carbon monoxide (CO) along with a variety of air pollutants, such as nitrogen oxides (NOx), sulfur dioxide (SO_2), toxic heavy metals and black carbon soot. The air pollution associated with flaring and venting natural gas puts the health of the local communities and people who work in the oil fields at risk [100, 101, 9]. Initiated by the World Bank's "Zero Routine Flaring by 2030", the Canadian and American governments in concert with major oil companies have committed to end routine gas flaring at oil production sites by 2030 [102]. It is also a tremendous waste of valuable energy resources : 140 billion cubic meters of flared gas is worth US$ 20 billion. In 2012, 24 % of the world total energy consumption comes from natural gas and a total of 4 % is flared. This gas could provide 750 billion kWh of electricity, which is sufficient for the annual consumption of Africa [102]. Moreover it could be a feedstock to produce value-added chemicals and fuels. Transforming the associated gas into added-value liquid products brings environmental and economic benefits [103, 104].

A mirco refinery unit (MRU) could economically convert undervalued natural gas to increase

revenues and decrease operating costs to support sustainable oil and gas production. Increased restrictions to venting or flaring (EPA/state/country legislation) will force companies to deal with this gas in order to produce oil. An MRU gives an opportunity to oil and gas operators to reduce GHG emissions while increasing profitability.

5.3 Gas-to-Liquid technologies

5.3.1 Fischer-Tropsch (FT) syncrudes

Gas-to-liquids (GtL) is a commercially successful industry to convert natural gas resources to high value transportation fuel and other petroleum products [105, 106, 107]. Feedstocks in GtL processes can be natural gas, or gas generated by gasification of biomass or coal. The synthesis gas (syngas) route can produce various liquid products, such as FT syncrudes (jet fuels, diesel, lubricates, waxes, etc.) or methanol oxygenates (methanol, acetic acid, dimethyl ether, etc.)[10]. FT synthesis is well-established technology that spans more than 60 years of research and development and has several world scale commercial facilities that operate [108, 109]. FT synthesis processes convert mixtures of H_2 and CO into aliphatic hydrocarbons, a multi-component mixture of linear and branched hydrocarbons and oxygenated products [110]. Its products resemble the composition of diesel fuel and have low aromaticity and sulfur content [111] :

1. Paraffins formation :

$$(2n+1)\mathrm{H_2} + n\mathrm{CO} \rightarrow C_nH_{2n+2} + n\mathrm{H_2O} \tag{5.1}$$

$$\Delta H_r = -167\,\mathrm{kJ\,mol^{-1}}$$

2. Olefins formation :

$$2n\mathrm{H_2} + n\mathrm{CO} \rightarrow C_nH_{2n} + n\mathrm{H_2O} \tag{5.2}$$

$$\Delta H_r = -146\,\mathrm{kJ\,mol^{-1}}$$

Main products are linear paraffins and α-olefins, namely : low molecular weight hydrocarbons (C_1-C_4), medium molecular weight hydrocarbons (C_4-C_{13}) and high molecular weight hydrocarbons (C_{13+})[112]. Low molecular weight hydrocarbons are a raw material for combustion fuels, polymers and fine chemicals. Medium molecular weight hydrocarbons resemble the composition of gasoline and are feedstock for lubricants and diesel fuels. High molecular

weight hydrocarbons are waxes or paraffins and are feedstocks for lubricants and are hydrocracked to diesel fuel. The reactors operate between 200°C to 350°C and from 10 bar to 60 bar [111].

5.3.2 Syngas production

The syngas (a mixture of CO and H_2) production is the key fundamental step to FT process. The bond dissociation energy of methane is very high at $439\,\mathrm{kJ\,mol^{-1}}$ [113]. Activating methane to react and produce syngas is challenging. Three conventional processes to produce syngas include :

1. Steam Methane Reforming (SMR) [105, 75]

In SMR, methane reacts with steam to produce hydrogen and carbon monoxide at a H_2/CO ratio of 3/1.

$$CH_4 + H_2O \rightarrow CO + 3H_2 \tag{5.3}$$

$$\Delta H_r = 206\,\mathrm{kJ\,mol^{-1}}$$

The process operates between 430°C to 1000°C at a steam partial pressure up to 30 bar. In the GtL industry, several companies, such as CompactGTL [114], Novargi and Carbon Sciences adopt the SMR process. It is a highly endothermic process, thus the large capital cost in heating system makes it uneconomical for small scale units.

2. Auto-thermal reforming (ATR) [105, 75]

In the ATR process, oxygen and steam (or carbon dioxide) react with methane to produce syngas. It combines homogeneous partial oxidation and steam reforming.

$$2CH_4 + \frac{1}{2}O_2 + H_2O \rightarrow 2CO + 5H_2 \tag{5.4}$$

$$2CH_4 + O_2 + CO_2 \rightarrow 3CO + 3H_2 + H_2O \tag{5.5}$$

The exothermic oxidation provides the energy to sustain the endothermic steam methane reforming reaction. Sasol, Velocys [115], and Toyo Engineering produce synthetic fuel by ATR as a first step. However, scaling down is not easily feasible.

3. Partial oxidation of methane (POX) [105, 75]

In POX reaction, methane reacts with a substoichometric amount of oxygen to hydrogen and carbon monoxide at a 2 :1 ratio.

$$CH_4 + \frac{1}{2}O_2 \rightarrow CO + 2H_2 \tag{5.6}$$

$$\Delta H_r = -36\,\mathrm{kJ\,mol^{-1}}$$

POX is mildly exothermic, which makes it convenient for industrial processes from an energy management perspective. The H_2/CO molar ratio of 2 is ideal for the FT reaction. The POX reaction rate is faster than SMR and requires shorter residence times [18]. As a consequence, the gas hourly space velocities are higher and the capital cost and production scale to achieve large capacity are lower [116]. Shell has commercialized the POX process and Gas-2 converts CH_4 to syngas in a porous membrane reactor with CPOX [117]. Typical POX reaction temperature is higher than 1400 °C. Catalytic partial oxidation of methane (CPOX) decreases the reaction temperature below 1000 °C. Improving catalyst stability and performance is one of the main challenges in developing CPOX catalysts [4].

5.4 Micro-refinery unit (MRU)

Converting associated gas (produced with oil) to FT fuel is economically feasible if capital costs can be kept below 100 $k\$bbl^{-1}d^{-1}$. This target is achievable for 1000 $bbld^{-1}$ mini gas-to-liquid plants but for the micro-scale (10 $bbld^{-1}$) it is ambitious. We designed a mobile and scalable Micro-refinery unit deployable at the well-head to eliminate greenhouse gas emissions, and process associated gas into high value liquid fuels ([107]).

Our MRU [29] converts waste associated gas to the desired H_2/CO ratio for FT synthesis, differently from the other syngas production technologies. Processes to convert methane involve multiple steps :

- gas cleaning to eliminate sulfur compounds and water and compressing to pressure of 20 bar ;
- conversion of methane to syngas through CPOX reaction ;
- transformation of syngas into liquids through the FT reaction ;
- FT products separation.

The complete unit consists in 3 main parts (Figure 5.2).

5.4.1 Pretreatment part

Sulfur is an inevitable impurity in associated natural gas, mainly presenting as hydrogen sulphide gas (H_2S). Environmental regulations strictly control the emission of corrosive and

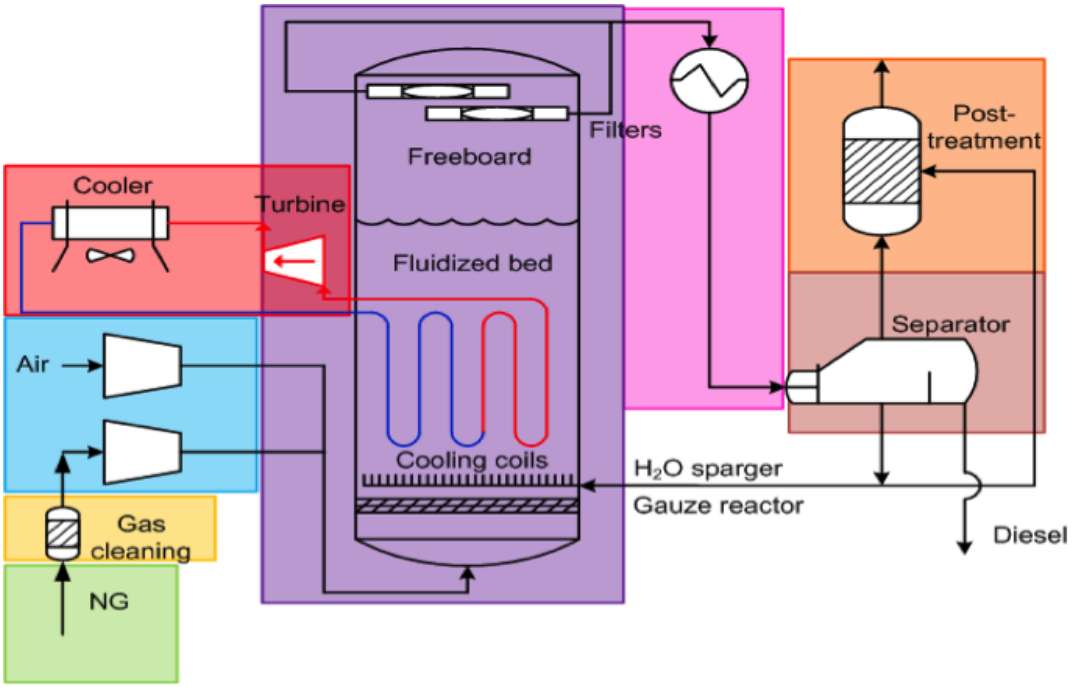

Figure 5.2 Scheme of the Micro-Refinery Unit.

toxic sulfide gas to the atmosphere. Also sulfur species poisons catalysts temporarily or permanently, largely decreasing their reactivity [118, 119]. Removal of sulfides to elemental sulfur for sale or safe disposal is necessary.

Emerging desulfurization technologies provide possibility for cleaning associated natural gas in remote oil fields include wet scrubbing, scavenger adsorption, selective oxidation, and biological oxidation [120].

The wet scrubbing process involves contacting the sulfur species with a liquid dimethylaniline or alkaline oxidative scrubbing solution, which can remove 99.9 % of the H_2S [121]. Wet scrubbing with an aqueous, nontoxic chelated iron solution can remove more than 99 % of the sulphides [120]. Scavenger adsorption is suitable for small scale units (as opposed to the Claus process) and can capture sulfur below $100\,\mathrm{kg\,d^{-1}}$ [122]. The H_2S forms pyrite with an iron based catalyst in a fixed bed. Maintenance costs may be prohibitive since the catalysts cannot be regenerated. In the selective oxidation process [120], oxygen reacts with sulfur compounds to for oxides. It can process about 97 % of the H_2S to elemental sulfur, but the capital costs are prohibitive for small scale plants [123]. A biofilter packed with oxidation bacteria removes 99 % of H_2S up to 1000 ppm. Both small and large scale trials demonstrated its feasibly [120].

The pretreatment part of an industrial MRU can recover, clean and compress associated

natural gas from petroleum fluids (along with water and impurities), which then returns to the pipeline. Besides a desulfurization unit, a separator contains a high efficiency mist eliminator to remove carry-over of water vapor aerosols, and a gas treatment column removes acids and other impurities. Compressors increase the pressure of both the natural gas and air lines to the reaction pressure of 20 bar.

5.4.2 Reaction zone

The reactor consists of a single vessel with two reactive stages : the CPOX reaction is the first stage and the FT reaction is the second stage [29]. This design decreases the reactor size and thus capital cost fit the unit in a mobile trailer that can be transported readily to oilfields.

In the reactor of a commercial MRU, the high pressure lines are heated and combined in the first stage where oxygen partially oxidizes the methane to syngas at temperature of 900 °C. The syngas then is partially cooled and enters the second stage, where FT catalyst reacts the CO and H_2 in the gas phase. The FT reaction is highly exothermic. Cooling coils control the reaction temperature of FT at between 250 °C to 350 °C. A steam turbine [86, 124, 125] produces extra power from steam generated in the cooling coils in the fluidized bed reactor and in the waste heat boilers. Waste heat boilers also generate steam to feed the boiler and heat exchangers remove heat. The hot gas exiting the waste heat boiler goes to a gas expander to produce power for the gas compressors. Therefore, electricity produced from the heat generated is an output of the process.

5.4.3 Post-treatment part

The gases exiting the reactor pass through a waste-heat boiler and a condenser. The product stream consists of three phases :

• the gas phase goes to a post treatment reactor to combust CO and the light hydrocarbons ;

• the dense aqueous phase circulates to either the reaction zone or to the post treatment reactor to control the temperature rise ;

• the organic phase goes to the pipeline or a storage tank, or to a separation unit to produce drop in fuels.

High pressure favors the FT reaction. The challenge is to combine the CPOX reaction (which operates best at atmospheric pressure) with FT at 20 bar. We are the first to report operating the high pressure CPOX reaction at the laboratory scale over a FeCralloy catalyst and

produced syngas suitable for FT (H_2/CO ratio of 2).

5.5 Methdology

5.5.1 Catalysts

• CPOX catalysts

Ni and Co catalysts deactivate at higher temperature than noble catalysts and form compounds with the alumina support. Carbon deposition and coking are other issues [126]. Claridge et al [5] reported the relative rate of coke formation on transition metals is : Ni > Pd > Rh > Ru > Pt, Ir. Therefore, we employ precious metal Pt as CPOX catalyst. We tested a Pt-based powder catalyst. The powder was a commercial 1 % Pt/Al_2O_3 catalyst (325 mesh from Sigma Aldrich).

• FT catalysts

Iron and cobalt are the two common active phases for FT catalysts. The catalyst composition we employ is a $Fe_{30\%}K_{2\%}Cu_{4\%}$ supported on Al_2O_3 (Sigma Aldrich), similar to one reported by Pirola (Pirola, Bianchi et al. 2010). After evacuating the support, we impregnated it with an aqueous solution of $Fe(NO_3)_3{\cdot}9H_2O$ (Riedel de Haen), KNO_3 (Merk) and $Cu(NO_3)_2{\cdot}xH_2O$ (Fluka). The solvent evaporated and the powder dried in a furnace, then it calcined at 500 °C for 4 h in static air.

5.5.2 Reactors

CPOX+FT Dual stage reactor

The system consisted of two tubular reactors, one on the top of the other : the stream exiting the CPOX reactor was the feed stream of the FT reactor. We fed 150 mL min^{-1} of CH_4 and 223 mL min^{-1} of 30 % O_2 in Ar to the reactor. The CPOX catalytic system was a fixed bed of 4 g of 1 % Pt/ Al_2O_3. We added a mass fraction of 50 % of Al_2O_3 as a diluent. The reactor operated at 900 °C and 20 bar. The FT catalyst was a fixed bed of 10 g of Fe/Cu/K supported on Al_2O_3, diluted with a mass fraction of 50 % of Al_2O_3. The average temperature was 240 °C.

CPOX

We tested 2 CPOX systems : fluidized bed and fixed bed. The operating conditions were 850 °C, 900 °C and 950 °C. The O_2/CH_4 ratio ranged from 0.45 to 0.55. The flow rate of the

gas exiting the reactor (Q) was 2 mmol min^{-1} at atmospheric pressure. The catalyst was the 1 % Pt/Al_2O_3 powder.

5.6 Results and discussion

5.6.1 Dual stage process

In these preliminary experiments, CH_4 conversion reached 52 %. The main product exiting the dual stage reactor was CO (34 % of CH_4) coming from the CPOX reaction. We collected 90 ml of liquid product after 70 hours. The organic phase weighted 0.5 g. The composition was 77 % C_{21+} and 23 % C_7-C_{20}. Coming CPOX and FT reactions in one single reactor proves feasible to convert methane to liquid oil products. It is fundamental and essential step to build a micro refinery unit for utilizing the waste flared gas in oil fields

5.6.2 Catalytic partial oxidation

We analyzed the effect of temperature on methane conversion and CO and H_2 yields (Figure 5.3). We measured CH_4 conversion and CO and H_2 yields at 850 °C, 900 °C and 950 °C : The maximum CH_4 conversion was 80 % and the maximum yield of CO and H_2 were 70 % and 65 %, respectively.

Increasing the O_2/CH_4 ratio increases methane conversion and CO and H_2 yield (Figure 5.4). With an O_2/CH_4 feed ratio of 0.55, CH_4 conversion and CO and H_2 yields reach 96 %, 88 % and 87 % respectively. The ratio of H_2/CO was close to 2 at 900 °C, suitable for further FT reaction.

At 20 bar and 850 °C, the maximum CH_4 conversion was 40 %, with a maximum CO and H_2 selectivity of 91The H_2/CO proportion was between 0.4-0.6 for the different CH_4/O_2 ratio (Figure 5.5).

5.6.3 Greenhouse gases reduction

Each MRU treats a minimum of 100 million cubic feet (MCF) everyday, which served as a basis to calculate greenhouse gas (GHG) emissions from flaring gas. We considered the average composition of associated gas in Alberta, Canada [8] and the stoichiometric amount of CO_2 from flaring (Table 5.1). The source of CO_2 emissions is crude oil that flares and/or vents associated gas.

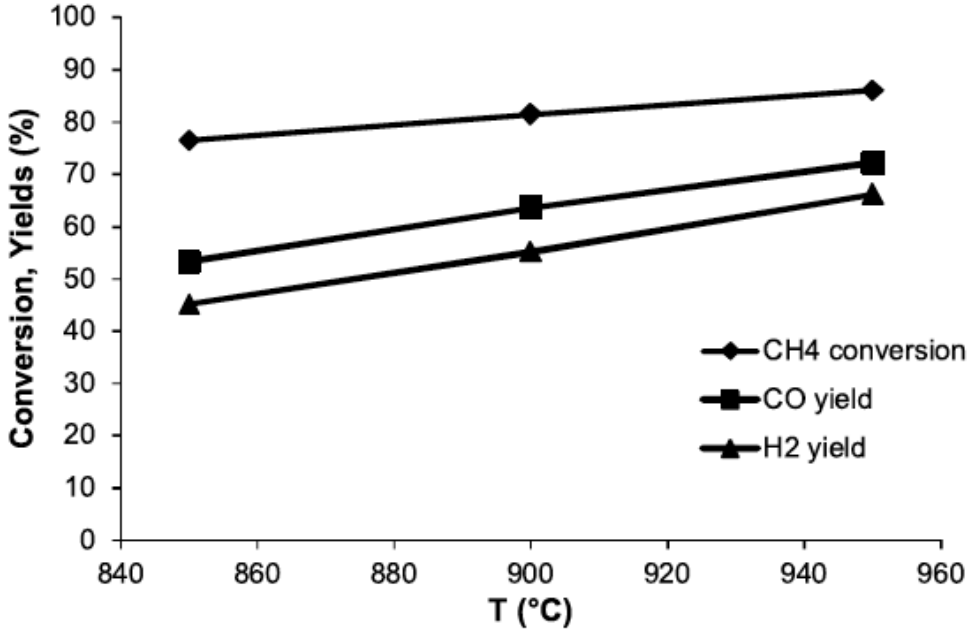

Figure 5.3 CH_4 conversion and CO and H_2 yields at different temperatures, fluidized bed, $O_2/CH_4 = 0.45$.

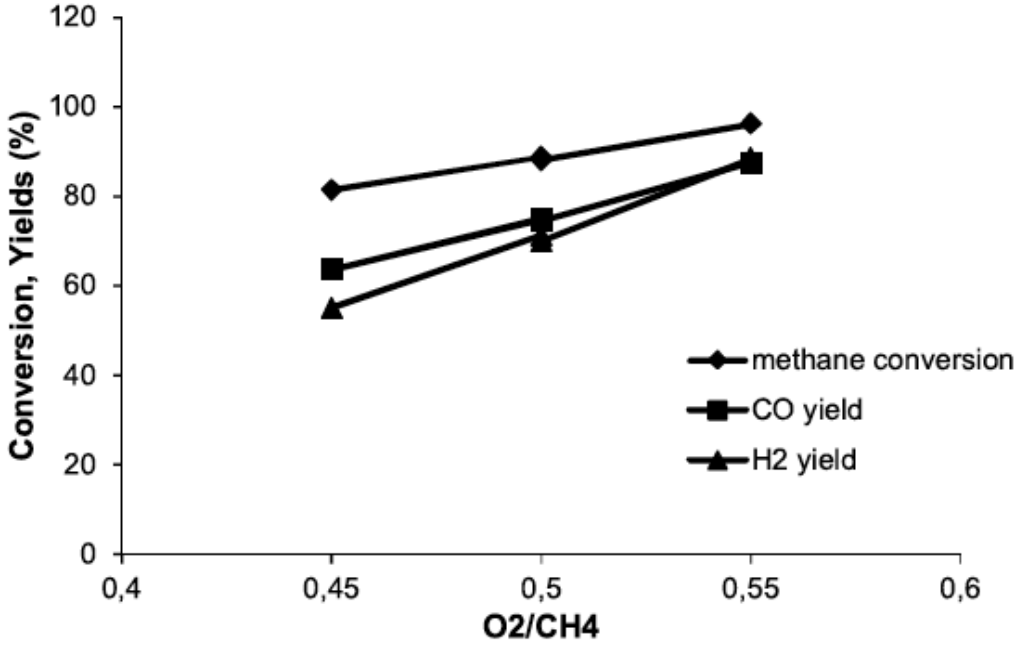

Figure 5.4 CH_4 conversion and CO and H_2 yields at different temperature, fluidized bed, T = 900 °C.

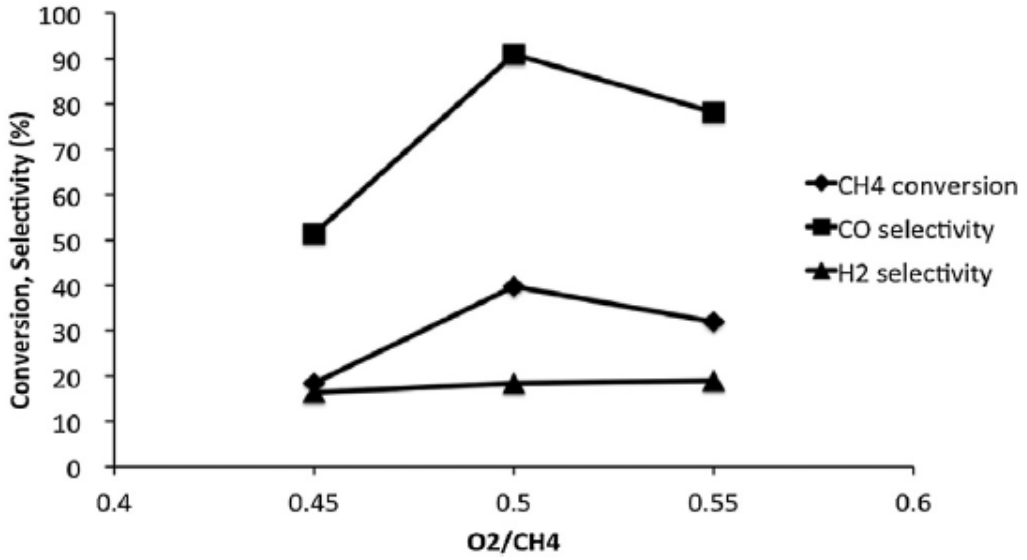

Figure 5.5 Conversion and selectivity at different O_2/CH_4. Fixed bed ; T = 850 °C ; P = 20 bar.

The CO_2 emission from complete combustion of 100 MCF is :

$$GHG = \frac{PF}{RT} \sum_i x_i \cdot N_{iCO_2} = 2.5 ktyr_{-1} CO_2 \tag{5.7}$$

Where

P = atmospheric pressure (101 kPa) ;

F = flow of treated associated gas ($2830\,m^3\,d^{-1}$ = 100 MCF d^{-1}) ;

T = ambient temperature (298 K) ;

x_i = molar fraction of component i in the associated gas.

N_{iCO_2} = number of moles from complete combustion of component i.

Considering 95 % of CH_4 conversion in the first CPOX step and 50 % yield of the diesel-like cut by FT (with respect to CH_4), the CO_2 emissions reduction is :

$$(1 - 0.475) \times 2.5 ktyr_{-1} CO_2 = 1.2 ktyr_{-1} CO_2 \tag{5.8}$$

The gas emission reduction target is 1.2 $ktyr^{-1}$ CO_2 for a single MRU. By deploying 10 MRU per month in 2020, the potential to reduce emissions are tremendous (Table 5.2).

The composition and the gas capacity vary from one well to another. The most important

Table 5.1 Average composition of associated gas in Alberta, Canada and stoichiometry of the flaring

Component	Composition	O_2, mol	CO_2 produced, mol
N_2	0.62	-	-
CO_2	5.24	-	1
CH_4	73.25	2	1
C_2H_6	11.97	3.5	2
C_3H_8	5.32	5	3
i-C_4H_{10}	0.88	6.5	4
n-C_4H_{10}	1.70	6.5	4
i-C_5H_{12}	0.36	8	5
n-C_5H_{12}	0.38	8	5
C_6H_{14}	0.24	9.5	6
C_7H_{16}	0.04	11	7

Table 5.2 Yearly CO_2 reduction vs. number of MRUs operating in the field.

Year	2017	2018	2019	2020	2021
Number of MRUs	1	10	40	160	280
kt yr^{-1} CO_2 Reduction	1.2	12	48	192	336
GHG emissions sink %, flared gas	0.1 %	0.86 %	3 %	14 %	44 %
GHG emissions sink %, vented gas	0.1 %	1.20 %	5 %	19 %	34 %

parameter for the greenhouse gas emissions is the volume of treated gas. Our baseline to calculate the CO_2 reduction is the industrial average of associated gas annually flared and vented in Alberta, Canada. The baseline is 1400 $ktyr^{-1}$ CO_2 and 1000 $ktyr^{-1}$ CO_2 for flared and vented gas, respectively. We estimate that the widespread adoption of MRU will generate a reduction of CO_2 emissions that increases gradually from 0.1 % to 44 % when treating flared gas and to 34 % when treating vented gas in the first 5 years.

5.6.4 Challenges

This work demonstrates the feasibility of reducing greenhouse gas emissions using a micro-refinery unit that converts waste flared gas into value added FT fuels. The first step in the process – methane partial oxidation – represents the major obstacle to implement the technology. We showed that Pt catalysts supported on FeCralloy knitted metal fibers convert methane at high conversion to H_2 and CO at ratio suitable for the FT synthesis step (Neagoe, Boffito et al. 2015, Ma, Ouzilleau et al. 2016). The challenges that remain include : coke build-up on the syngas catalyst, fully integrating the two reactions, heat integration, power regeneration, and remote control.

5.7 Conclusions

Flaring associated natural gas increases greenhouse gas emissions that impacts the global environment and wastes valuable natural resources. Flared natural gas, bio-gas, and coalbed methane are low volume, low value hydrocarbons that could be transformed to high value FT fuels. The World Bank is exhorting governments and industry to end routine gas flaring by 2030. Gas-to-Liquid processes are promising technologies to treat flared gas but both elevated operating and capital costs frustrate broad application to both large and small scale units. A micro refinery that combines both steps – partial oxidation of methane and FT synthesis – addresses both operational and investment costs. Here we demonstrated that we could react methane at high conversion and selectivity to feed directly to a FT unit. Every MRU will process 100 MCF of natural gas flared or vented. This corresponds to a CO_2 sink of 1.2 $ktyr^{-1}$ per unit. We expect to reach the full production capacity of 10 MRU per month in 2020, reducing 336 $ktyr^{-1}$ CO_2. By then the total greenhouse gas emissions reduction will equal 44 % for flared natural gas and 34 % for vented natural gas in Alberta, respectively. Challenges going forward with the technology include catalyst life, safety, operating multiple remote units, heat integration and power generation.

5.8 Acknowledgements

The authors gratefully acknowledge the financial support of the Natural Sciences and Engineering Research Council of Canada and equipment grants from the Canadian Foundation for Innovation. Dr. Boffito acknowledges financial support from the NSERC Banting Postdoctoral Fellowship.

CHAPTER 6 ARTICLE 2 - PARTIAL OXIDATION OF METHANE TO SYNGAS OVER PT/RH/MGO CATALYST SUPPORTED ON FECRALLOY WOVEN FIBRE

Zhenni Ma, Philippe Ouzilleau, Cristian Trevisanut, Cristian Neagoe, Samira Lotfi, Daria C. Boffito and Gregory S. Patience

Published : Canadian Journal of Chemical Engineering, 96, 2016, 642–649

6.1 Abstract

Integrating a high pressure syngas step with Fischer-Tropsch (FT) in a single vessel reduces investment and operating costs to synthesize GtL liquids. Methane catalytic partial oxidation (CPOX) to produce syngas for FT is an economic opportunity for micro-refineries. Many metals and metal oxides selectively convert natural gas to CO and H_2 but they also form coke, which must be removed intermittently otherwise it deactivates the catalyst and can foul the reactor and process lines. Here, we prepared a mass fraction of 1 % Pt/Rh (Pt/Rh = 9) catalyst supported on MgO over FeCralloy woven fibre via Solution Combustion Synthesis. At 900 °C, from 0.1 MPa to 2 MPa and with a 2 :1 feed composition of CH_4 to O_2, we consumed all the oxygen and obtained a H_2/CO ratio of 2 (ideal for FT). The catalyst at low pressure and a 0.1 s residence time converted 90 % of the methane at 90 % CO selectivity. At 2 MPa, we obtained a CO yield of 50 % (<88 % conversion and 57 % selectivity). Thermodynamics predict that less than 5 % coke forms below 900 °C. At high pressure and short residence time (0.1 s), the coke yield (presumed to be coke crystallites) was 24 %. Increasing the residence time to 0.3 s reduced the amount of coke by 33 % because it is metastable.

6.2 Introduction

EIA (U.S. Energy Information Administration) projects a 56 % increase in the world's energy consumption by 2040, with fossil fuels accounting for nearly 80 % of it [104]. In North America, natural gas, including tight gas, shale gas and coal bed methane, is the fastest-growing carbon source. It competes with coal as the world's second largest energy source (Figure 6.1). The world relies on liquid fuels as the predominant energy vector, but environmental, geopolitcal and macroeconomic events greatly affect their price [103]. This motivated many nations to develop alternative solutions to produce liquid fuels [57, 25, 127], such as gas-to-liquids GtL products [103]. Natural gas is as abundant as oil and coal but most of it is trapped in hydrates

underneath the ocean or in remote regions of the world.

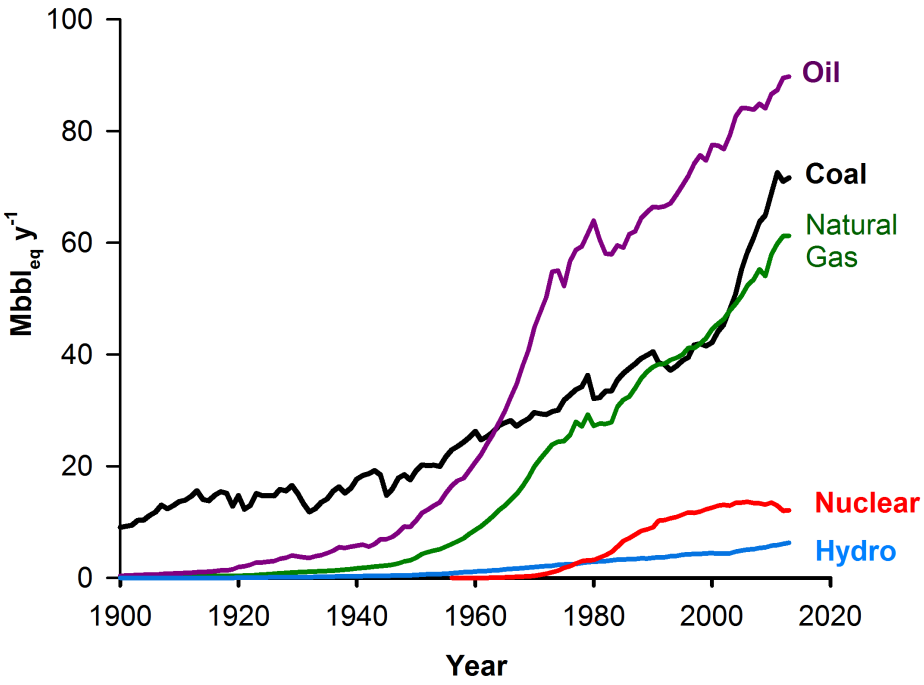

Figure 6.1 Until 1960, coal was the leading energy source in the world. Natural gas rivals coal, while nuclear and hydroelectric energy represent less than 10 % of the total. In 2013, renewable energy contributed 1.5 % of the total energy supply.

Associated natural gas that is dissolved in petroleum is often flared or, worse, vented. Instead of wasting this resource, converting it to a liquid fuel not only reduces its negative environmental impact [9], but also generates an additional revenue stream. The first step to diesel (FT fuels) is to partially oxidize methane to syngas with air (POX), steam (steam methane reforming, SMR) or a combination of the two (auto thermal reforming, ATR). POX reaction temperature runs as high as 1500 °C, but metals and metal oxides catalyze the reation below 1000 °C [4]. The reaction is mildly exothermic ($\Delta H^o_{298} = -36\,\mathrm{kJ\,mol^{-1}}$) and the product H_2/CO ratio is close to 2, which is optimum for FT liquid fuels [111]. This process requires a relatively pure hydrocarbon stream : sulphur compounds and metals must be removed upstream of the syngas reactor. Therefore, besides reducing anthropogenic CO_2 and CH_4 emissions, the process eliminates toxic pollutants.

The choice of catalyst is a crucial component of the CPOX reaction. Structured catalysts like gauze and woven fibres combine mechanical elasticity and resistance to thermal stress at

extremely high space velocities ($12\,000\,000\,h^{-1}$) [25, 52]. Catalysts are mainly noble metals, such as Pt, Pd, Rh and Ir, because of their high reactivity [34]. Another advantage of a structured catalyst is that the final design of the reactor allows greater throughput. Reactors are compact and easy to handle for conducting experimental studies and are readily designed for an industrial scale [4, 34].

Following the initial discovery of Schmidt and Hickman [25, 22], researchers have studied various metallic gauze catalysts. Methane conversion and CO selectivity are low on Pt gauze operating between 200 °C to 900 °C [4]. Adding Rh to the Pt (Pt/Rh = 9) increased the conversion to 30 % [26]. Surface oxides of Pd, Pt and Pt-Ir form and degrade catalytic activity more than Pt/Rh [4, 26, 27, 28, 29]. CO selectivity was 95 % at 1000 °C and 0.1 MPa in a 15 mm quartz reactor operating with a CH_4/O_2 ratio of 2 [27].

Pd/ZrO_2 supported on cordierite and FeCralloy partially combusts low concentrations of methane in air while maintaining the temperature below 1000 °C at 1.6 MPa [128]. Pd and Ni metals on stainless steel gauzes and FeCralloy woven metal fibres convert almost 100 % of the methane at 90 % CO selectivity with little coke (0.1 %) [30, 31].

Washcoating is the most common method to deposit metals and binders onto structured supports. Other methods also includes eletrochemical deposition [129, 130, 131, 132] and in situ spray pyrolysis [133, 134], etc. Solution Combustion Synthesis (SCS) is a quick process to prepare powders but can be adapted to coat nanocrystalline metal oxides, such as Al_2O_3, and zero-valent metal onto monoliths, honeycombs and gauzes. Prepared by SCS, Ru/Al_2O_3 loaded on monolith catalyst for oxy-steam reforming of methane [58], and palladium on zirconiastabilised lanthanum manganese oxide perovskite on FeCralloy gauzes for natural gas combustion [50] are quite active.

Coke deactivates catalyst but also promotes methane combustion to CO_2 rather than CO. MgO supports resist carbon formation on Ni and Pt based catalysts [4, 135, 136, 137, 5]. Rather than encapsulating active sites, the carbon on MgO is amorphous and in the form of non-deactivating whiskers due to the formation of ductile cast iron [138].

In this paper, we prepared a new structured catalyst by depositing Pt/Rh/MgO on FeCralloy woven fibres by SCS, and evaluated the catalyst's performance in a CPOX reaction. We also discuss coke formation with respect to equilibrium thermodynamics. We focused on the impact of pressure : conditions ranged from atmospheric pressure to the high required pressures of a Fischer-Tropsch reaction (typically 2 MPa).

6.3 Experimental

6.3.1 Catalyst preparation

The support was a FeCralloy woven fibre, with a mass fraction of 20 % chromium, 5 % aluminum, yttrium > 0.1 %, 0.3 % silicon, 0.08 % manganese, 0.03 % copper, 0.03 % carbon and the balance is iron. We cut the woven fibres 10 mm×10 mm squares. They were then washed in a water/acetone solution (1 :1) in an ultrasonic bath for 30 min. A muffle furnace (a Neytech model 3-550, Vulcan Multi-stage programmable furnace) dried the samples at 120 °C for 1 h.

We deposited MgO by dipping the 1.8 g FeCralloy squares in a 10 mL aqueous solution containing magnesium nitrate ($Mg(NO_3)_2{\cdot}6H_2O$, Sigma Aldrich) as a precursor and urea ($CO(NH_2)_2$, Sigma Aldrich) as the organic fuel. We calculated the masses of the reagents according to Vita et al. [58]. The stoichiometric ratio between oxidizing (O : total valences of oxidizers, i.e. nitrates) and reducing species (F : total valences of fuel, i.e. urea) was 1. The concentration of the solutions were 1.7 mol L^{-1} and 3.6 mol L^{-1} for $Mg(NO_3)_2{\cdot}6H_2O$ and $CO(NH_2)_2$ respectively. We placed the solution in the furnace at 600 °C for 2 min. This procedure was repeated 3 times to reach a mass fraction of 36.3 % of MgO on the bare woven fibres. To test the mechanical stability, we put MgO coated fecralloy fibre in a 40 % intensity ultrasonic bath for 30 min. The mass was constant after 1 h drying at 120 °C.

Before depositing the active components (Pt and Rh), the samples calcined at 1000 °C for 3 h at a heating and cooling rate of 5 °C min^{-1}. To minimize the catalyst cost, we must minimize the mass of the precious metals while simultaneously maximizing the activity. An autothermal methane catalytic partial oxidation reaction was rather insensitive to noble metal loading from 0.05 % to 10 % [139]. A middle loading of 5 % is common for the initial study [7]. We compare the catalyst activity of a pure Pt/Rh (Pt/Rh=9) metal gauzes, with 1 % Pt and Rh which is a much lower metal loading for starting. We deposited Pt and Rh with the same procedure adopted for MgO. We repeated the dipping 3 times with 2 mL aqueous solution containing tetraammineplatinum(II) nitrate ($Pt(NH_3)_4(NO_3)_2$, Sigma Aldrich), Rhodium(III) chloride ($RhCl_3$, Sigma Aldrich) and urea at a concentration of 0.057 mol L^{-1}, 0.012 mol L^{-1} and 0.125 mol L^{-1} respectively. The final mass fraction of Pt and Rh was 1 % with a Pt/Rh weight ratio of 9 :1. Finally, the catalyst calcined at 1000 °C in static air for 4 h with a heating and cooling rate of 5 °C min^{-1}. To confirm that the total mass fraction of Pt and Rh on the catalyst was 1 %, we weighed the catalyst before and after deposition and analyzed the catalyst by EDS. We inspected the morphological change of the FeCralloy during the preparation steps with a 44302-B Deluxe Handheld digital Microscope(Figure 6.2).

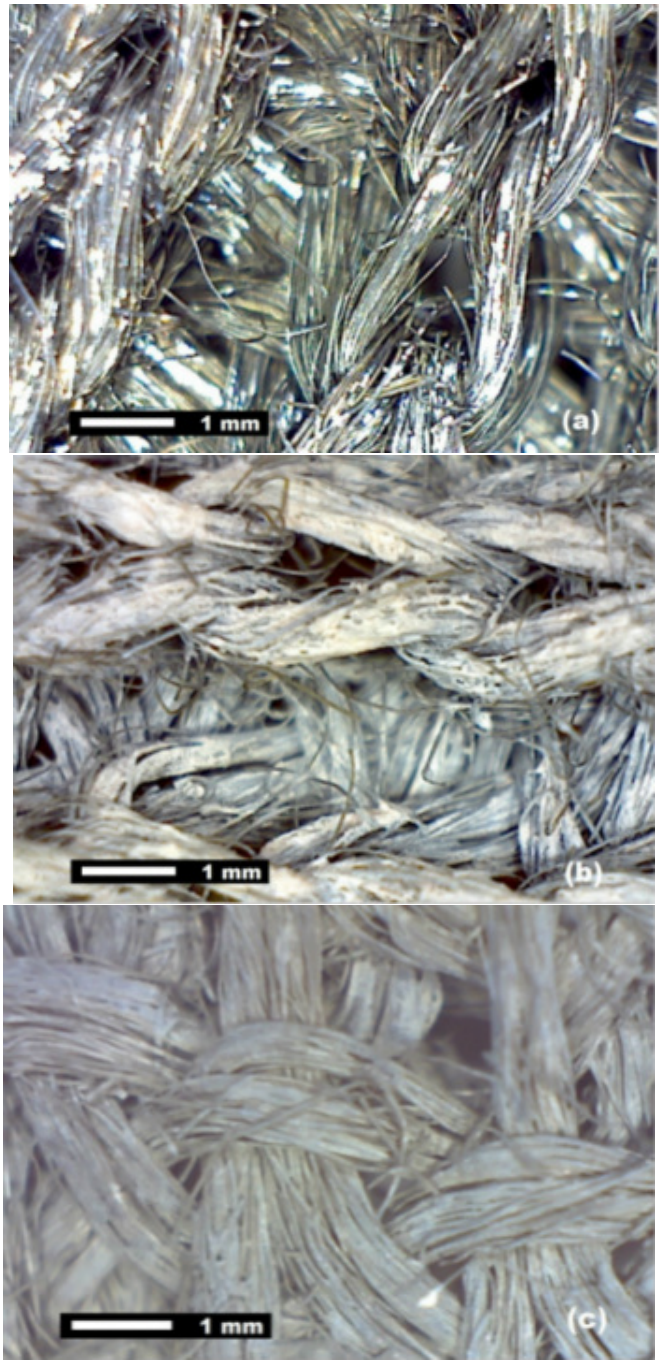

Figure 6.2 (a) uncoated FeCralloy woven fibre ; (b) coated MgO over FeCralloy ; (c) 1 % Pt/Rh on MgO over FeCralloy

6.3.2 Catalyst characterization

A Philips X-Pert MPD diffractometer equipped with a Cu Kα radiation at 50 kv and 40 mA measured the diffraction of the crystalline phases of the 1 % Pt/Rh on MgO over FeCralloy

catalyst. The scanning rate was $0.02\,^{\circ}\,s^{-1}$ with 2θ varying from 20° to 90°. We attributed the peaks according to the PCPFWIN database and calculated the crystallite size of MgO and Pt with the Scherrer equation (particle shape factor = 0.9). We performed scanning electron microscopy (JSM-7600A) with an EDS (Energy Dispersive Spectroscopy) detector to assess the surface composition [99].

6.3.3 Experimental setup

The reactor for methane partial oxidation was a 60 cm long quartz reactor with an ID of 8 mm (Figure 6.3). We cut three circular disks of the fecralloy woven metal so that they fit snugly inside the reactor. The total weight of the three disks was 0.27 g and we placed them in the centre of the reactor without reduction pretreatment [140]. An electrical furnace heated the reactor to 900 °C. A thermocouple within the catalyst monitored the temperature. A back pressure regulator maintained a constant reactor pressure. The gases entered from the bottom of the reactor. An Agilent gas-chromatograph 7890 B measured the gas composition following the ASTM D1945 standard. A mass-spectrometer (Hiden, HPR-20/QIC) monitored the gas phase composition on-line at the exit of the reactor for the duration of the experiments.

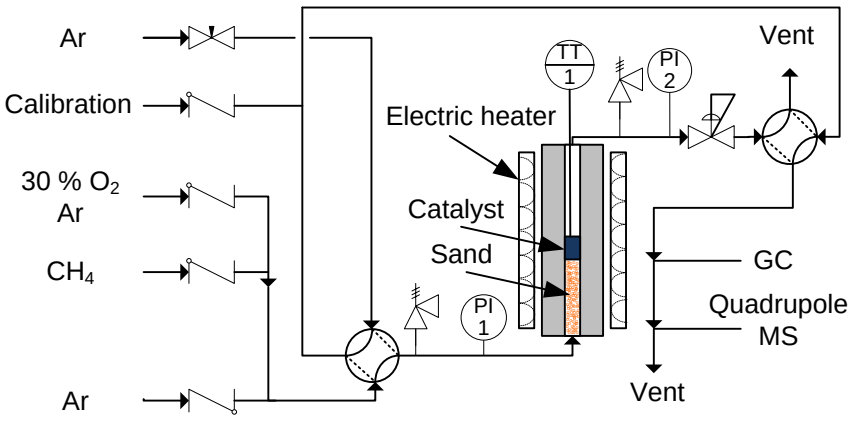

Figure 6.3 The reactor was an 8 mm ID quartz tube filled to 300 mm with sand to preheat and distribute the gases to the catalyst. Four mass flow controllers (MKS) metered the gases to the reactor and the analytical instruments to calibrate the feed composition as well as the MS.

The conversion of methane (X_{CH_4}) and selectivity towards CO (S_{CO}), H_2 (S_{H_2}), CO_2 (S_{CO_2}) and the coke based on the inlet CH_4 (S_C) were calculated as follows :

$$X_{\mathrm{CH_4}}(\%) = \frac{q^{in}_{\mathrm{CH_4}} - q^{out}_{\mathrm{CH_4}}}{q^{in}_{CH4}} \times 100 \tag{6.1}$$

$$S_{\mathrm{CO}}(\%) = \frac{q^{out}_{CO}}{q^{in}_{\mathrm{CH_4}} - q^{out}_{\mathrm{CH_4}}} \times 100 \tag{6.2}$$

$$S_{\mathrm{H_2}}(\%) = \frac{q^{out}_{H2}}{(q^{in}_{\mathrm{CH_4}} - q^{out}_{\mathrm{CH_4}}) \times 2} \times 100 \tag{6.3}$$

$$S_{\mathrm{CO_2}}(\%) = \frac{q^{out}_{CO2}}{q^{in}_{\mathrm{CH_4}} - q^{out}_{\mathrm{CH_4}}} \times 100 \tag{6.4}$$

$$S_{\mathrm{C}}(\%) = \frac{q^{in}_{\mathrm{CH_4}} - q^{out}_{\mathrm{CH_4}} - q^{out}_{\mathrm{CO_2}} - -q^{out}_{\mathrm{CO}}}{q^{in}_{CH4}} \times 100 \tag{6.5}$$

Where : $q^{in}_{\mathrm{CH_4}}$ and $q^{out}_{\mathrm{CH_4}}$ are the molar flow rates of methane at the reactor entrance and exit, respectively ; q^{out}_{CO}, $q^{out}_{\mathrm{H_2}}$ and $q^{out}_{\mathrm{CO_2}}$ are the molar flow rates of CO, H_2 and CO_2 at the reactor exit.

We changed pressure, residence time for each 60 min catalytic test. We fed O_2/Ar (O_2 % = 30 %) to remove the coke and regenerate the catalyst between tests.

6.4 Results and discussion

6.4.1 Catalyst characterization

The XRD analysis of the 1 % Pt/Rh over MgO/FeCralloy detected the phases of Pt (JCPDS no. 04-0802), MgO (JCPDS no. 45-0946) and FeCr (JCPDS no. 34-0396) (Figure 6.4). It did not detect any diffraction peak attributable to Rh, due to its low concentration. The sharp Pt peaks at 2θ equal to 40.0°, 46.5° and 67.7° correspond to large crystallites on the MgO surface. We calculated the particle size of the main crystallites with the Scherrer equation, which was 54 nm and 47 nm for Pt and MgO, respectively.

The SCS deposited a uniform MgO layer on the bare FeCralloy woven fibres (Figure 6.2). The SEM analysis also detected a thick homogeneous layer of MgO. (Figure 6.5 (a). The MgO on the FeCralloy surface sintered to give a thicker and more uniform layer after 40 h of operation (Figure 6.5 (b)). This indicates that MgO effectively covered the bare FeCralloy, and thereby decrease any coking that would be due to Fe.

On the catalyst surface (Figure 6.6 (a)), we confirmed the deposition of Mg, O, Pt and Rh on the catalyst surface by EDS analysis (Figure 6.6 (b)-(d)). The dispersion of Pt and Rh are

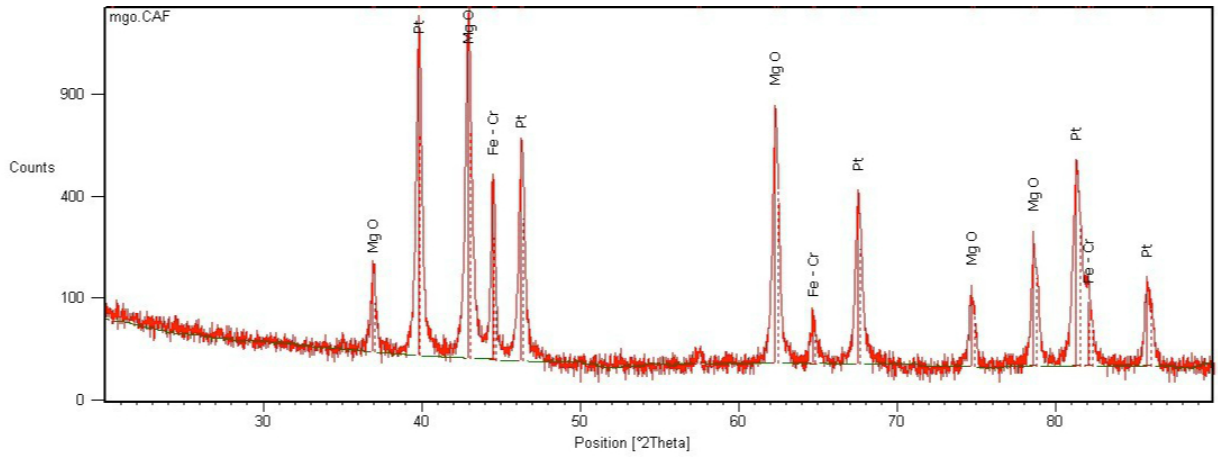

Figure 6.4 XRD pattern of 1 % Pt/Rh on MgO/FeCralloy woven metal fibre catalyst

uniform on the catalyst surface. We did not detect Fe on the surface (Figure 6.7). Comparing with the sum of Mg and O (95.4 % in EDS), the total mass fraction of Pt and Rh is close to 1 % (2.5 % in EDS). We did not find obvious coke on the surface of used catalyst. The regeneration with O_2/Ar is effective to remove the coke, and also maintain the catalytic activity of the catalyst.

6.4.2 Catalytic tests

We tested the catalyst activity under CPOX conditions (Table 6.1). In the first tests we kept the feed flow rate constant at a weight hourly space velocity (WHSV) equal to 15 $g_{CH_4} g_{cat}^{-1} h^{-1}$ at elevated pressure (Figure 6.8 (a) to (d)). At atmospheric pressure the methane conversion decreased to 45 % and stabilized after 30 min (Figure 6.8 (a)). Methane conversion increased to 80 % when the pressure increased to 2 MPa. At 0.1 MPa, the selectivity of CO rapidly increased in the first 30 min to 45 % (Figure 6.8 (b)).

The CO selectivity improved as the pressure increased and reached a maximum at 0.5 MPa (above 55 %). H_2 selectivity followed the same trend (Figure 6.8 (c)). The CPOX reaction at 2 MPa gave the highest H_2 selectivity (60 % after 30 min) among all the tested pressures. The CO_2 selectivity is lower at elevated pressures (Figure 6.8 (d)). It decreased from around 40 % to 23 % when going from atmospheric pressure to 2 MPa. Based on the carbon mass balance, higher pressure produces more coke. More importantly, the average H_2/CO ratio at 2 MPa is 2 (1.9 at 0.5 MPa and 1 MPa, 1.7 at 0.1 MPa), which is ideal for the Fischer-Tropsch reaction.

The gas residence time across the FeCralloy was 0.015 s at a WHSV of 15 $g_{CH_4} g_{cat}^{-1} h^{-1}$ at

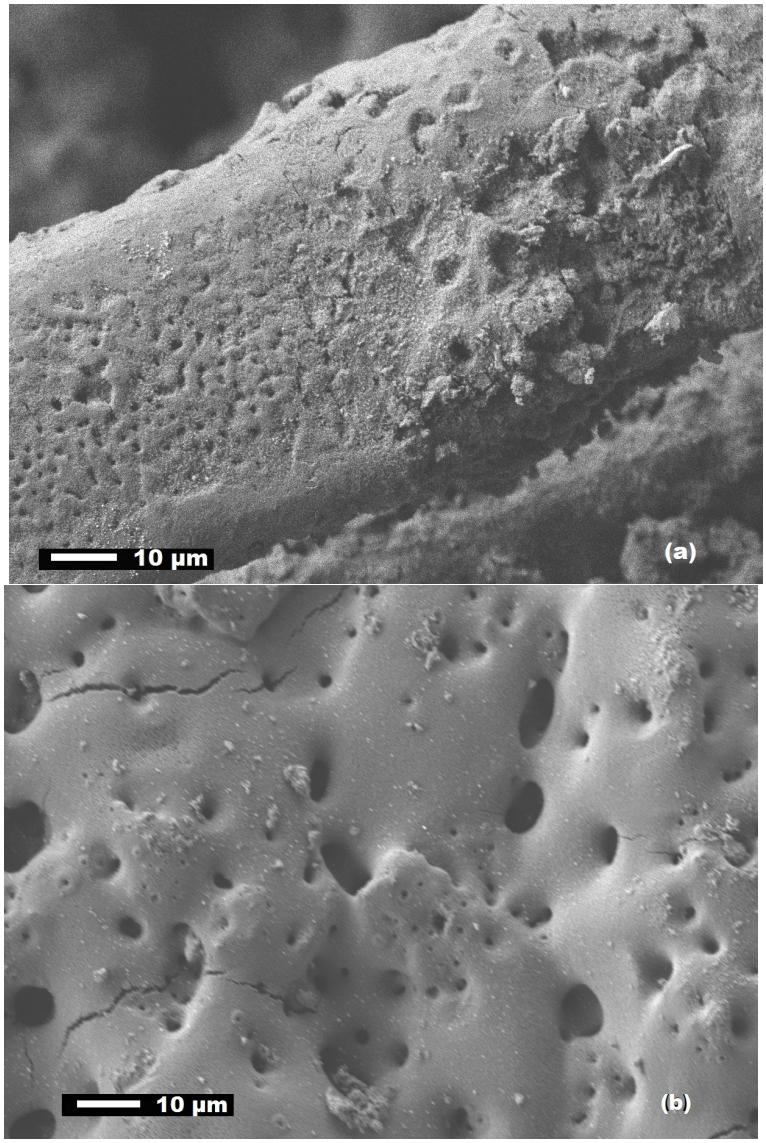

Figure 6.5 SEM micrographs of 1 % Pt/Rh on MgO/FeCralloy (a) x1000 before reaction ; (b) x1000 after reaction.

0.1 MPa. With such short contact time, methane conversion is only 45 %. At higher pressures while keeping WHSV constant, the residence time increases (0.075 s at 0.5 MPa, 0.15 s at 1 MPa and 0.3 s at 2 MPa), which is the main contribution to the increase of the methane conversion. Therefore, to study the effect of pressure, we then test the CPOX reaction with the constant residence time of 0.1 s under pressures up to 2 MPa with the same methane to oxygen ratio of 2 and temperature of 900 °C.

Methane conversion was high at atmospheric pressure and a residence time of 0.1 s (around 90 %, Figure 6.9 (a)). At higher pressure, the conversion of methane drops to around 75 % ;

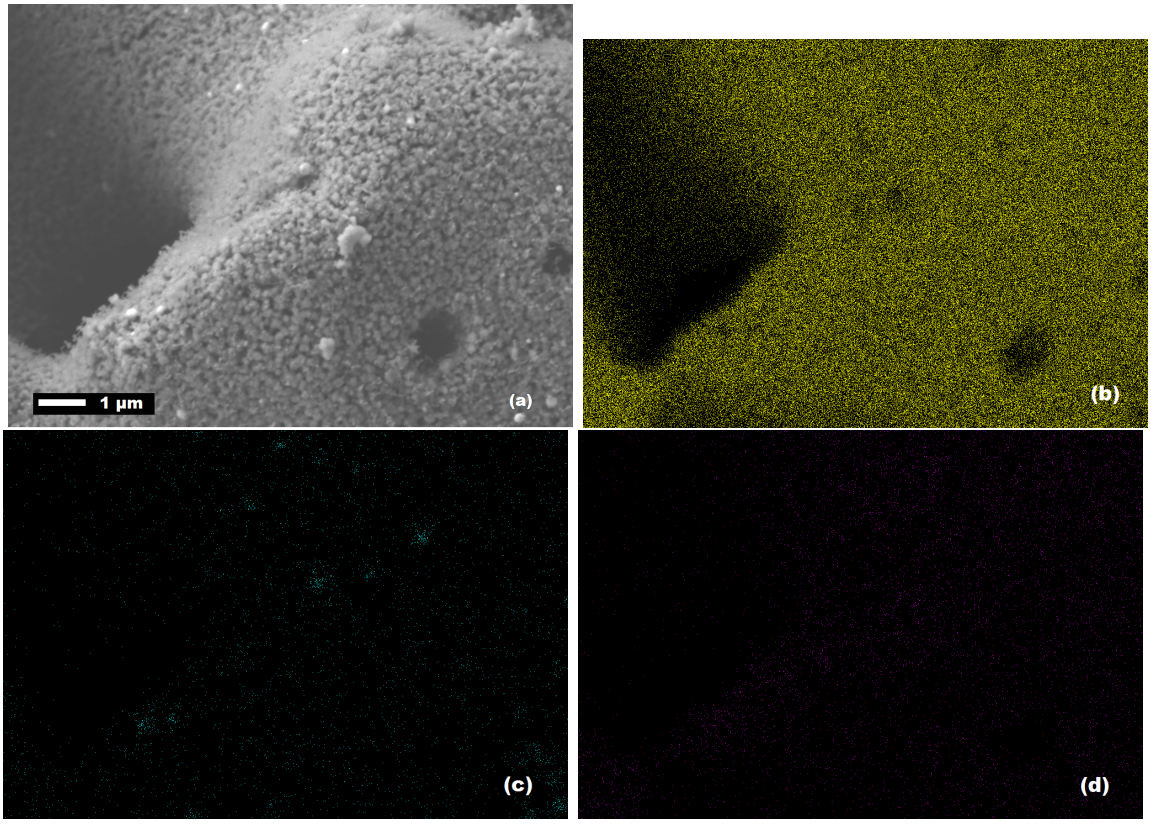

Figure 6.6 (a) x10 000 SEM micrographs of the one typical surface of Pt/Rh/MgO FeCralloy (b) Mg dispersion ; (c) Pt dispersion ; (d) Rh dispersion.

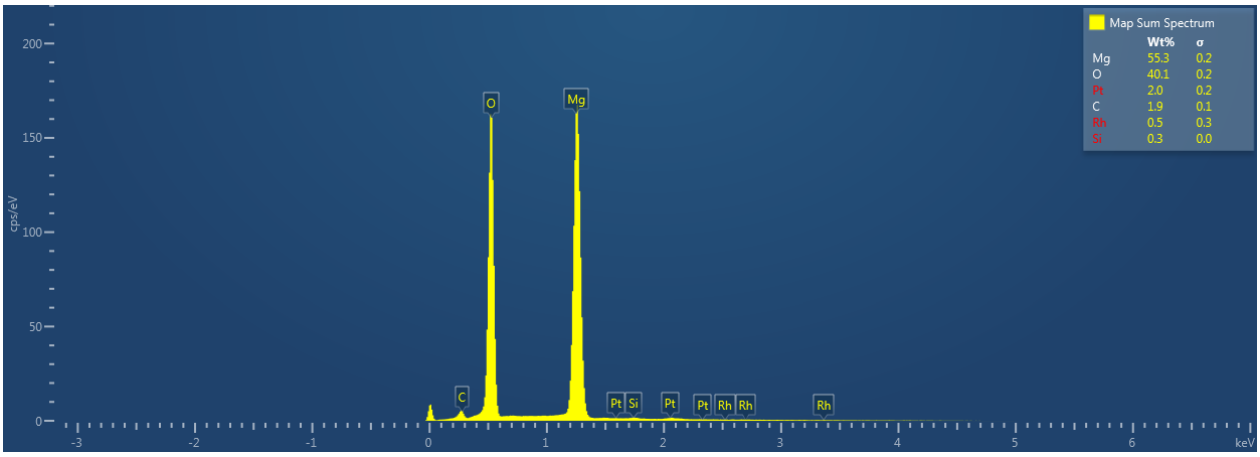

Figure 6.7 The composition of the surface of Pt/Rh/MgO fecralloy via SEM-EDS analysis.

however, it changes little from 0.5 MPa to 2 MPa. Pressure affects both CO and H_2 selectivity (Figure 6.9 (b) and (c)). At 0.1 MPa and 0.5 MPa both selectivities increase quickly in the

Table 6.1 Design of experiments. Reaction conditions : T = 900 °C, CH_4/O_2 = 2, mass of catalyst = 0.27 g (mass of catalyst* = 0.2 g). The value of gas flow Q is under 25 °C and atmosphere pressure.

Test	Q_{CH_4} $ml\,min^{-1}$	Q_{O_2} $ml\,min^{-1}$	Q_{Ar} $ml\,min^{-1}$	τ s	WHSV $g_{CH_4}g_{cat}^{-1}h^{-1}$	Pressure MPa
1	106	53	199	0.015	15	0.1
2	106	53	199	0.075	15	0.5
3	106	53	199	0.15	15	1.0
4	106	53	199	0.3	15	2.0
5*	11	6	21	0.1	2	0.1
6	79	40	149	0.1	12	0.5
7	159	79	298	0.1	23	1.0
8	317	159	597	0.1	46	2.0

first 30 min and then S_{CO} remains constant around 90 % while S_{H_2} increases up to 99 %. The average selectivities (after 30 min operation) are 9 % and 53 % at 1 MPa and 44 % and 34 % at 2 MPa, respectively. The CO_2 selectivity (Figure 6.9 (d)) is around 10 % at 0.1 MPa and 0.5 MPa, around 20 % at 1 MPa and 2 MPa, which also indicates an increasing coke formation with the rising pressure. The average H_2/CO ratio lies between 1.8 to 2.1 from 0.1 MPa to 1 MPa, however dropping to 1.6 at 2 MPa. To maintain constant residence time, we increased the flow rates of methane and oxygen/argon proportionally to the operating pressure, but this disrupted the reactor operation.

6.4.3 Coke formation analysis

Coke formation is an inevitable problem when catalytically converting methane to syngas : it deactivates the catalyst and disrupts the reactor and process lines. Previous work has either neglected the impact of carbon formation on the thermodynamics [4, 141] or ignored the thermodynamic difference between solid carbon in its graphite form and in its coke form [142, 143].

Considering the importance of carbon deposition [23], we recalculated the thermodynamic equilibrium of coke with a thermodynamic model (FactSage® Thermochemical Software) [144] [145].

The thermodynamic calculations considers the thermodynamic equilibrium of all possible reactions including the following chemical species : H_2, CH_4, N_2, O_2, H_2O, CO, CO_2. Partial oxidation and Boudouard reactions are included as well as the following :

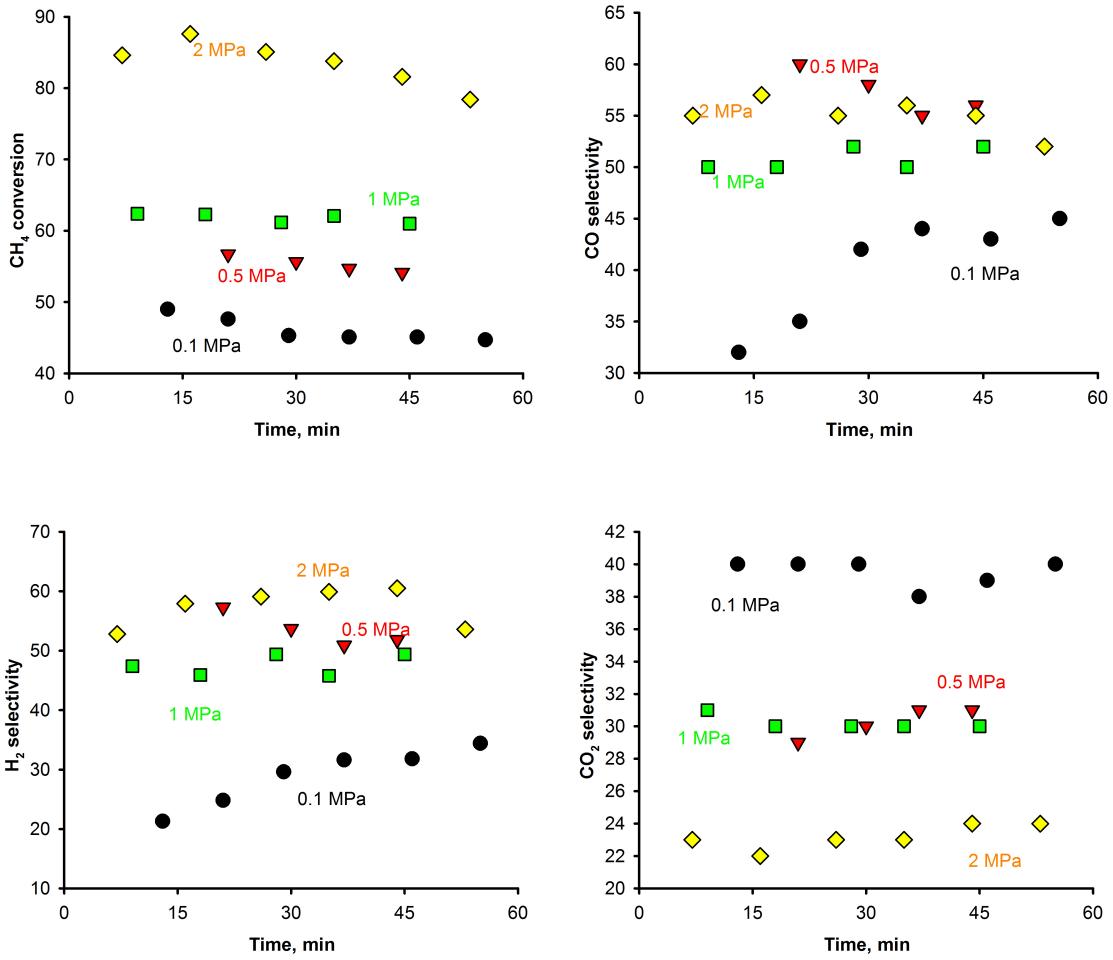

Figure 6.8 (a) Methane conversion ; (b) CO selectivity ; (c) H_2 selectivity ; (d) CO_2 selectivity vs. time under elevated pressures with CH_4/O_2 of 2, 900 °C, WHSV = 15 $g_{CH_4} g_{cat}^{-1} h^{-1}$.

$$H_2 + \frac{1}{2}O_2 \rightleftharpoons H_2O \tag{6.6}$$

$$CO + \frac{1}{2}O_2 \rightleftharpoons CO_2 \tag{6.7}$$

$$CH_4 \rightleftharpoons C + 2H_2 \tag{6.8}$$

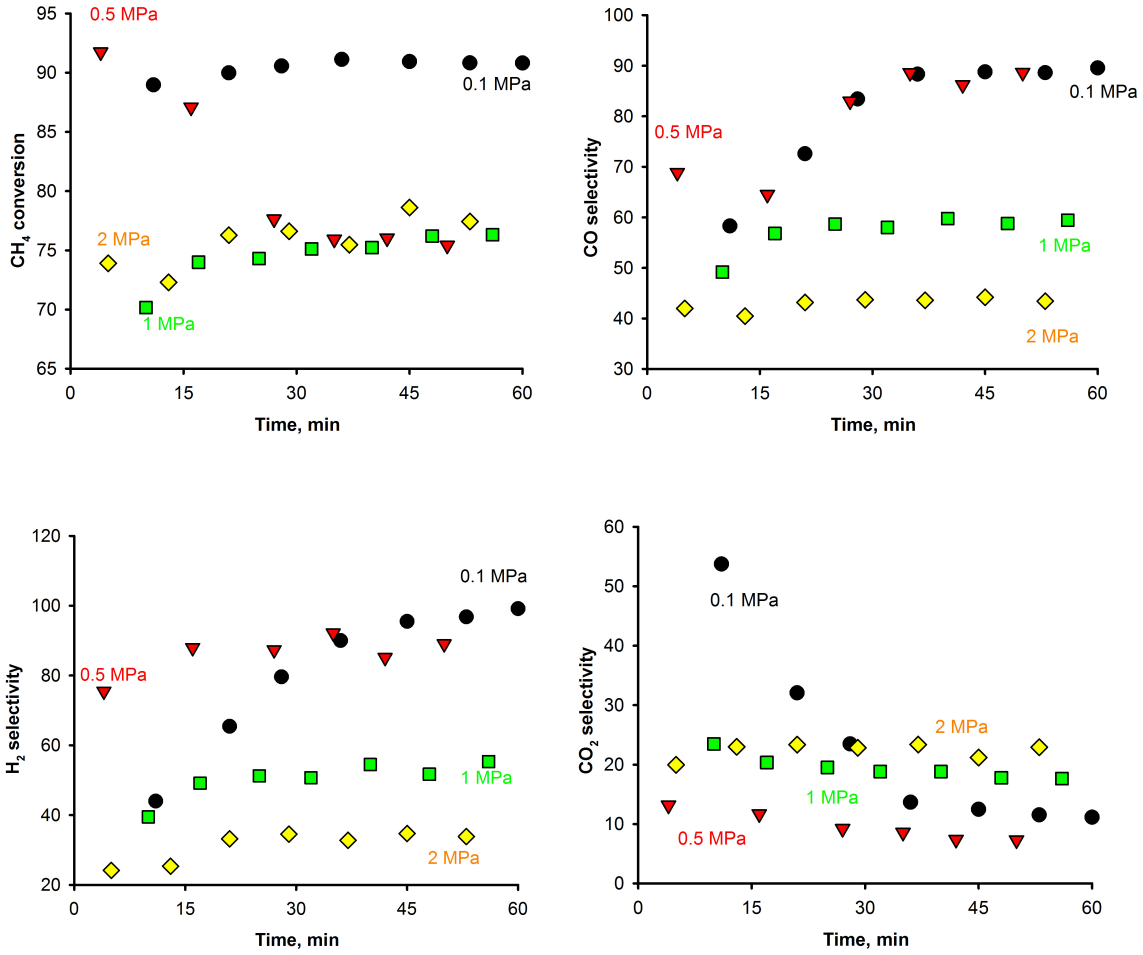

Figure 6.9 (a) Methane conversion ; (b) CO selectivity ; (c) H_2 selectivity ; (d) CO_2 selectivity vs. time under elevated pressures with CH_4/O_2 of 2, 900 °C, residence time of 0.1 s.

$$CO + H_2 \rightleftharpoons C + H_2O \tag{6.9}$$

$$CH_4 + CO_2 \rightleftharpoons 2CO + 2H_2 \tag{6.10}$$

$$CH_4 + H_2O \rightleftharpoons CO + 3H_2 \tag{6.11}$$

$$CO + H_2O \rightleftharpoons CO_2 + H_2 \tag{6.12}$$

The Gibbs energy minimization procedure finds the minimum of Gibbs energy of the system at constant T and total P by distributing the moles of C and H between the coke and different gas species (Factsage). This results in the equilibrium phase assemblage (with the internal composition of the phases given as species composition). The resulting partial pressures of the gaseous species then fully respect all equilibrium constants resulting from all potential reaction between the chosen species. These techniques of Gibbs energy minimization using Lagrange multipliers were developed around 1960 [146, 147] and are very standard today in computing phase equilibria.

We selected the 7 chemical species to compare with the thermodynamic calculations of Enger [4]. However, extending this selection of species to 472 did not affect the thermodynamic calculations presented in the present paper (For example, methane conversion was modified by less than 0.07 %). The selected species are the most stable at 900 °C and 0.1 MPa to 2 MPa.

The key advantage of the FactSage software is the vast solution database to calculate the solution thermodynamics based on pure substance properties. The database for coke is unique to FactSage and relies on established principles such as the assumed turbostratic structure of coke crystallites. and the kinetic/thermodynamic aspects of graphitization of pyrocarbons (which is relevant to methane coking).

Solid carbon (i.e. coke or graphite) formation regime (Figure 6.10) varies with crystallite size L_a (the diameter of crystallites composing the coke). The larger the L_a (nearing graphite) results in a more stable coke due to high surface energies. Generally, the formation of large coke crystallites proceeds through the growth of smaller ones, which requires an equivalent activation energy. It requires a higher activation energy at higher temperatures to form large crystallites of stable coke. The minimal size for stable solid carbon can be 4 times larger at an operating temperature of 900 °C than 750 °C. The presence of active metals on the surface of the support lowers this activation energy, kinetically hindering coke formation at high temperatures.

We compared equilibrium coking of CH_4 calculated by FactSage® with experimental S_C based on a mass balance (Figure 6.11). Experimental coking is significantly higher than equilibrium values. This indicates that CPOX reaction does not reach the Boudouard equilibrium, which is expressed by

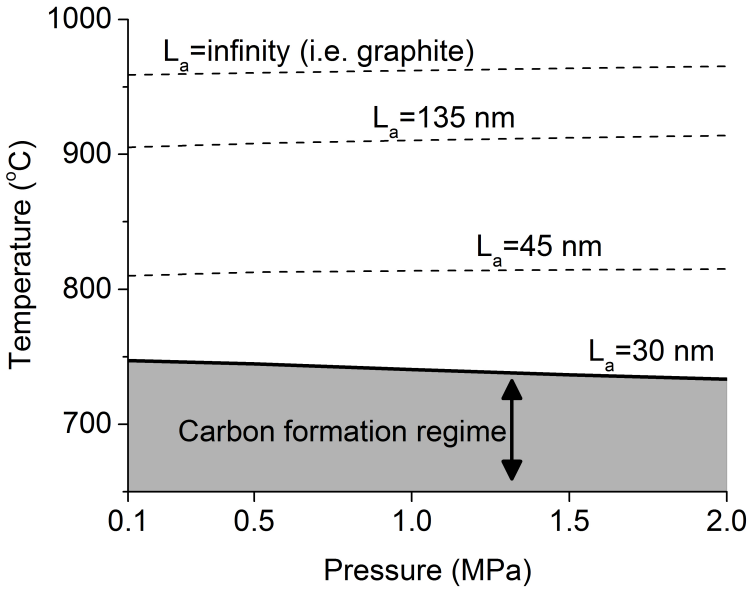

Figure 6.10 Coke formation regime for CPOX calculated at various crystallite sizes (i.e. activation energies) and pressures with a CH_4/O_2 ratio of 2

$$C + CO_2 \rightleftharpoons 2CO \tag{6.13}$$

The experimental results (Figure 6.8 and 6.9) also suggest that high coking rates are associated with a high selectivity of CO_2. Higher pressure promotes the reverse Boudouard reaction and thus more coke and CO_2 form. At lower pressures (0.1 and 0.5 MPa), CPOX produces coke much closer to the equilibrium value.

Residence time also affects coking : the coke selectivity (S_C) decreased from 24 % ($\tau = 0.1$ s) to 18 % ($\tau = 0.3$ s) at 2 MPa. This is possibly due to a higher methane conversion and CO selectivity at a relatively longer residence time of 0.3 s. Lower coke also corresponds to a higher H_2 seletivity at 2 MPa. Based on the thermodyanmic calculations, the coke formed is metastable.

According to equilibrium thermodynamics, pressure has little impact on the equilibrium conditions for temperatures closte to 1200 K (900 °C) or higher [4]. Our kinetic data indicate that the CPOX reaction has not reached equilibrium, the amount of coke is above the equilibrium thermodynamic value. Thermal decomposition of methane (8), as the first reaction step, is faster than the other reaction steps of CPOX, because it is not strongly limited

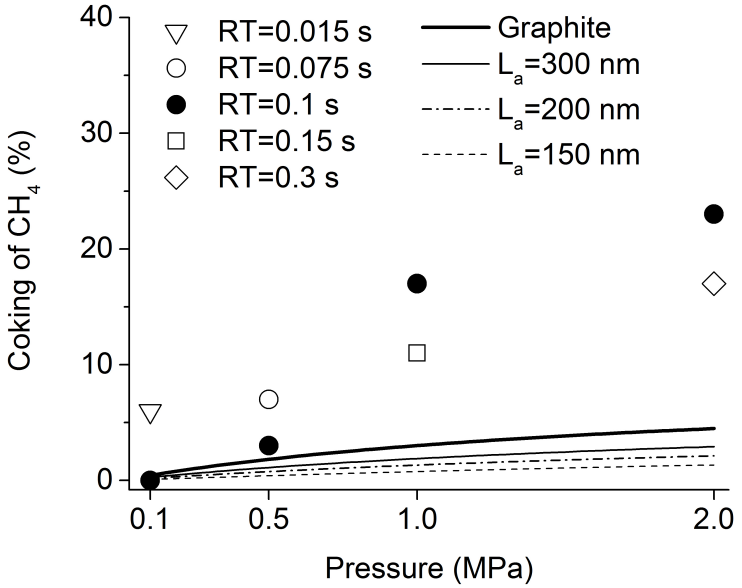

Figure 6.11 Experimental and thermodynamically predicted coking of CH_4 at 900 °C for various pressures and residence times (RT) with a CH_4/O_2 ratio of 2

by diffusion [4]. Therefore the generation of metastable coke through thermal decomposition of methane will be greater than the consumption of metastable coke to produce CO or CO_2. Increasing pressure will lower the generation of metastable coke as it will restrain the decomposition rate of CH_4 to form H_2. This kinetic effect is more important than the thermodynamic impact of increasing pressure on catalyst performance. The global kinetics of the CPOX reaction are assumed to be fast because of the short reactor residence time (less than 0.3 s). As we increase the residence time, the amount of metastable coke is reduced and both selectivity and conversion approach equilibrium.

6.5 Conclusion

Combining CPOX with FT to make synthetic fuel has advantages over standard technologies with respect to operation and investment. The challenge of integrating CPOX and FT is converting methane to suitable syngas at high pressure. Methane cokes CPOX catalyst at high pressure and consequently both CO and H_2 selectivity are low High operating temperatures may partially alleviate the negative effects of coke. However, the catalyst and the FeCralloy thermal stability can become limiting factors. The FeCralloy woven fibre is thermally stable only up to 1050 °C.

Coating the FeCralloy support with a layer of MgO layer may minimize coke. We synthesized a 1 % mass fraction of Pt/Rh catalyst supported on MgO over FeCralloy woven fibre. At 2 MPa and a residence time of 0.3 s, syngas yields were 50 % CO with a H_2/CO ratio of 2. All the oxygen was consumed for all experiments, which is critical for the FT step that requires reducing conditions.

Comparison with thermodynamics clearly demonstrate that the measured coke formation is metastable. Coke conversion to CO through the Boudouard reaction is assumed to be the limiting factor in metastable coke elimination. Increasing residence time should thus reduce metastable coke formation and the associated negative effects on conversion and H_2 selectivity. At 2 MPa, a residence time of 0.3 s reduced coke formation by 33 % and increase CO and H_2 yield than a residence time of 0.1 s . The present study did not explore the effect of temperature. Higher temperatures should further reduce the amount of metastable coke.

CHAPTER 7 ARTICLE 3 - FECRALLOY PARTIALLY OXIDIZES METHANE SELECTIVELY

Zhenni Ma, Diego C. Pelegrin, Patrice Perreault, Daria C. Boffito and Gregory S. Patience

Under review : Catalysis Today, 2018

7.1 Abstract

Micro Gas-to-Liquids technology (GtL) reduces flared natural gas and carbon emissions while producing diesel. Integrating high pressure syngas step (catalytic partial oxidation of methane, CPOX) with Fischer-Tropsch (FT) in a single vessel reduces investment and operating cost. CPOX catalyst must resist high temperature and high pressure stresses. FeCralloy knitted fibres are ideal materials because the surface alumina layer resists temperature over 1000 °C.

Virgin FeCralloy and oxidized FeCralloy are active to convert methane, and promote partial oxidation of methane without a pre–reduction treatment. We deposited Pt/Rh on the fibre surface via solution combustion synthesis. Methane conversion and syngas selectivity was superior to unsupported FeCralloy at 900 °C and from 0.1 MPa and 2 MPa. SEM analysis and a carbon mass balance demonstrated that its coke levels were imperceptible in 1 h test. The FeCralloy surface morphology remains intact after 12 reaction-regeneration cycles.

7.2 Introduction

Associated natural gas that is pumped with crude oil from high pressure reservoirs has little value. The economic incentive to invest in infrastructure for remote wells is lacking thus producers prefer flaring this gas. However, this contributes to carbon emissions globally and the toxic compounds that accompany this gas contaminate the local environment. Global flaring contributes 300 million tons of CO_2 annually and it wastes 3.5 % of world's natural gas [148] that is sufficient to meet the power needs of the African continent [149]. An overall growth in oil production, especially in Iraq and the United States, has increased world flaring rates over the past five years [102]. A global initiative of Zero Routine Flaring by 2030 [150], endorsed by 62 oil companies, governments and development institutions, calls for technical and economic alternatives to end flaring.

Gas-to-Liquid (GtL) technology is an attractive opportunity to monetize remote natural

gas [10]. The Fischer-Tropsch (FT) technology is widely established in both large-scale and small-scale projects. To eliminate associated gas flaring in remote oil reservoirs requires micro-refineries. Some companies pursue small-scale systems at a capacity of 1000 bbl d^{-1}, while more ambitious projects seek to produce as little as 10 bbl d^{-1} [149, 106]. A single MRU (Micro Refinery Unit) vessel [29] houses both the synthesis gas (syngas) unit and FT reactor. This compact design makes it possible to fit a single unit on a trailer that travels to remote reservoirs to convert the gas to oil.

One challenge is to produce syngas at high pressure without producing coke. Syngas, a mixture of H_2 and CO, reacts with Co or Fe to diesel – Fischer Tropsch synthesis. Conventional processes to produce syngas include steam methane reforming (SMR), dry-reforming (DRM) [151], auto-thermal reforming (ATR) and partial oxidation of methane (POX) [105, 75]. POX is mildly exothermic (Δ H $= -36\,\mathrm{kJ\,mol^{-1}}$), which makes it convenient for industrial processes from an energy management perspective ; the H_2/CO molar ratio of 2 is ideal for FT ; it avoids large capital costs to superheat steam ; it allows higher gas hourly space velocities and thus capital costs are lower. Catalysing the partial oxidation of methane (CPOX) decreases the reaction temperature below 1000 °C while the POX reactors operate as high as 1400 °C.

The thermodynamic equilibrium of the FT reaction favours high pressure to produce large molecules ($\geqslant$2 MPa) [152] while the thermodynamic equilibrium of the CPOX reaction favours low pressure for methane conversion, and CO and H_2 selectivity. Syngas selectivity suffers at high pressure but operating CPOX at high temperature mitigates the low selectivity towards H_2 and CO [21]. A few studies of high pressure CPOX tested pressures from 0.8 MPa to 1.5 MPa [94, 153, 96, 95, 154, 97]. Fichtner et al [98] operated at 2 MPa and 1100 °C. Catalyst selection must account for sintering, coking, and mechanical stability to withstand the high pressure and temperature [94, 155, 96, 97]. Rh monoliths operate well up to 1.5 MPa [155, 97].

CO selectivity over Pt/MgO and Pt/Al_2O_3 catalysts supported over FeCralloy knitted fibres reached 57 % and 47 % at 2 MPa [156, 157]. FeCralloy is an outstanding metal alloy designed to operate over 1000 °C, and is the primary element in gas fired burners to distribute heat uniformly, and as catalyst supports [158, 159, 160, 161] and automobile catalyst substrate [162, 163]. Monolith type reactors are easier to operate than fluidized beds but FeCralloy knitted fibres are superior to both because of their excellent mechanical properties and high thermal conductivity that allow high space velocities and a low pressure drop [164, 165] ; because of their flexibility, scale-up criteria are more straightforward compared to fluidized beds. The specific surface area is low, so the volume required for the catalyst might be an issue for scaling up. Nevertheless, they are more economical than noble metal gauzes (Pt,

Rh, etc. [4, 26, 27, 28, 29]).

In this work, we tested virgin and oxidized FeCralloy knitted fibres and Pt/Rh FeCralloy catalysts. We explored their reactive and regenerative abilities at ambient pressure and at 2 MPa to meet the demand of combing high pressure FT.

7.3 Experimental

7.3.1 Catalyst preparation

The catalyst support was a FeCralloy metal fibre in the form of a flexible knitted textile structure, with a mass fraction of 20 % chromium, 5 % aluminum, yttrium > 0.1 %, 0.3 % silicon, 0.08 % manganese, 0.03 % copper, 0.03 % carbon over 74 % iron. We cut the woven fibre into 10 mm×10 mm squares then sonicated them in a water/acetone solution (1 :1) for 30 min. Then a muffle furnace (a Neytech model 3-550, Vulcan Multi-stage programmable furnace) dried the FeCralloy fibres at 120 °C for 1 h.

We refer to the unsupported Fecralloy as virgin FeCralloy. The virgin FeCralloy calcined at 1000 °C for 3 h under air at a heating and cooling rate of 5 °C min^{-1} to form oxidized FeCralloy. To modify the performance of FeCralloy catalysts, we added other active components, Pt, Rh, by solution combustion synthesis (SCS). To minimize surface deformation of FeCralloy, we deposited the metals on oxidized FeCralloy. Aqueous solutions containing metal precursors ($Pt(NH_3)_4(NO_3)_2$, Sigma Aldrich ; $RhCl_3$, Sigma Aldrich) and the fuel ($CO(NH_2)_2$, Sigma Aldrich) wet the knitted fibres. Fine powders formed when the moistened fibres reached ignition temperature at 600 °C [156].

To minimize the catalyst cost, we minimize the mass of the precious metals while simultaneously maximizing their activity. Noble metal loading varied from 0.05 % to 10 % [139]. An average loading of 5 % was common for the screening experiments [7]. The pre-determined mass fraction of Pt + Rh was 1 % by weight with a Pt/Rh weight ratio of 9 :1. After deposition via SCS, the catalysts calcined at 1000 °C in static air for 3 h at a heating and cooling rate of 5 °C min^{-1}.

To confirm that the total mass fraction of Pt/Rh catalyst was 1 %, we weighed the catalyst before and after SCS.

An Autosorb-1 measured the surface area of each catalyst by N_2 adsorption/desorption. The sample degassed for 3 h at 200 °C to evaporate residual water and volatile impurities (Table 7.1).

A Philips X-Pert MPD diffractometer equipped with a Cu Kα radiation at 50 keV and 40 mA

Table 7.1 Catalyst composition and surface area. CPOX reaction at 2 pressure with 3 FeCralloy catalysts, at a contact time of 0.15 s under 900 °C with a O_2/CH_4 ratio of 0.5 (balance Ar to match N_2 concentration in air). m_{cat} : the weight of the catalyst ; h_{cat} : the height of the catalyst bed.

Catalyst	Pt %	Rh %	BET surface area $m^2\,g^{-1}$	m_{cat} g	h_{cat} mm
Virgin Fecralloy	–	–	0	0.50	5.0
Oxidized Fecralloy	–	–	0.020	0.50	8.0
Pt/Rh Fecralloy	0.9	0.1	0.021	0.45	5.0

measured the diffraction of the crystalline phases of these FeCralloy catalysts. The scanning rate was $0.02\,^\circ\,s^{-1}$ with 2θ varying from 20° to 90°. We attributed the peaks according to the PCPFWIN database. We performed scanning electron microscopy (SEM, model : JSM-7600A) and EDS (Energy Dispersive Spectroscopy) analysis to screen the surface morphology and analyze the elemental composition [99].

7.3.2 Experimental setup

The reactor for methane partial oxidation was a 300 mm long quartz reactor with an ID of 8 mm (Figure 7.1). We cut two or three circular FeCralloy disks to fit snugly in the reactor. We positioned them in the middle of the reactor at a height of 175 mm (the total thickness equals the sum of 10 mm glasswool and the height of the catalyst). We did not pretreat the catalyst further [140]. An electrical furnace heated the reactor. A type K thermocouple of 175 mm monitored the temperature at the top of the catalyst bed. A back pressure regulator maintained a constant reactor pressure. The gases entered from the top of the reactor. An Agilent gas-chromatograph 7890 B measured the inlet gas composition before reaction and the outlet gas during reaction following the ASTM D1945 standard.

The conversion of methane (X_{CH_4}) and selectivity towards H_2 (S_{H_2}), CO (S_{CO}), CO_2 (S_{CO_2}) and the coke based on the inlet CH_4 (S_C) were calculated as follows :

$$X_{CH_4}(\%) = \frac{F^{in}_{CH_4} - F^{out}_{CH_4}}{F^{in}_{CH4}} \times 100 \tag{7.1}$$

$$S_{H_2}(\%) = \frac{F^{out}_{H2}}{(F^{in}_{CH_4} - F^{out}_{CH_4}) \times 2} \times 100 \tag{7.2}$$

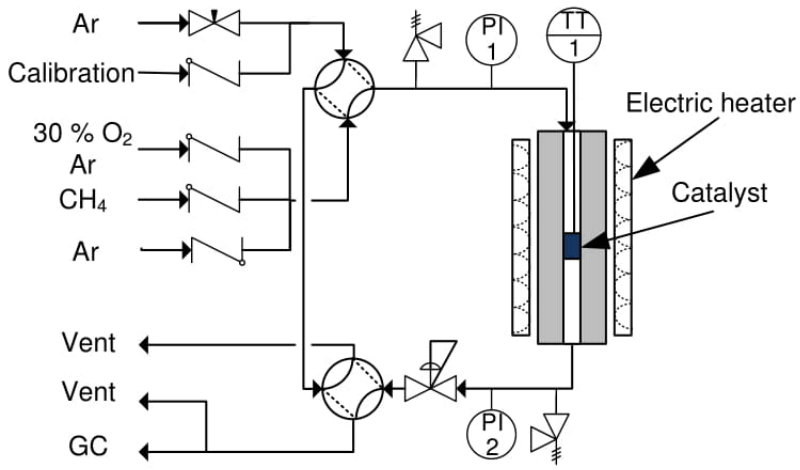

Figure 7.1 Experiment setup. The reactor was an 8 mm ID quartz tube, with a 10 mm high glasswool in the middle supported the catalyst.

$$S_{\mathrm{CO}}(\%) = \frac{F^{\mathrm{out}}_{CO}}{F^{\mathrm{in}}_{\mathrm{CH_4}} - F^{\mathrm{out}}_{\mathrm{CH_4}}} \times 100 \tag{7.3}$$

$$S_{\mathrm{CO_2}}(\%) = \frac{F^{\mathrm{out}}_{CO2}}{F^{\mathrm{in}}_{\mathrm{CH_4}} - F^{\mathrm{out}}_{\mathrm{CH_4}}} \times 100 \tag{7.4}$$

$$S_{\mathrm{C}}(\%) = \frac{F^{\mathrm{in}}_{\mathrm{CH_4}} - F^{\mathrm{out}}_{\mathrm{CH_4}} - F^{\mathrm{out}}_{\mathrm{CO_2}} - F^{\mathrm{out}}_{\mathrm{CO}}}{F^{\mathrm{in}}_{CH4}} \times 100 \tag{7.5}$$

Where : $F^{\mathrm{in}}_{\mathrm{CH_4}}$ and $F^{\mathrm{out}}_{\mathrm{CH_4}}$ are the molar flow rates of methane at the reactor entrance and exit, respectively ; $F^{\mathrm{out}}_{\mathrm{CO}}$, $F^{\mathrm{out}}_{\mathrm{H_2}}$ and $F^{\mathrm{out}}_{\mathrm{CO_2}}$ are the molar flow rates of CO, H_2 and CO_2 at the reactor exit.

We compared the reactivity of each FeCralloy catalyst at atmospheric pressure and elevated pressure (2 MPa) while maintaining a constant contact time at 0.15 s. Each test lasted 65 min and GC sampled the effluent stream every 10 min. To maintain the same catalytic condition and remove the coke produced by the previous test, we regenerated the catalyst before each test by feeding 50 mL $\mathrm{min^{-1}}$ oxygen (O_2 : 30 %, Ar : balance), and monitored the regeneration process by GC to avoid over oxidation.

7.4 Results and Discussion

7.4.1 Catalyst characterization

FeCralloy fibres are non-porous materials. After calcination at 1000 °C for 3 h, the specific surface area of the oxidized FeCralloy increases to 0.02 $\mathrm{m^2\,g^{-1}}$ due to the formation of alumina

scale. Through solution combustion synthesis, we deposited 1 % Pt/Rh (Pt/Rh = 9) over the oxidized FeCralloy surface, and the surface area of the catalyst slightly increases (Table 7.1). The surface area insignificantly impacts the FeCralloy catalyst performance and syngas selectivity.

XRD

The X-ray diffraction pattern of the virgin FeCralloy has three peaks (Figure 7.2 – 1, intensity 0 – 1400) at $2\theta = 44.6°$, 64.8° and 81.7°, representing the bulk components - FeCr (JCPDS 34-0396, marked with black square). Al, with a mass fraction of 5 %, was not detectable in the virgin FeCralloy. Al preferentially becomes oxidized, as alumina has a lower Gibbs free energy than other alloy element oxides illustrated in the Ellingham diagram [166]. After calcination at 1000 °C, only α-Al_2O_3 (JCPDS 42-1468, marked with red dot) forms over the FeCralloy surface (Figure 7.2 – 2, intensity 0 – 1400).

In previous study [157], we coated α-alumina by spray pyrolysis instead of calcination and deposited 1 % Pt. Peaks at 2θ equal to 40.0°, 46.5° and 67.7° correspond to Pt crystallites (Fig. 7.2 – 3, JCPDS 04-0802, marked with blue star, intensity 0 – 1400).

By replacing the stainless steel sample holder with a silicon sample holder, we eliminated noisy peaks overlapping with FeCr. From Fig. 7.2 – 4a (intensify from 0 – 3500) we observed very low peaks of FeCr. From Fig. 7.2 – 4b (intensify from 0 – 500), intensity of FeCr was approximately $\frac{1}{3}$ of peaks of 1 % Pt/Al_2O_3/FeCralloy catalyst prepared by spray pyrolysis. Two low Pt peaks reveal non-crystalline state and/or indicates a well dispersion. We assume that after the direct deposition of Pt on oxidized FeCralloy, Pt is well dispersed and the surface of supported oxidized FeCralloy is amorphous. We confirmed this assumption by SEM analysis.

SEM with EDS

Electron microscopy surveyed the surface morphology of the i) virgin/fresh, ii) used, and iii) regenerated catalyst (Figures 7.3 - 7.5). The surface of virgin FeCralloy is non porous and relatively smooth (Figure 7.3 (a)). Surface elemental map analysis confirmed the composition of metal elements Fe, Cr and Al.

The calcination of virgin FeCralloy to oxidized FeCralloy mostly formed an alumina scale (Figure 7.4 (a))[166]. This oxidative scale protects the surface Fe and Cr from oxidation, as long as Al is not depleted, the structure of FeCralloy is stable up to 1050 °C. At calcination temperature lower than 1000 °C under air, outward diffusion of Al generates transition

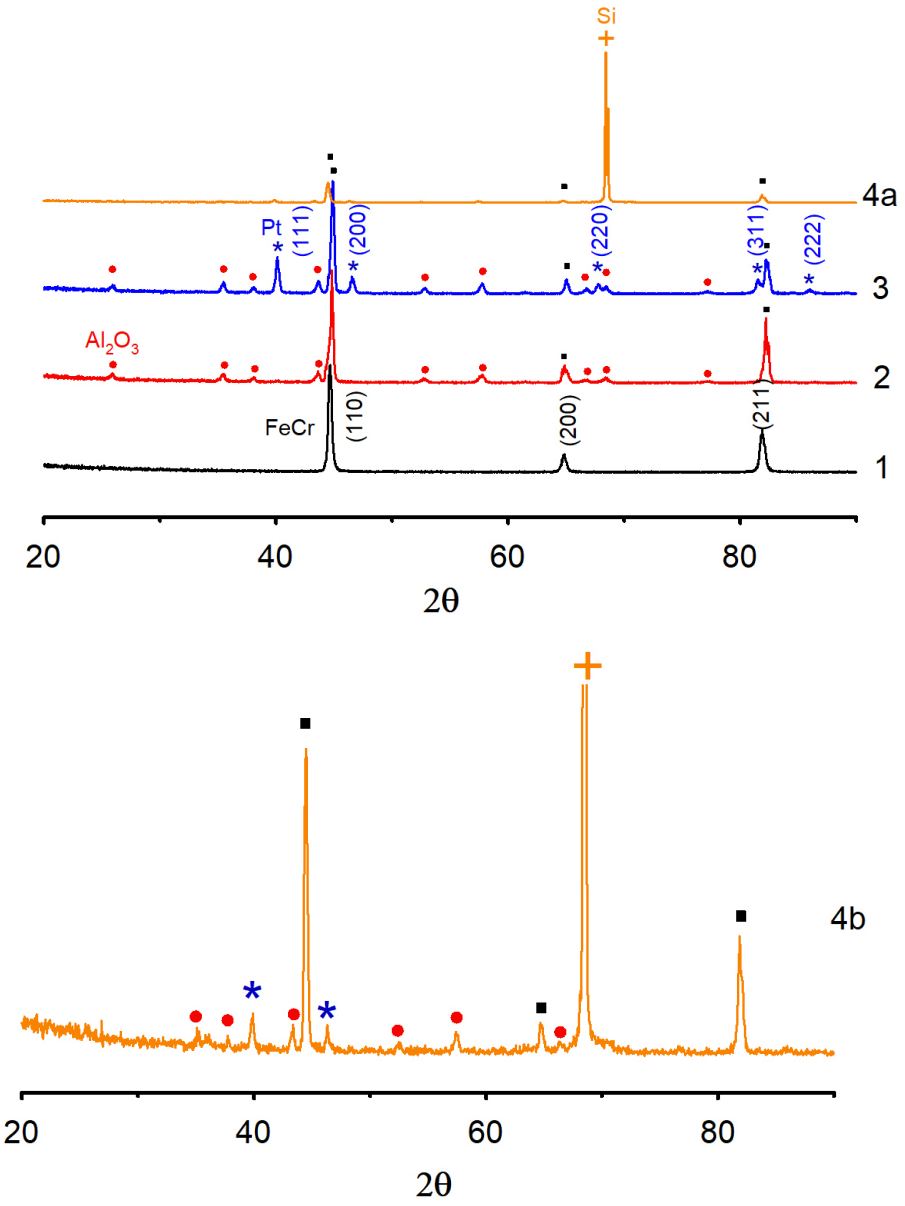

Figure 7.2 XRD characterization of 1) virgin FeCralloy; 2) oxidized FeCralloy; 3) 1 % Pt/Al_2O_3/FeCralloy catalyst synthesized by spray pyrolysis; 4a) 1 % Pt over oxidized FeCralloy by solution combustion synthesis (intensity 0 – 3500); 4b) 1 % Pt over oxidized FeCralloy by solution combustion synthesis (intensity 0 – 500).

(γ, δ, θ) alumina at the oxide-gas interface, resulting in whiskers and sharp-edged flakes [167]. Annealing oxidized FeCralloy at 1000 °C for 3 h produces α-Al_2O_3, as the X-Ray Diffraction analysis confirms [157]. The surface area of oxidized FeCralloy is only $0.020\,m^2\,g^{-1}$ (Table 7.1), the main oxide scale is non-porous α-Al_2O_3.

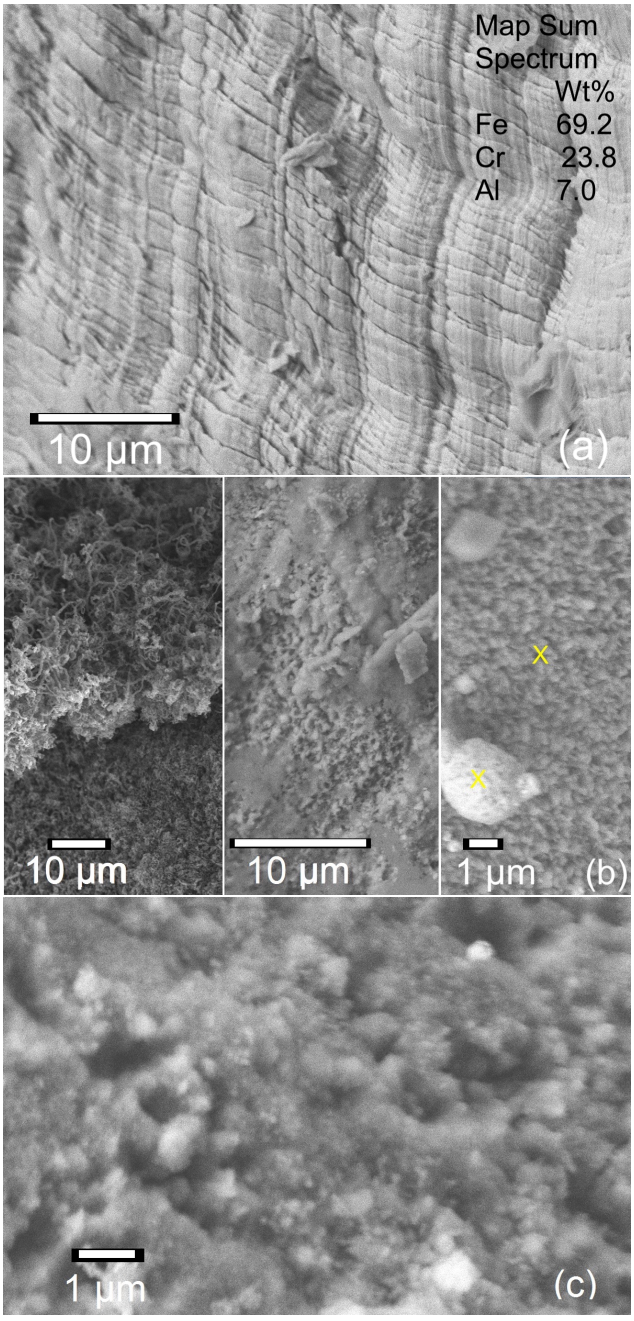

Figure 7.3 (a) Fresh virgin FeCralloy is non-porous and mainly consists Fe, Cr and Al. (b) Used virgin FeCralloy after CPOX reaction. From left to right are the first, the middle and the last piece of catalyst. The first piece that first contacted the inlet stream coked the most, while the last piece had no coke but an oxidized layer. (c) Regenerated virgin FeCralloy, its surface was completely oxidized.

After CPOX reaction at 2 MPa, three disks of the used virgin FeCralloy changed morphology (Figure 7.3 (b)). The first disk that confronts the inlet feed gas was fully covered by whisker

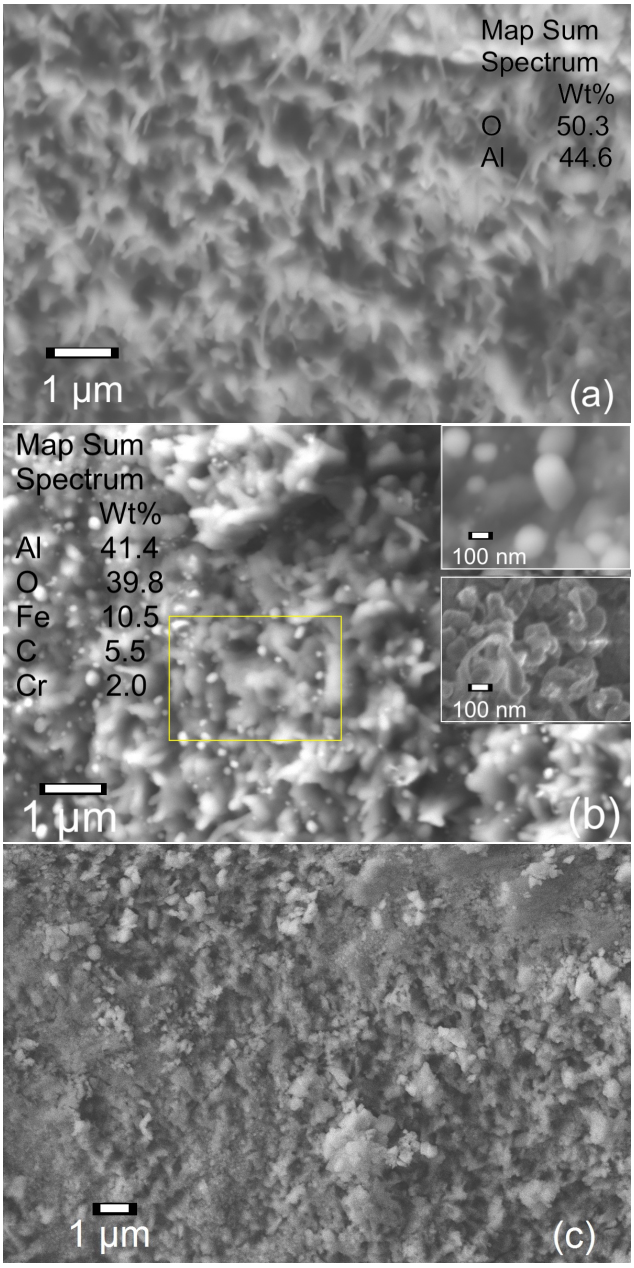

Figure 7.4 (a) Fresh oxidized FeCralloy. An EDS map analysis confirmed an alumina layer predominantly formed. (b) Used oxidized FeCralloy after CPOX reaction. The lower right picture shows the whisker coke formed on oxidized FeCralloy ; the upper right one magnifies the newly formed globular alumina grains. An EDS map analysis of the rectangular region presented the surface composition. (c) Regenerated oxidized FeCralloy.

coke. The middle disk displayed much less coke and an oxidized surface with whiskers and amorphous alumina. The third disk was the least coked and its surface was similar to the fresh oxidized FeCralloy. An EDS point analysis (marked by a yellow cross) demonstrated

a similar surface composition, mainly consisting of Al_2O_3. The regenerated virgin FeCralloy catalyst grew a further oxidized layer of alumina (Figure 7.3 (c)). Whisker carbon has high strength and breaks the pores or channels of the catalyst [168] and increases pressure drop. The non-porous structure of FeCralloy prevents encapsulating coke formation and ensures an easy coke removal process and catalyst regeneration step.

After CPOX reaction, spherical grains of alumina with a particle size in the range of a few hundred nanometers uniformly dispersed over the surface alumina scale (Figure 7.4 (b)). This may be because alumina scale forms in two stages : at first the alumina scale is compact and planer as Al atoms uniformly distribute over the alloy surface ; then the initial grain nucleus grows due to the diffusion and Al accumulates at unevenly distributed grain boundaries [163]. EDS analysis detects the volumetric elemental composition at a surface thickness up to 2 µm. At 10 eV, it detected more than 10 % Fe, so the thickness of alumina scale is less than 2 µm. The coke deposited on the oxidized FeCralloy catalyst displayed a whisker structure. After regenerating the used oxidized FeCralloy in an oxygen rich flow (30 %), further oxidation produces more protruding grains (Figure 7.4 (c)).

We deposited 1 % Pt/Rh (9/1) over oxidized FeCralloy via solution combustion synthesis (Figure 7.5 (a)). EDS analysis confirmed the deposition of Pt and Rh. A map spectrum revealed that Pt and Rh distributes well over alumina scale but Pt tends to agglomerate with a particle size on the order of hundred nanometers. The surface alumina has a amorphous and fluffy structure, which corresponds to XRD analysis. Compared to spray pyrolysis method, Pt particle size from 80 to 3000 nm [157], solution combustion synthesis prepares much uniform Pt particles. A point spectrum pointed that the weight ratio of Pt/Rh particle was close to 7. The catalyst surface was intact after reacting at 2 MPa with no visible coke (Figure 7.5 (b)). A map spectrum analysis detected a mass ratio of carbon less than 2 %. After regeneration, amorphous alumina covered the surface more uniformly, while Pt granules remained isolated (Figure 7.5 (c)). This stable structure prevents Pt from migration and agglomeration. Compared to conventional supported catalysts, oxidized FeCralloy as supports avoids the delamination or cracking of the coated support, which deactivates catalysts.

7.4.2 Catalytic tests

We tested the catalyst activity in CPOX reaction without any pre-reduction procedure. CPOX catalysts usually needs activation in reducing gas such as hydrogen, to produce a stable metallic state [61]. We tested both non-pretreatment Pt FeCralloy catalyst and pre-reduced (2 h reduction in 10 % H_2 at 300 °C), and the results were similar with variance less than 5 %. This test confirmed that Pt was in the metallic state.

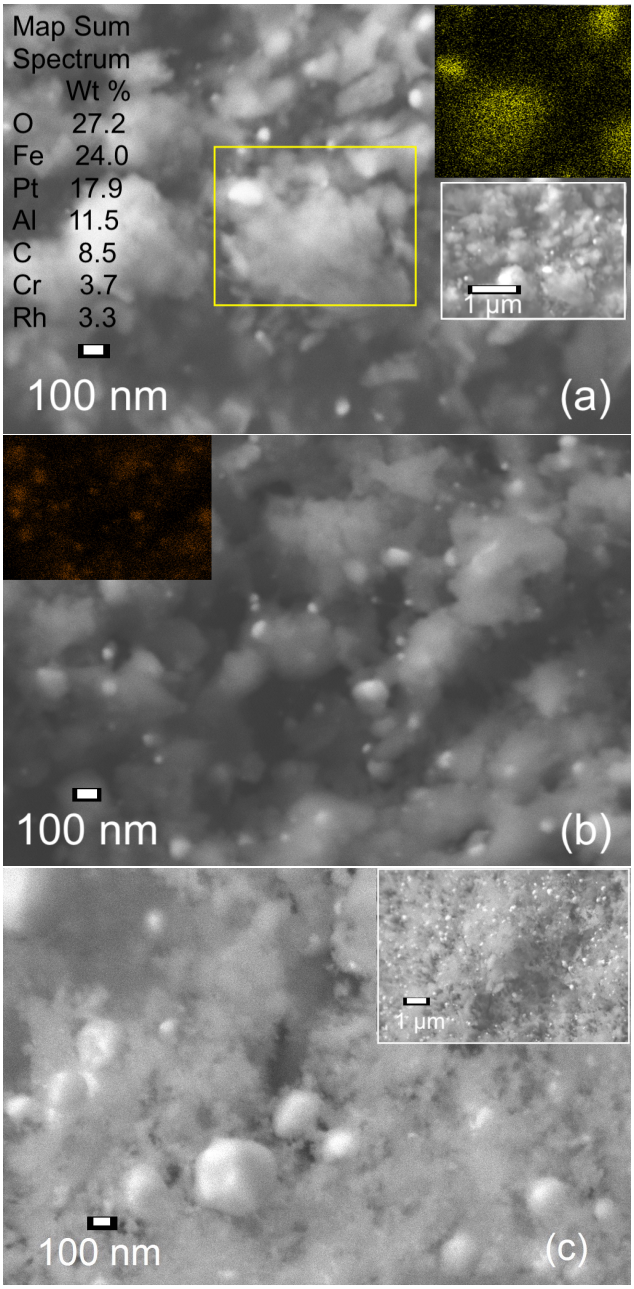

Figure 7.5 (a) Fresh Pt/Rh FeCralloy. The upper right picture shows the Pt distribution in the selected region; a map sum spectrum displays the element composition. (b) Used Pt/Rh FeCralloy after CPOX reaction. The upper left picture reveals the Pt distribution after rection. (c) Regenerated Pt/Rh FeCralloy.

At a pressure of 0.1 MPa or 2 MPa, we kept the contact time constant at 0.15 s (Table 7.1). The composition of oxygen in Argon is the same as it is in air (21 %). During each 65 min reaction, we measured the composition of the outlet products by GC 7 times, starting from 5 min and every 10 min thereafter. We calculated the average conversion and selectivity

and standard error. We also carried out blank tests at 0.1 MPa and 2 MPa, 900 °C without catalyst, but with 10 mm inert glass wool as a reactor filling.

Tests at atmospheric pressure

At 900 °C, 0.1 MPa, in the blank test, 26 % of the CH_4 (Figure 7.6, symbol : cross) reacted preferentially to complete oxidation products, CO_2.

Virgin FeCralloy, whereby Fe is the main active component, converted 50 % of CH_4 with 55 % selectivity to H_2 and 65 % selectivity to CO (Figure 7.6, symbol : hollow with plus). Among non-noble CPOX catalysts, Fe catalysts received the least consideration as it readily oxidizes when exposed to oxygen atmosphere at high temperature and is prone to produce CO_2 [21]. However, Fe has a melting point higher than nickel, so it is more stable. In FeCrAlloy, surface Al oxidizes more readily than Fe. As long as the Al reservoir is not depleted, the alumina scale protects Fe from oxidation. All oxygen was consumed ; however, oxygen moles from carbon monoxide and carbon dioxide did not add up to the feed oxygen, as it also oxidized the alumina layer. The variability of the virgin FeCralloy performance may be due to the competition between methane partial oxidation and surface Al oxidation. From the SEM pictures of the used virgin FeCralloy, the reacted methane forms coke mostly on the top the catalyst bed while the rest the catalyst bed becomes oxidized (Figure 7.4 (b)). According to the carbon balance, coke selectivity increased with time from 0 to 15 % (average : 7 %).

Oxidized FeCralloy, covered by an inert alumina scale, is considered inactive. EDS analysis reveals the maximum thickness of the alumina scale is 2 µm. Fe detected on the used oxidized FeCralloy (Figure 7.4 (b)) acted as active component and alumina scale grows during the reaction. It is reactive but hardly selective. During the first 25 min, its performance was similar to the virgin FeCralloy, but methane conversion and H_2 selectivity slowly decreased with time (Figure 7.6, symbol : hollow). CH_4 conversion averaged 49 % and H_2 and CO selectivity were 43 % and 53 %, respectively. Little coke (selectivity less than 7 %) formed based on a carbon balance. The oxidized FeCralloy with alumina scale as support were more stable than virgin FeCralloy.

Precious metals convert more methane at a higher rate and produce less coke compared to transition metals [4]. A low loading of precious metal catalyst with high activity can compensate for their high cost. The combination of transition metals with a low loading of precious metals decreases the catalyst cost while ensuring sufficient catalyst activity. Pt/Rh FeCralloy (Figure 7.6, symbol : solid) catalyst increased the methane conversion to 94 %. The CO selectivity increased concurrently to 78 %. It was outstanding in H_2 production with a selectivity of 94 %. CO_2 selectivity decreased to less than 10 % but coke selectivity was

slightly above 10 % according to the carbon balance. From SEM analysis, no visible coke was found on used Pt/Rh FeCralloy (Figure 7.5 (b)). However, coke forms over the reactor wall and the thermocouple.

Virgin and oxidized FeCralloy are both active at 0.1 MPa and 900 °C, however non-selective. FeCralloy catalysts with Pt and Rh are highly selective and resist coke formation.

To further investigate the reactivity of Pt/Rh FeCralloy catalyst, we recalculated the thermodynamic equilibrium with FactSage® Thermochemical Software (FACT pure substances database) [144] [145] and compared with catalytic performance as a function of temperature. The thermodynamic calculations considers all the possible reactions by minimizing the Gibbs energy.

At 0.1 MPa, the thermodynamic equilibrium (Figure 7.7, solid line) of methane conversion, H_2 and CO selectivity increases with temperature. Above 900 °C approaches to complete methane conversion and maximum H_2 and CO selectivity. 600 °C is the light-off temperature. Above 600 °C, the reactivity of Pt/Rh FeCralloy catalyst increased linearly. At 900 °C, we reached 95 % of equilibrium methane conversion and 90 % of equilibrium H_2 and 85 % of equilibrium CO selectivity. CO_2 selectivity increases while complete oxidation dominates below 450 °C, and drops while water-gas shift and dry reforming become significant. CO_2 selectivity with Pt/Rh FeCralloy catalyst follows the same trend, however more narrow and sharp, the peak temperature shifts to higher temperature, 700 °C. Coke preferably forms at low temperature according to the equilibrium calculation ; increasing temperature lowers C selectivity. Over 600 °C, Pt/Rh FeCralloy is coke free.

Tests at 2 MPa

The reactivity of virgin FeCralloy catalysts decreased with time (Figure 7.8, symbol : hollow with plus), mainly due to the asymmetrical carbon deposition and surface oxidation of the three catalyst disks (Figure 7.3 (b)). On average, 6 % less methane reacted at 2 MPa than at 0.1 MPa. The H_2 and CO selectivity dropped to 42 % and 49 %. Coke forms at higher rate with increasing pressure [156]. Based on a carbon balance, coke selectivity was twice as high at 2 MPa compared to 0.1 MPa.

The performance of oxidized FeCralloy was more stable versus virgin FeCralloy (Figure 7.8, symbol : hollow). The methane conversion was almost steady and only 1.0 % lower than at ambient pressure. H_2 declined 3 % more while CO selectivity dropped 7 % more. Coke selectivity was only 6 %, which is less than at ambient conditions.

Although pressure of 2 MPa restrained the activity of FeCralloy catalysts, the Pt/Rh FeCral-

loy was stable with time, and converted 47 % of the methane to H_2 and to CO with selectivity of 67 % and 62 %, respectively (Figure 7.8, symbol : solid). Based on the carbon balance, the coke selectivity during the 65 min reaction was steady and close to zero. Also EDS did not detect coke on the catalyst surface and its structure maintained its morphology after reaction (Figure 7.5 (c)). The addition of Pt/Rh presented outstanding resistance to coke formation at high pressure. Thus it is a suitable candidate for CPOX reaction at elevated pressure.

High pressure disfavors CPOX thermodynamically : methane conversion and H_2 and CO selectivity at 2 MPa (Figure 7.9, dash line) are lower than 0.1 MPa (Figure 7.9, solid line). In order to reach the same conversion and selectivity, it requires higher temperature. However, byproduct CO_2 and C selectivity increase above 600 °C. At 850 °C, 900 °C and 950 °C with Pt/Rh FeCralloy catalyst, methane conversion and H_2 and CO selectivity increased 7 %, 6 % and 9 %, respectively. At 850 °C, methane reached 72 % of equilibrium conversion, while H_2 and CO reached 79 % and 78 % of equilibrium selectivity. CO_2 selectivity dropped 11 %. C selectivity was below 10 %.

We investigated the effect of O_2/CH_4 on high pressure CPOX (Figure 7.10). Feeding more oxygen reduced coke accumulation and increased methane conversion from 47 % at 0.5 to 82 % at 0.7. The O_2/CH_4 ratio affected the CO selectivity less. An O_2/CH_4 ratio of 0.7 was superior in H_2 selectivity (72.0 %).

At 2 MPa, 900 °C, with an O_2/CH_4 feed ratio of 0.7, we performed a 255 min CPOX reaction with the regenerated Pt/Rh FeCralloy catalyst (Figure 7.11). Methane conversion decreased with time and became stable after 100 min with approximately 10 % drop. H_2 selectivity fluctuated over time with a 15 % decline and CO selectivity gradually reduced around 15 %. Also we compared its performance with the previous 65 min CPOX reaction (Figure 7.10, ratio of 0.7) under the same condition. The beginning of the extended test almost duplicated the methane conversion of the 65 minute reaction. CO selectivity followed the same trend and decreased slightly. The H_2 selectivity of the extended test declined continuously.

We regenerated the catalyst after each test with a mole fraction of 30 % O_2 stream (balance Ar). FeCralloy loaded with Pt/Rh produced much less coke. Oxygen combusts coke within 10 min at reaction temperature at 0.1 MPa and longer at at 2 MPa (based on GC traces). With the regenerated Pt/Rh FeCralloy catalyst, the repeatability was good for the 65 min tests at both 0.1 MPa and 2 MPa. Including the screening tests as well as the repeat tests at 0.1 MPa and 2 MPa, this catalyst operated over 80 h and reached the same performance after the regeneration steps. Figure 7.12 compares the regenerated Pt/Rh FeCralloy catalyst performance at 2, 6 and 12 run at temperature of 900 °C, 2 MPa, CH_4/O_2=2, at a contact time of 0.15 s. The regeneration process monitored by GC has delay due to offline analysis. Methane

conversion and H_2 and CO selectivity fluctuated, mainly due to the different regeneration time and oxidative state of the catalyst.

7.5 Conclusions

Combining CPOX with FT in a Micro-Refinery Unit to make synthetic fuel brings both environmental and economic benefits. The challenge of integrating CPOX and FT is converting methane to suitable syngas at high pressure. A suitable catalyst needs to resist both high temperature and mechanical stresses introduced by high pressure.

FeCralloy knitted fibres are active for the CPOX reaction. With a protective alumina scale, the oxidized FeCralloy is stable. Adding precious metals of Pt/Rh highly increased the methane conversion and syngas selectivity : it converted over 90 % of methane with a 94 % H_2 selectivity and 78 % CO selectivity at atmospheric pressure. Although high pressure reduced reactivity of CPOX catalysts, Pt/Rh FeCralloy catalyst still achieved 67 % H_2 selectivity and 62 % CO selectivity with a H_2/CO ratio of 2.2 at 2 MPa. More significantly, little coke formed at high pressure. Increasing the O_2/CH_4 ratio to 0.7, we obtained 82 % methane conversion and 72 % H_2 selectivity and 59 % CO selectivity. Overall Pt/Rh FeCralloy catalyst is a strong candidate for high pressure CPOX catalyst ; while, it is best suited for forced concentration cycling operation like a redox reactor.

Acknowledgement

The authors acknowledge the financial support from the Natural Sciences and Engineering Research Council of Canada (NSERC).

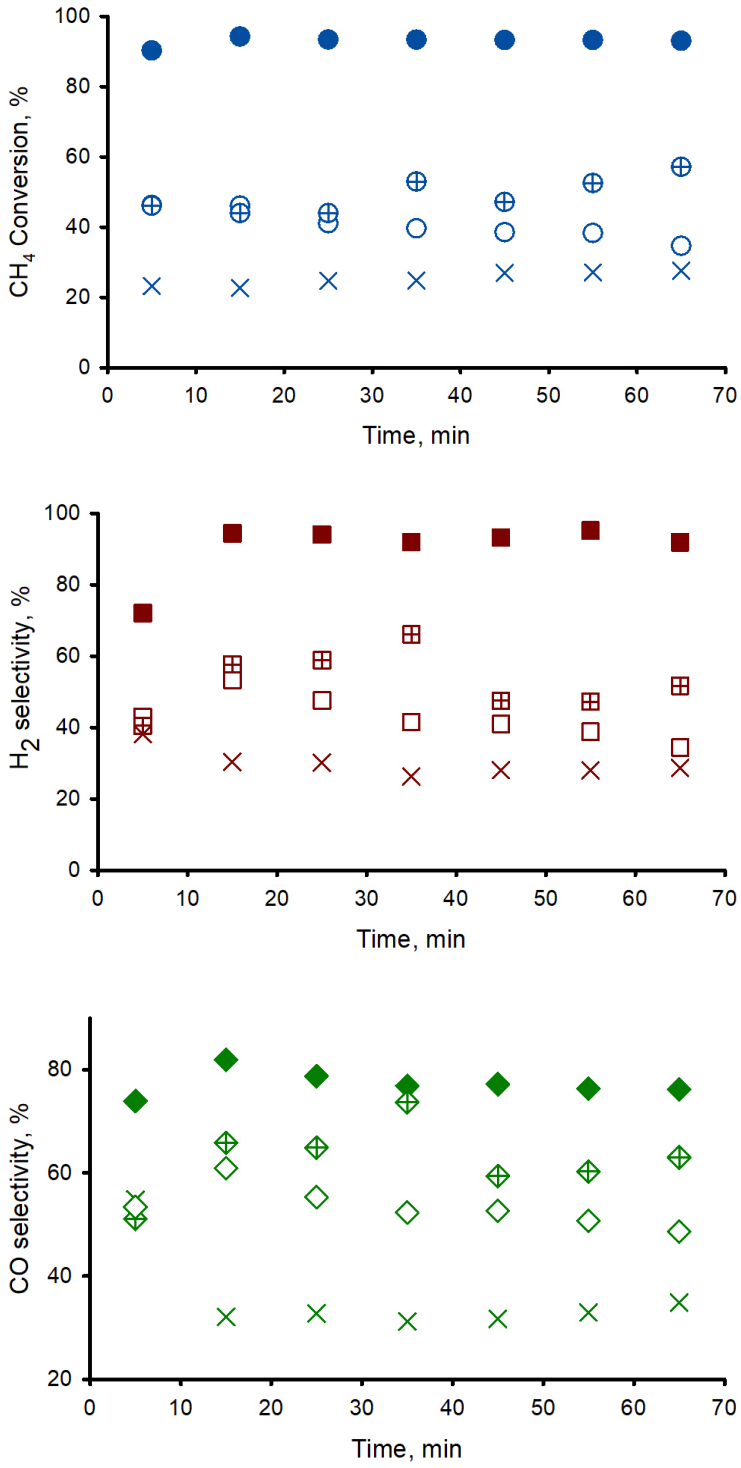

Figure 7.6 (a) Methane conversion; (b) H_2 selectivity; (c) CO selectivity vs. time under atmosphere pressure with CH_4/O_2 of 2, 900 °C, $\tau = 0.15$ s. Cross : blank; solid symbol : Pt/Rh FeCralloy; hollow symbol with plus : virgin FeCralloy; hollow symbol : oxidized Fecralloy.

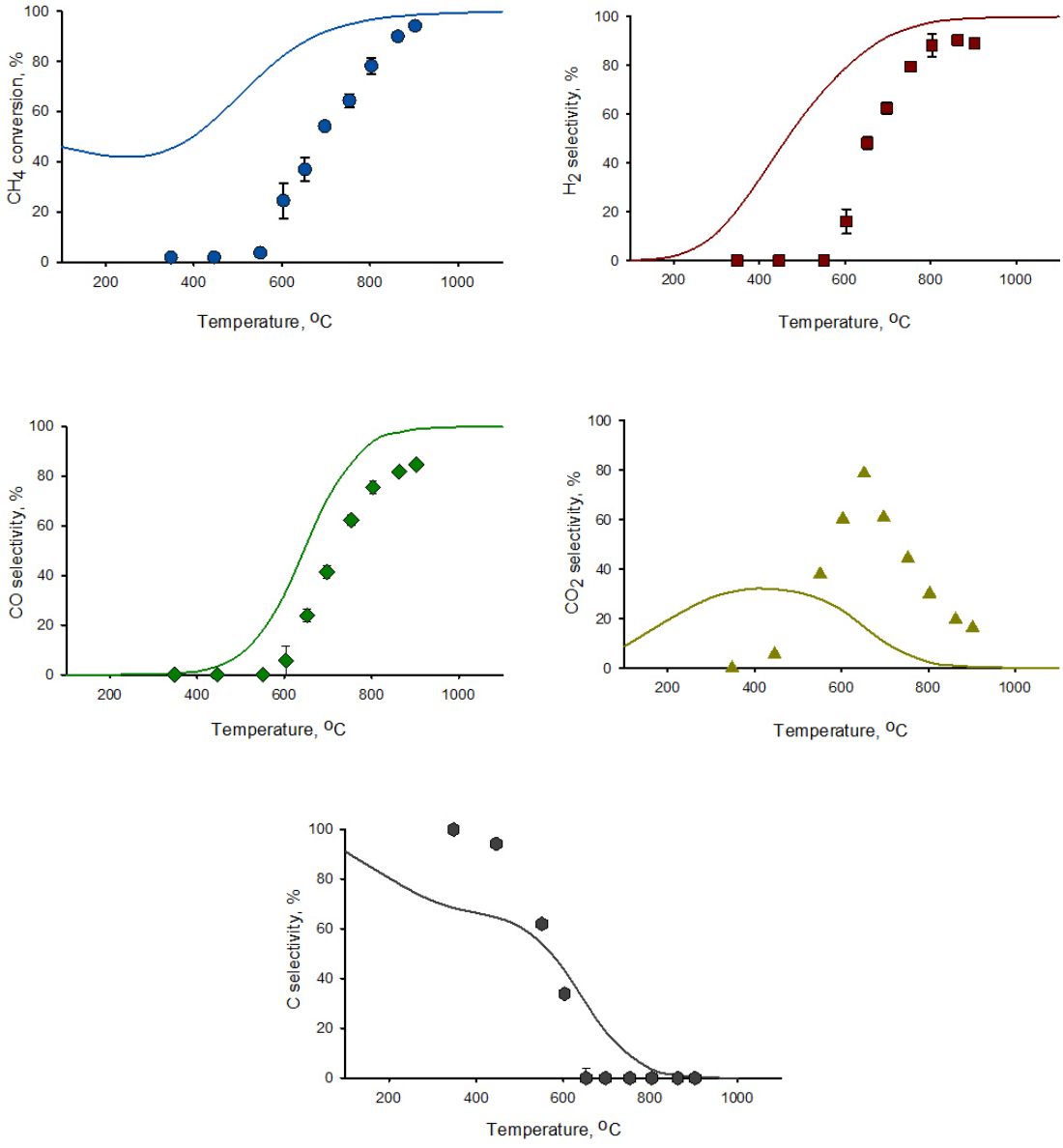

Figure 7.7 Compared with equilibrium of 0.1 MPa (solid line) calculated by Factsage, the effect of temperature on methane conversion (blue cicle), H_2 selectivity (red square), CO selectivity (green diamond), CO_2 selectivity (yellow triangle) and C selectivity (grey circle) with Pt/Rh FeCralloy catalyst at 0.1 MPa, CH_4/O_2=2, at a contact time of 0.15 s.

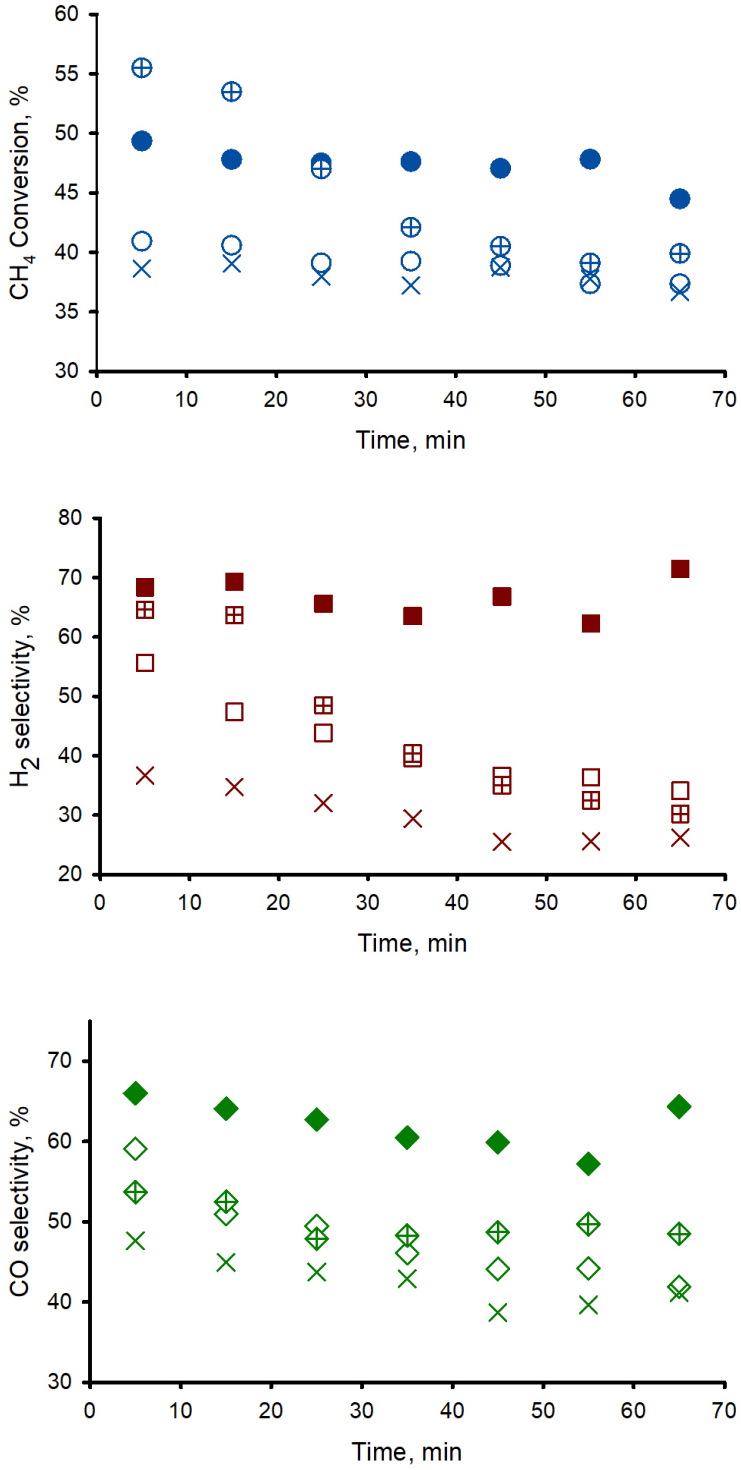

Figure 7.8 (a) Methane conversion ; (b) H_2 selectivity ; (c) CO selectivity vs. time under elevated pressure of 2 MPa with CH_4/O_2 of 2, 900 °C, $\tau = 0.15$ s. Cross : blank ; solid symbol : Pt/Rh FeCralloy ; hollow symbol with plus : virgin FeCralloy ; hollow symbol : oxidized Fecralloy.

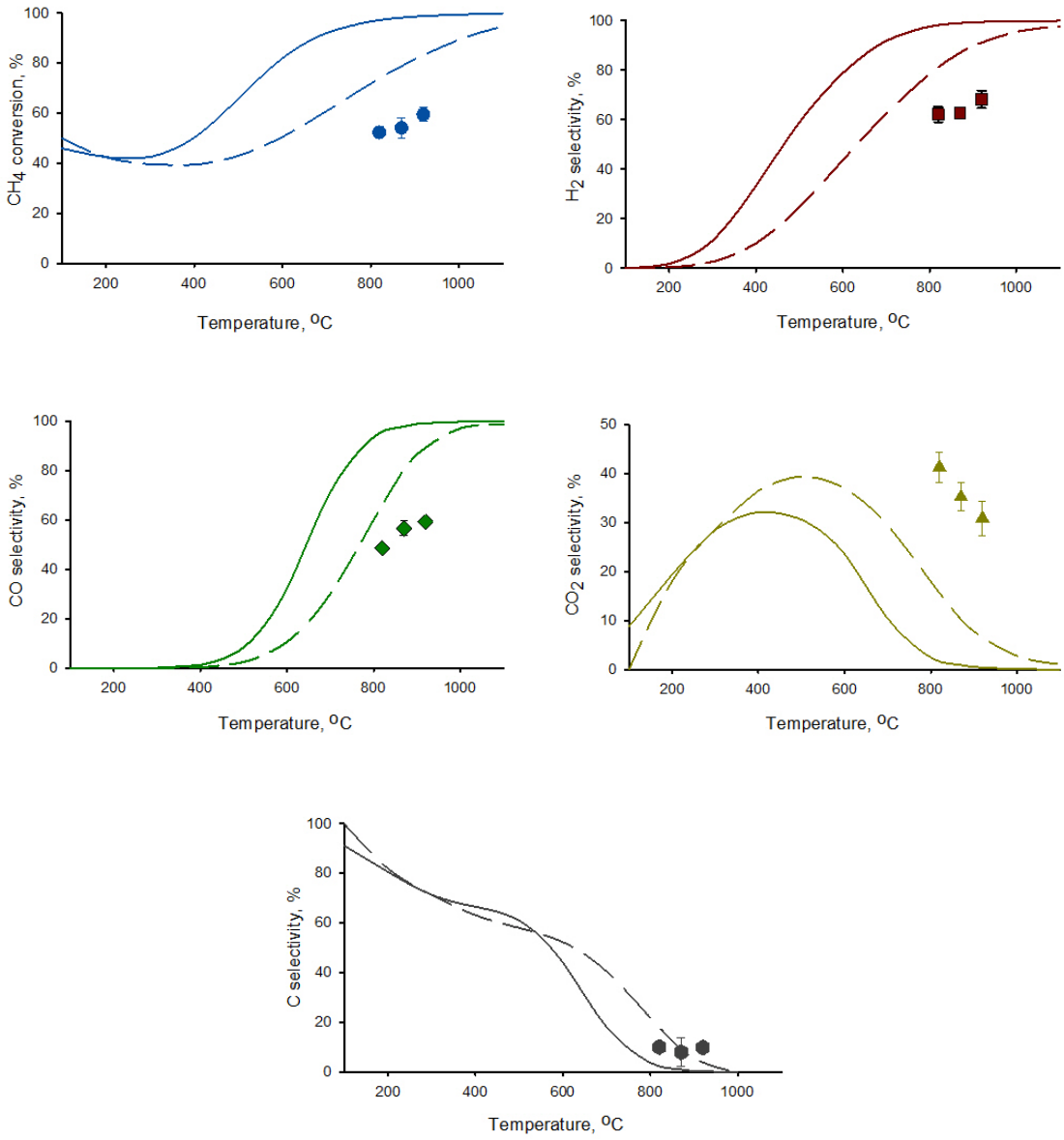

Figure 7.9 Compared with equilibrium of 0.1 MPa (solid line) and 2 MPa (dash line) calculated by FactSage, methane conversion (blue cicle), H_2 selectivity (red square), CO selectivity (green diamond), CO_2 selectivity (yellow triangle) and C selectivity (grey circle) with Pt/Rh FeCralloy catalyst at 2 MPa, CH_4/O_2=2, at a contact time of 0.15 s.

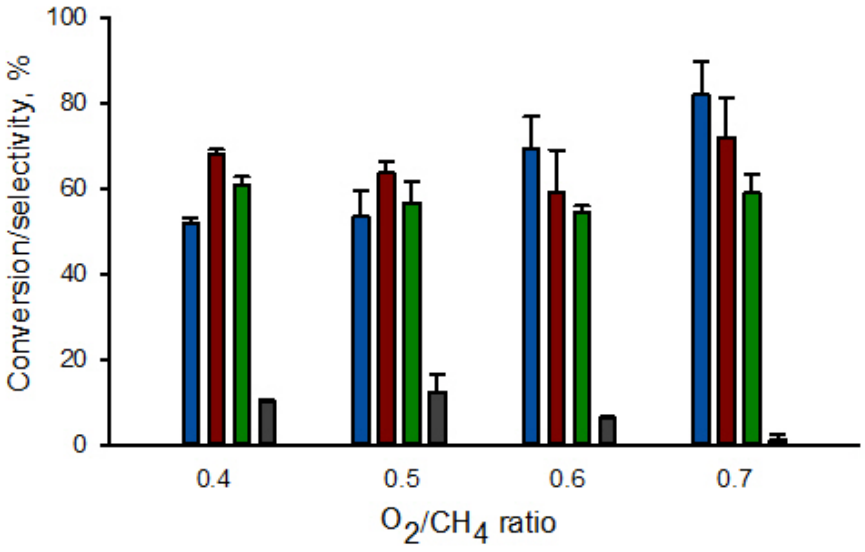

Figure 7.10 The effect of CH_4/O_2 ratio on methane conversion (blue), H_2 selectivity (red), CO selectivity (green) and C selectivity (grey) with Pt/Rh FeCralloy catalyst at 2 MPa, 900 °C, at a contact time of 0.15 s.

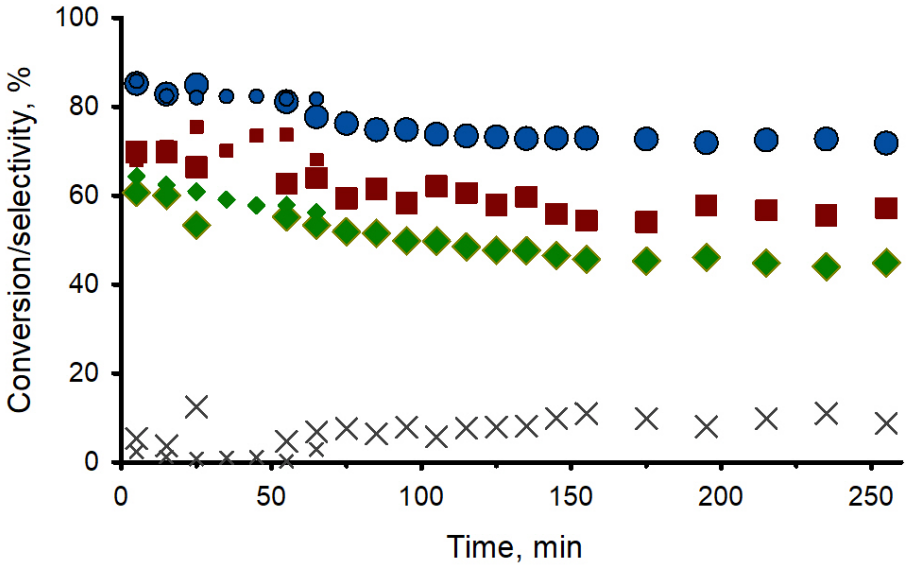

Figure 7.11 A 255 min CPOX reaction at 900 °C, 2 MPa, CH_4/O_2=0.7, with Pt/Rh FeCralloy catalyst (due to the breakdown of mass flow controller, we lost two data points at 35 and 45 min). We also compared the methane conversion (blue cicle), H_2 selectivity (red square), CO selectivity (green diamond) and C selectivity (grey cross) of the 255 min test with the previous 65 min test (smaller symbols) under the same condition.

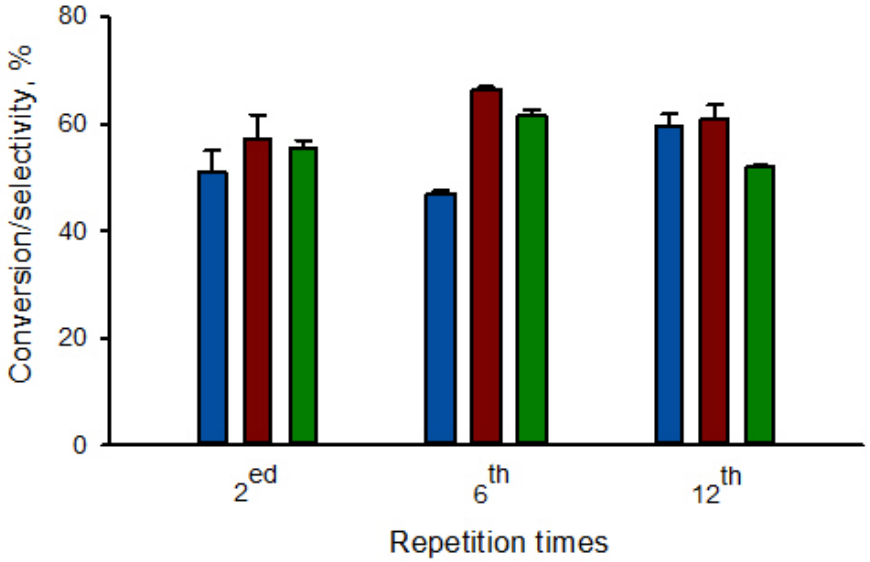

Figure 7.12 The repeatability of 1 % Pt/Rh FeCralloy catalyst in CPOX reaction at 900 °C, 2 MPa, CH_4/O_2=0.5, at a contact time of 0.15 s. Methane conversion (blue), H_2 selectivity (red), CO selectivity (green)

CHAPTER 8 ARTICLE 4 - THERMODYNAMICALLY UNCONSTRAINED FORCED CONCENTRATION CYCLING OF METHANE CATALYTIC PARTIAL OXIDATION OF CEO2 ON FECRALLOY KNIT

Zhenni Ma, Patrice Perreault, Diego C. Pelegrin, Daria C. Boffito and Gregory S. Patience

Sumitted to : Applied Energy, 2019

8.1 Abstract

Converting waste associate gas lacks economical techniques. Micro Gas-to-Liquids technology (μGtL) transforms flared natural gas into value-added synthetic fuel. A high pressure syngas step (catalytic partial oxidation of methane, CPOX) meets the demand of combing with Fischer-Tropsch (FT) in a compact unit.

FeCralloy knitted fibres with high thermal conductivity and low pressure drop, resist thermal and mechanical stresses from high pressure CPOX. The FeCralloy catalysts are free of pre-reduction treatments. We deposited Pt and/or CeO_2 over the fibre surface via solution combustion synthesis. CeO_2 FeCralloy catalyst revealed superior activity in converting methane to syngas under atmosphere pressure ; but high pressure restrained its activity. Pt/CeO_2 FeCralloy was inert at both 0.1 MPa and 2 MPa. However, both catalysts demonstrated high activity in quasi chemical looping partial oxidation of methane : methane completely convert to H_2 and only CO was produced during the oxidation step. kinetic models and 3 oxidation-reduction cycles at high pressure assumed the mechanism of surface reaction on CeO_2 based FeCralloy catalyst.

8.2 Introduction

Natural gas presents as associated gas in oil fields [14]. Oil producers sometimes reinject the associated gas to reinforce the oil recovery, however, a significant fraction (5 % of the total natural gas production) is flared [15], due to economical issues and technical limitations. "Zero Routine Flaring by 2030" [150], globally advocated by major oil companies, governments and environmental institutions, requests technical and economic alternatives to stop flaring.

Syngas creates flexibility for the chemical industry and the manufacture of synthetic fuels (synfuels) thus is important in energy conversion [16, 169]. Recent trends in syngas application focus on the conversion of inexpensive remote natural gas into liquid fuels (GtL), such as oil

which is the most versatile fossil fuel with high energy density and is easy to transport with the existing pipelines and frastructure.

The Fischer-Tropsch (FT) technology is well–established in both large-scale and small-scale plants. A compact MRU (Micro Refinery Unit) [29] housing reactions of syngas production and FT in a single unit, is feasible to travel to remote reservoirs and convert flared gas to value–added oil.

Compared to steam methane reforming (SMR), dry reforming (DRM) and auto-thermal reforming (ATR) [105, 75], POX is mildly exothermic and produces H_2 and CO at a molar ratio of 2 (ideal for FT). Catalytic partial oxidation of methane (CPOX) reduces the reaction temperature below 1000 °C is suitable for micro and small scale. In practice, capital cost is lower without expensive superheated steam generation systems and because it allows higher gas space velocity.

Thermodynamically, FT reaction favors pressure over 2 MPa to produce long chain hydrocarbons [152], however, CPOX reaction favors low pressure for CH_4 conversion, and CO and H_2 selectivity. Producing syngas at high pressure to meet the downstream requirement of FT process is challenging. There is few work on high pressure CPOX [94, 95, 96, 97, 98]. Lyubovsky et al [94] demonstrated CPOX with microlith based catalysts at pressures up to 0.8 MPa. The product composition profiles indicated high initial selectivity to CO (> 85 %) and low initial selectivity to H_2. Burke et al [95] carried out CPOX with $Rh/\gamma\text{-}Al_2O_3$ foam monolith catalyst at pressures up to 1.5 MPa. Methane conversions was up to 54 % with O_2 conversion of 86 % and selectivities of CO and H_2 are 89 % and 65% respectively. Larsen et al [96] presented CPOX with Rh and Pt coated foams from 0.1 to 1.1 MPa total pressure. Fichtner et al [98] tested microstructured honeycomb catalysts at operating pressure up to 1.2 MPa with oxygen and up to 2.0 MPa with air at a catalyst temperature of 1100 °C. The methane conversion rate drops from 90 % at 0.15 MPa to 77 % at 2 MPa. H_2 and CO selectivity declined 83 % and 76 % repectively. Basini et al [97] demonstrated the possibility to perform a bench-scale reactor at short contact time at a pressure of 20 atm.

Despite the thermodynamic disadvantage, the choice of catalyst is crucial to CPOX reaction under condition of high temperature and high pressure simultaneous [94, 155, 96, 97].

FeCralloy knitted fibres are superior to conventional supports because of their excellent mechanical properties and high thermal conductivity. FeCralloy is an outstanding alloy material which could work continuously under temperature of 1000 °C over 3000 h [162, 163]. In gas-fired burners, it distributes heat uniformly. Figure 8.1 exhibits FeCralloy when heated over 600 °C and by infrared camera we see a uniform temperature distribution. Also, FeCralloy allows high space velocities and a low pressure drop [164, 165]. Figure 8.2 compares the

pressure drop between traditional inert reactor fillings, glasswool and sand, and FeCralloy under different gas flow rate. FeCralloy allows gas passing freely, and its pressure drop is negligible at room temperature and ambient pressure. Its flexibility makes scale-up more straightforward and achievable. Furthermore, the price of noble metal supported FeCralloy is competitive to precious metal gauzes (Pt, Rh, etc. [4, 26, 27, 28, 29]).

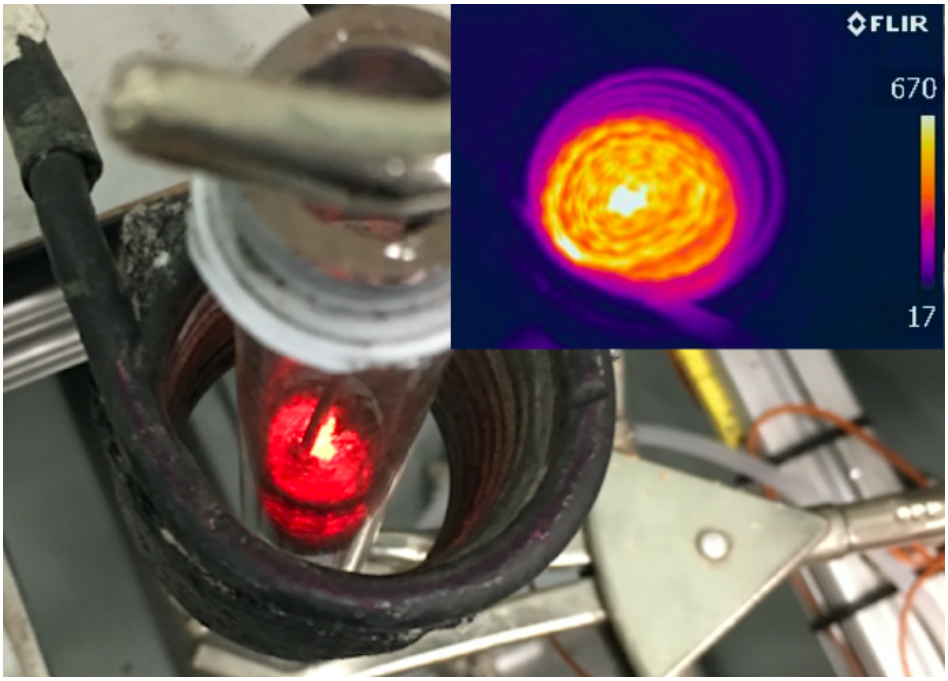

Figure 8.1 Heated FeCralloy (>600 °C) and its temperature distribution taken by FLIR T420 infrared camera.

CeO_2 has a cubic fluorite structure [170]. It stores and releases oxygen via cycling the Ce^{3+}/Ce^{4+} redox couple [171, 172] :

$$CeO_2 \leftrightarrow CeO_{2-x} + \frac{x}{2}O_2 \tag{8.1}$$

CeO_2 maintains its fluorite crystal structure even after loses considerable lattice oxygen and forms oxygen vacancies. Surface oxygen and oxygen vacancies are more active than bulk oxygen [173]. CeO_2 is attractive as catalyst or support for heterogeneous catalytic reactions, such as CO oxidation [174], water gas shift [175, 176, 177], steam reforming [178] and methane partial oxidation [179, 180].

In this work, we prepared two CeO_2 based FeCralloy catalyst : 5 % CeO_2 and 1 % Pt/5 % CeO_2 supported on oxidized FeCralloy knitted fibres. We explored their reactivities from 300 °C to 900 °C and pressure of 0.1 MPa and 2 MPa. Inspired by chemical looping process,

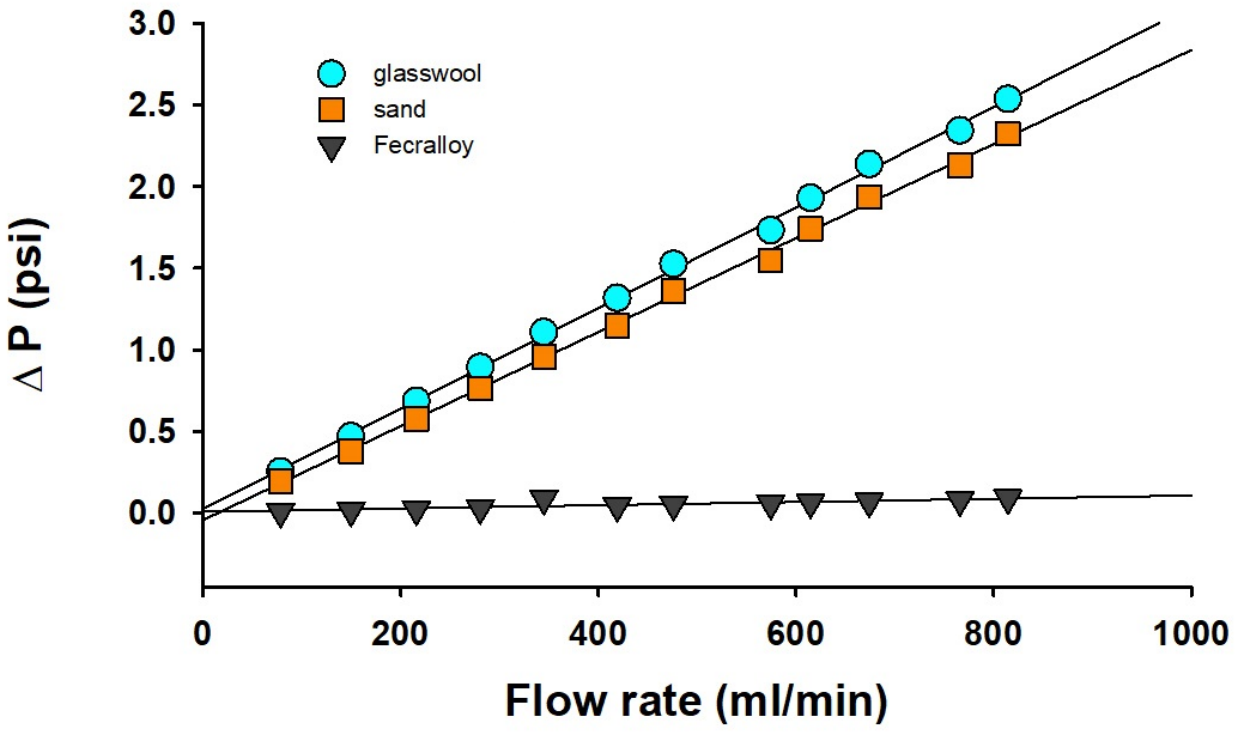

Figure 8.2 Comparison of the pressure drop of common inert reactor fillings, glasswool and sand, and FeCralloy under different flow rate at room temperature and ambient pressure.

we separately fed methane and oxygen and investigate the kinetics of methane activation and oxidation on the CeO_2 based FeCralloy catalyst.

8.3 Experimental

8.3.1 Catalyst preparation

FeCralloy as support has a flexible knitted textile structure. The main components are Fe (74 %), Cr (20 % chromium) and Al (5 %). We sonicated the virgin FeCralloy in a water/acetone solution (1 :1) for 30 min to remove surface organic dirts. Then a muffle furnace (a Neytech model 3-550) dried the FeCralloy fibres at 120 °C for 1 h and calcined them at 1000 °C for 3 h at a heating and cooling rate of 5 °C min^{-1}. The oxidized FeCralloy lost metal lustre and became dark.

We cut the woven fibres into 10 mm×10 mm squares. Then we coated active components, Pt and/or CeO_2 by solution combustion synthesis (SCS). To minimize surface deformation of

FeCralloy, we deposited the metals on oxidized FeCralloy. Aqueous solutions containing metal precursors ($Pt(NH_3)_4(NO_3)_2$, Sigma Aldrich ; $Ce(NO_3)_3{\cdot}6H_2O$, Sigma Aldrich) and the fuel ($CO(NH_2)_2$, Sigma Aldrich) wet the knitted fibres. Fine particles formed on the FeCralloy fibres when the moistened fibres reached ignition temperature at 600 °C [156].

To minimize the catalyst cost, we must minimize the mass of the noble metals while maintaining their activity. Precious metal loading ranges from 0.05 % to 10 % [139]. An average loading of 5 % is common for the screening tests [7]. The pre-determined mass fraction of the CeO_2 FeCralloy catalyst contained a mass of 5 % of CeO_2 ; the Pt/CeO_2 FeCralloy catalyst contained a Pt and CeO_2 mass fraction of 1 % and 5 %, respectively. To confirm that the total mass fraction of Pt and/or CeO_2, we weighed the catalyst before and after deposition. Finally, we calcined the catalysts at 1000 °C in the muffle furnace for 3 h at a heating and cooling rate of 5 °C min^{-1}.

An Autosorb-1 analyzed the surface area of each sample via N_2 adsorption/desorption (Table 8.1). 3h degasing at 200 °C eliminates residual water and volatile impurities.

A Philips X-Pert MPD diffractometer equipped with a Cu Kα radiation at 50 kv and 40 mA analyzed the diffraction of the crystalline phases. The scanning rate was 0.05 ° s^{-1} with 2θ ranging from 20° to 90°. We fitted the peaks with the PCPFWIN database.

Scanning electron microscopy (SEM, model : JSM-7600A) with Energy Dispersive Spectroscopy (EDS) inspected the surface morphology and the type and surface content of elements. [99].

8.3.2 Experimental setup

The reactor for CPOX was a 300 mm long reactor with quartz (ID of 8 mm) as interior and stainless steel as exterior [157]. Two or three circular disks of CeO_2 based FeCralloy catalysts settled in the middle of the reactor at a height of 175 mm. The total height of the catalyst bed equals the sum of 10 mm glasswool and the height of the catalysts. We did not pre–reduce the catalyst [140]. A type K thermocouple above the catalyst bed at a height of 175 mm observed the temperature at the top of the catalyst. A back pressure valve sustained a constant reactor pressure. We fed the cold gases from the top to bottom. A water adsorbent between the reactor outlet and GC inlet traps water and protects MS and GC. We weighed the water adsorbent before and after each test and calculated average water formation rate. A Hiden QIC-20 Quadrupole Mass Spectrometer online monitored the reaction and an Agilent gas-chromatograph 7890 B offline analyzed the inlet gas composition before reaction and the outlet gas during reaction following the ASTM D1945 standard. Calibration gases (mixture

of CH_4, CO, CO_2, O_2 in Ar, Air Liquide) corrected GC and MS.

We replaced 21 % O_2 in Ar of air as the oxidant and fed CH_4 and O_2 at a ratio of 2 (CH_4 : O_2 : Ar = 30 : 15 : 45). The conversion of methane (X_{CH_4}) and selectivity towards H_2 (S_{H_2}), CO (S_{CO}) and CO_2 (S_{CO_2}) were calculated as follows :

$$X_{\mathrm{CH_4}}(\%) = \frac{F^{\mathrm{in}}_{\mathrm{CH_4}} - F^{\mathrm{out}}_{\mathrm{CH_4}}}{F^{\mathrm{in}}_{CH4}} \times 100 \tag{8.2}$$

$$S_{\mathrm{H_2}}(\%) = \frac{F^{\mathrm{out}}_{H2}}{(F^{\mathrm{in}}_{\mathrm{CH_4}} - F^{\mathrm{out}}_{\mathrm{CH_4}}) \times 2} \times 100 \tag{8.3}$$

$$S_{\mathrm{CO}}(\%) = \frac{F^{\mathrm{out}}_{CO}}{F^{\mathrm{in}}_{\mathrm{CH_4}} - F^{\mathrm{out}}_{\mathrm{CH_4}}} \times 100 \tag{8.4}$$

$$S_{\mathrm{CO_2}}(\%) = \frac{F^{\mathrm{out}}_{CO2}}{F^{\mathrm{in}}_{\mathrm{CH_4}} - F^{\mathrm{out}}_{\mathrm{CH_4}}} \times 100 \tag{8.5}$$

Where : $F^{\mathrm{in}}_{\mathrm{CH_4}}$ and $F^{\mathrm{out}}_{\mathrm{CH_4}}$ are the molar flow rates of methane at the reactor entrance and exit, respectively ; $F^{\mathrm{out}}_{\mathrm{CO}}$, $F^{\mathrm{out}}_{\mathrm{H_2}}$ and $F^{\mathrm{out}}_{\mathrm{CO_2}}$ are the molar flow rates of CO, H_2 and CO_2 at the reactor exit.

We calculated the selectivity of coke based on the C mass balance. We determined the O mass balance as :

$$O_{\mathrm{MB}} = \frac{2F^{\mathrm{out}}_{O2} + 2F^{\mathrm{out}}_{CO2} + F^{\mathrm{out}}_{CO} + \overline{F}^{\mathrm{measured}}_{H2O}}{2F^{\mathrm{in}}_{\mathrm{O_2}}} \times 100 \tag{8.6}$$

We compared the reactivity of FeCralloy catalysts at different temperature at ambient pressure with a constant weight hourly space velocity of 1.1 $g_{CH_4}/g_{cat}/h$ and at mosphere pressure (0.1 MPa) and elevated pressure (2 MPa) maintaining a constant contact time at 150 ms ($\frac{V_{\mathrm{cat}}}{Q_{\mathrm{total}}}$). Each test lasted 65 min and was measured by GC at an interval of 10 min. In order to keep the same catalytic condition and remove the coke produced by last test, we regenerated the catalyst before each test by feeding 50 mL min^{-1} oxygen flow (O_2 : 21 %, Ar : balance), and monitored the regeneration process by MS to avoid over oxidation.

8.4 Results and Discussion

8.4.1 Catalyst characterization

Specific surface area

FeCralloy fibres are non-porous materials. After calcination at 1000 C for 3h, the specific surface area of the oxidized FeCralloy didn't change as the oxidative scale is α–alumina. Through solution combustion synthesis, we coated 5 % CeO_2 over the oxidized FeCralloy surface, and the coating layer didn't increase the specific surface area of the catalyst. When we deposited 1 % Pt and 5 % CeO2 over the surface, the surface area increased to 6.242 $m^2\,g^{-1}$ (Table 8.1).

XRD

The X-ray diffraction patterns of fresh CeO_2 and Pt-CeO_2 catalysts (Figure 8.3. 1 and 2 respectively) supported on oxidized FeCralloy suggested that CeO_2 and Pt phase are crystalline. 1 % Pt is a low loading thus usually invisible in XRD patterns [179]. As an example, in previous work of 1 % Pt/CeO_2-Al_2O_3 FeCralloy (Figure 8.3. 3, [157]), we only noticed peaks of FeCr and Al_2O_3.

SEM with EDS

Electron microscopy surveyed the surface morphology of each sample as i) fresh, ii) used, and iii) regenerated catalyst (Figure 8.4 - 8.5).

The surface of original FeCralloy (virgin FeCralloy) is non porous and relatively smooth. The calcination of virgin FeCralloy to oxidized FeCralloy formed an uniform alumina layer, which prevents the bulk Fe and Cr from oxidation and extends the lifetime of FeCralloy under high temperature operation.

Table 8.1 Catalyst composition and surface area.

Catalyst	Pt %	CeO_2 %	BET surface area $m^2\,g^{-1}$
Virgin Fecralloy	–	–	0
Oxidized Fecralloy	–	–	0.020
CeO_2 Fecralloy	–	5.0	0
Pt/CeO_2 Fecralloy	1.0	5.0	6.242

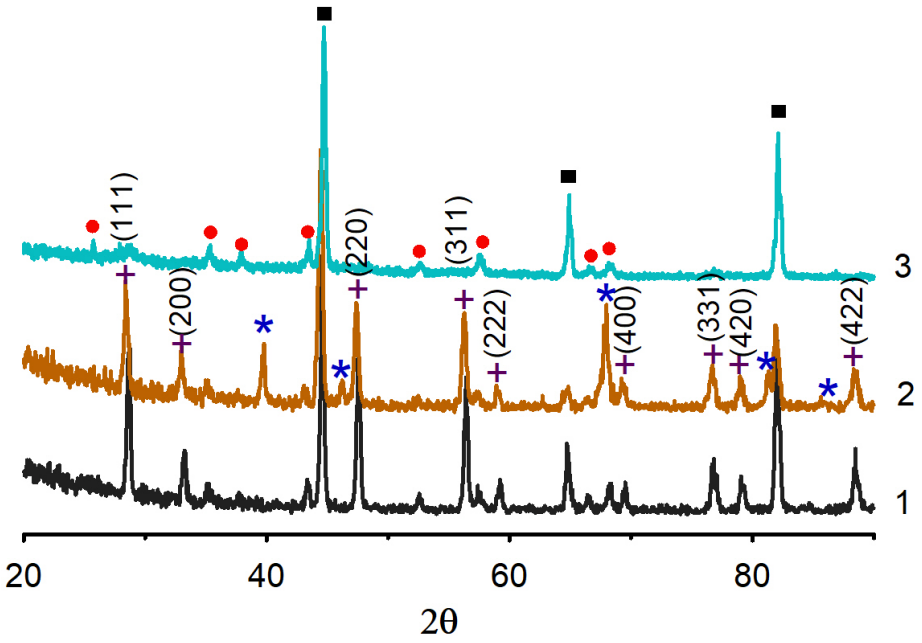

Figure 8.3 XRD patterns : 1) 5 % CeO_2 FeCralloy ; 2) 1 % Pt/ 5 % CeO_2 FeCralloy ; 3) 1 % Pt/CeO_2-Al_2O_3 FeCralloy (CeO_2 : Al_2O_3 = 79 : 21). Black squre : FeCr ; red circle : α-Al_2O_3 ; blue star : Pt ; purple plus : CeO_2.

We depositied 5 % CeO_2 over oxidized FeCralloy by solution combustion synthesis (Figure 8.4 (a)). Cerium oxide particles agglomerated to a pile of humps on the amorphous alumina surface. Each separate particle is rod-shaped. A map spectrum at 10 eV detected much less alumina and little Fe than oxidized FeCralloy, therefore CeO_2 coated on oxidized FeCralloy thoroughly and uniformly.

After reaction at 2 MPa, massive coke whiskers covered the reactive surface. In bare regions covered by less coke, rod–like cerium oxide independently distributed (Figure 8.4 (b)).

Regeneration of used CeO_2 FeCralloy catalysts led to more uniform clavate cerium oxide particles with a diameter of around 200 nm (Figure 8.4 (c)). The regeneration effectively cleared away the superficial whisker coke and completely exposed the active phase. Rod–shaped ceria particles revealed good stability and resistance to high temperature and pressure stresses. CeO_2 with rod–like or cube–like shapes exhibit higher oxygen storage capacity than spheroidal particles [181, 182, 183]. Lattice oxygen migrates more easily from the bulk to the surface [184].

On the surface of Pt/CeO_2 Fecralloy catalyst, CeO_2 agglomerates spread over the oxidized

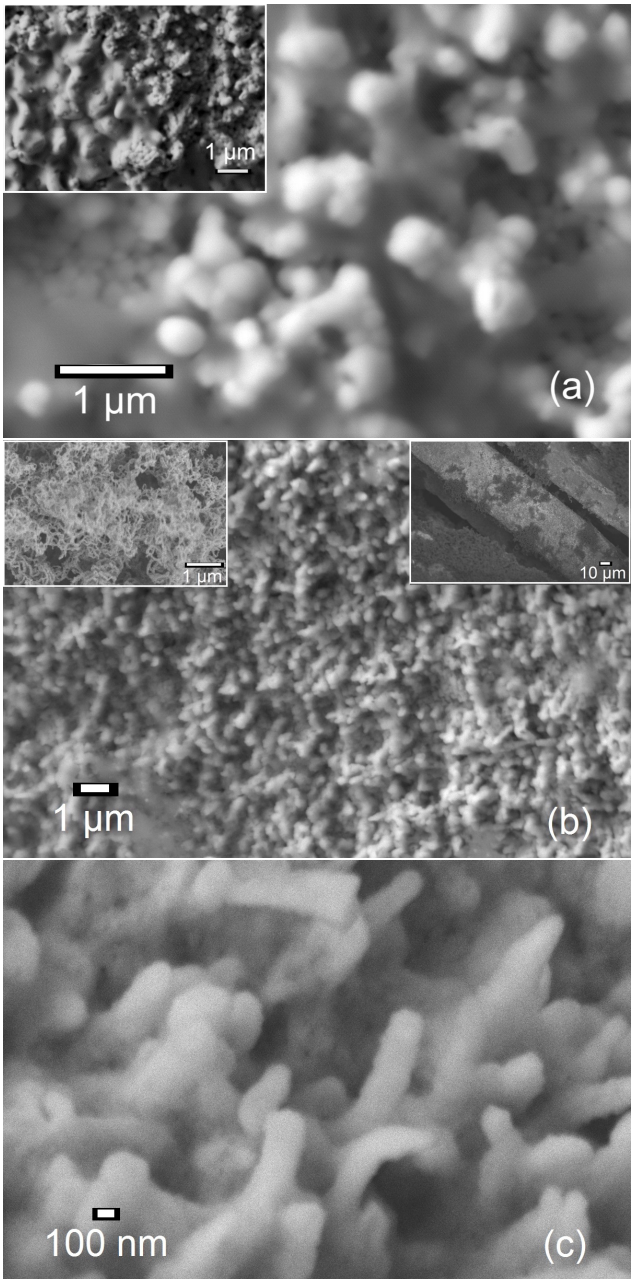

Figure 8.4 (a) Fresh CeO_2 FeCralloy (Map spectrum Wt % : Ce, 56.9 ; O, 18.9 ; C, 14.1 ; Al, 6.4 ; Fe, 2.3). The upper left picture magnifies and exposes the aggolomeration of cerium oxide. (b) The bare part of used CeO_2 FeCralloy after CPOX reaction. The upper left picture shows the whisker coke that attached to the fibre surface. The upper right picture manifies a catalyst fibre not fully covered with whisker coke. (c) Regenerated CeO_2 FeCralloy.

FeCralloy surface, while Pt particles (particle size smaller than a few hundred nanometers) populated on the agglomerates' apex or surrounded by the CeO_2 particles (Figure 8.5 (a)). We assumed that it was the initial stage of Pt encapsulation. A map sum spectrum analysis

indicated that the mass ratio of CeO_2/Pt was close to 4.

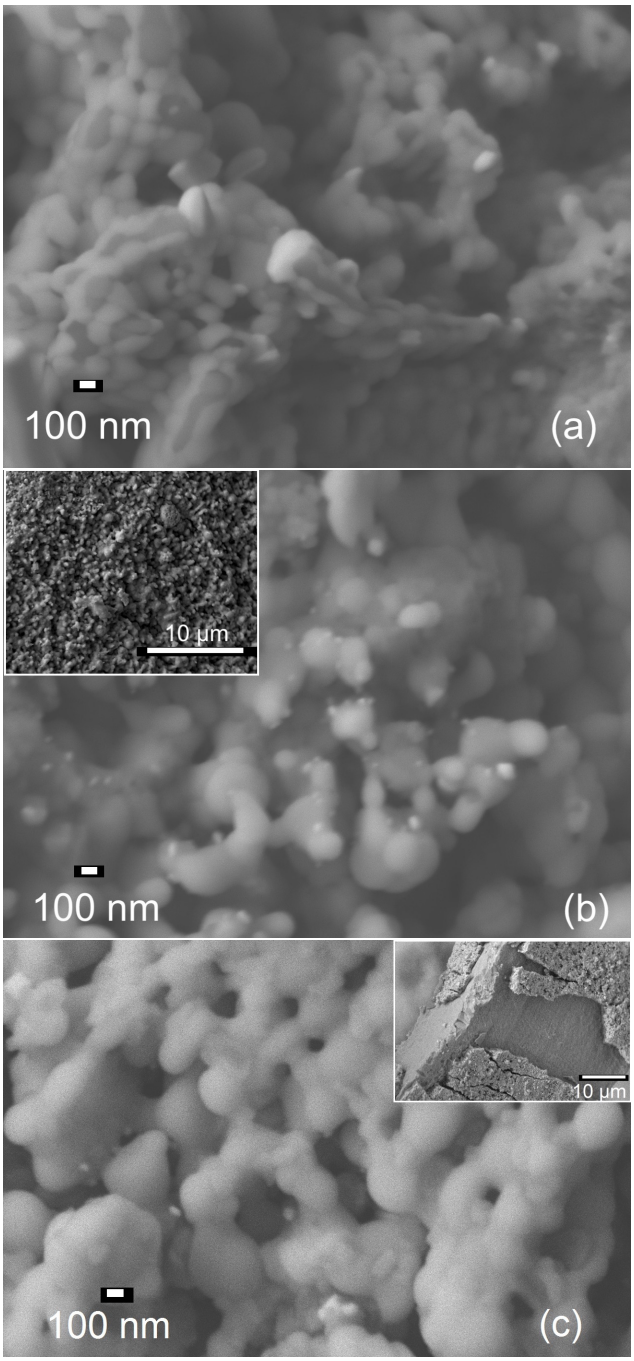

Figure 8.5 (a) Fresh Pt/CeO_2 FeCralloy (Map spectrum Wt % : Ce, 48.1 ; O, 21.0 ; Pt, 15.2 ; Al, 11.8 ; Fe, 2.5). (b) Used Pt/CeO_2 FeCralloy after CPOX reaction (Map spectrum Wt % : Ce, 59.9 ; O, 19.5 ; Pt, 11.0 ; Fe, 5.5 ; Al, 3.9). (c) Regenerated Pt/CeO_2 FeCralloy.

After CPOX reaction at 2 MPa, no whisker coke formed (Figure 8.5 (b)). Also EDS analysis detected no carbon. Fine Pt particles (particle size smaller than 50 nanometers) spread over

the CeO_2 particles, while some merged with CeO_2 and buried inside. A point EDS detected a large CeO_2 particle (marked with yellow cross) with 5 % Pt.

After regeneration, the extent of the agglomeration increased. Cerium oxide agglomerates tended to grow longitudinally and form larger particles and encapsulated Pt more severely. Fewer fine Pt particles exposed on the surface. Over a small scale of the exterior surface, delamination cracks led to the exfoliation of the oxidation layer and exposed bare Fe surfaces, probably due to the weak adhesion between the thermally grown oxide layer and the metal base [163].

One mechanism of noble metal aging reflected as the deep encapsulation by support is the collapse of the support. In our case, CeO_2 gradually encapusulated Pt. Fan [185] reported Pt catalyst supported on low surface area oxides (CeO_2 – ZrO_2 – La_2O_3). Pt crystallites buried by the mixed oxides occurs at the calcination temperature above 700 °C. Fan [185] indicated the interdiffusion/interaction between Pt and supported mixed oxides is vital for metals supported on low surface area oxides. At the metal/oxides interface there are crystal defects and a distortion of the mixed oxides lattice. Through creating crystal imperfections along the metal/oxide interfaces, the encapsulation of Pt enhances the formation of Ce^{3+} or oxygen vacancies both on the surface and in the bulk of the supports and also increase the number of labile oxygen. However, actives sites on the surface of metal decrease as well.

8.4.2 Catalytic tests

All catalysts in CPOX reaction are without any pre-reduction procedure.

Activity vs. temperature

We tested the catalytic performance of CeO_2 and Pt/CeO_2 FeCralloy catalyst under different temperature at a constant weight hourly space velocity of $1.1\,g_{CH_4}/g_{cat}/h$, and compared conversion and selectivities with thermodynamic equilibrium calculated by FactSage® Thermochemical Software (FACT pure substances database) [144] [145]. FactSage® considers all the possible reactions and gives all species composition at equilibrium state by minimizing the Gibbs energy.

At 0.1 MPa, the thermodynamic equilibrium (Figure 8.6 and 8.7, dashed line) of methane conversion, H_2 and CO selectivity increases with temperature. Temperature over 900 °C approaches to complete methane conversion and maximum H_2 and CO selectivity. CO_2 selectivity increases while complete oxidation dominates below 450 °C, and drops with increasing temperature while water-gas shift and dry reforming become significant.

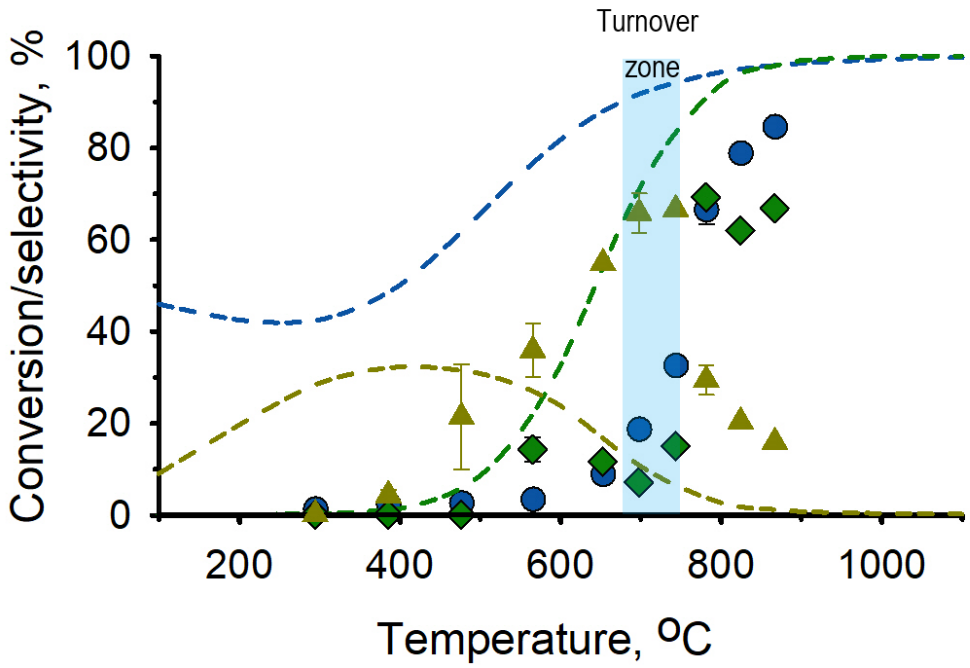

Figure 8.6 CPOX at ambient pressure with CeO_2 FeCralloy under different temperature. There is a narrow turnover zone around 700 °C. Methane conversion : blue circle ; CO selectivity : green diamond ; CO_2 selectivity : ginger triangle. Dash line of calculated thermodynamic equilibrium vs. temperature : methane conversion : blue ; CO selectivity : green ; CO_2 selectivity : ginger.

With CeO_2 FeCralloy catalyst, all gases composition change significantly at a temperature window around 700 °C (Figure 8.6) which referred as a ″turnover zone″ [186]. Selectivity of H_2 (not shown) and methane conversion of CeO_2 FeCralloy catalyst linearly increases. Considering carbon products, CO and byproduct of CO_2, we observed the same phenomenon reported by Liu et al (temperature of turnover zone around 600 °C)[186]. In the turnover zone, there is the competition between CO and CO_2 formation. At temperature below this zone, total oxidation to CO_2 governs the overall reaction. In the turnover zone, as temperature increases, the increase of CO_2 formation rate declines and CO formation rate reaches a maximum. At temperature above this zone, methane partially oxidized to CO becomes dominent.

Pt/CeO_2 FeCralloy catalyst comparing to CeO_2 FeCralloy catalyst is much less active in CPOX reaction (Figure 8.7). With increasing temperature, methane conversion slowly increases below 600 °C. The maximum conversion of methane (54 %) occurs at 800 °C, then decreasing with elevated temperature. It may not have a ″turnover zone″ as the depressing activity of Pt/CeO_2 in CPOX led to low CH_4 conversion ; or a much wider zone range

from approximately 550 °C to 800 °C, since the competition between CO and CO_2 formation followed the same trend.

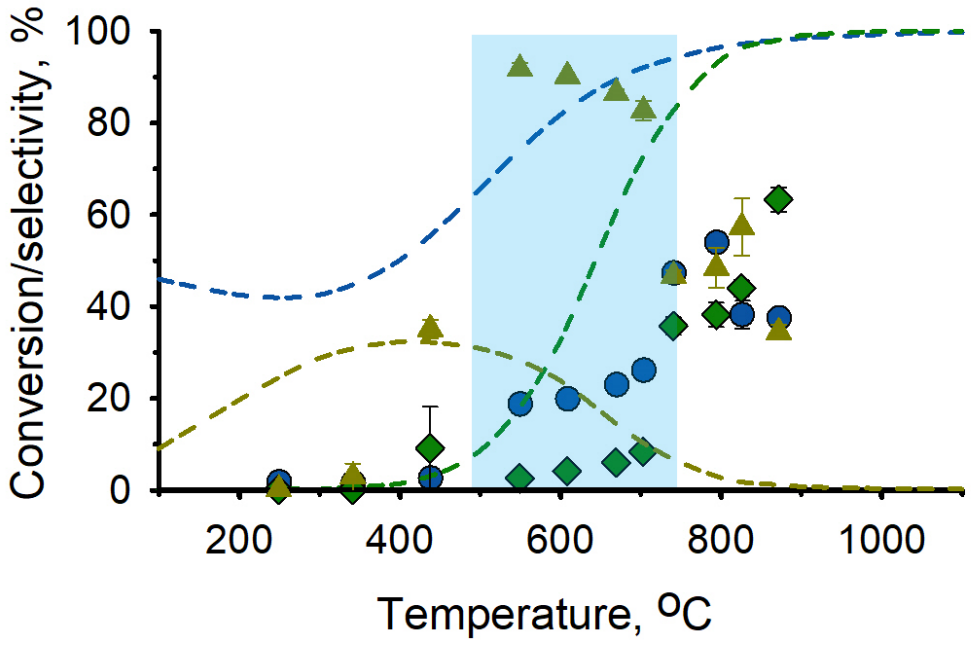

Figure 8.7 CPOX at ambient pressure with Pt/CeO_2 FeCralloy under different temperature. Low activity caused a much wider temperature range around 600 °C where methane starts to activate. Methane conversion : blue circle ; CO selectivity : green diamond ; CO_2 selectivity : ginger triangle. Dash line of calculated thermodynamic equilibrium vs. temperature : methane conversion : blue ; CO selectivity : green ; CO_2 selectivity : ginger.

Activity vs. pressure

To further investigate the activity of CeO_2 and Pt/CeO_2 FeCralloy catalysts, we compared their performance under different pressure. At a pressure of 0.1 MPa (thermodynamically favored pressure) and 2 MPa (industrially favored pressure), we kept the contact time constant at 150 ms at 900 °C (Figure 8.8). Each test (including repeated tests) lasts 65 min, we measured the composition of the outlet starting from 5 min at an interval of 10 min by GC. We carried out blank tests with 10 mm inert glasswool as a reactor filling.

At ambient pressure, the homogeneous methane partial oxidation reaction (Figure 8.8, barn red, second row) converted 25 % CH_4. Formation of CO_2 and H_2O occurred preferentially versus partial oxidation products of CO (36 % selectivity) and H_2 (30 % selectivity) .

CeO_2 FeCralloy (Figure 8.8, apricot, second row) catalysts increased the methane conversion

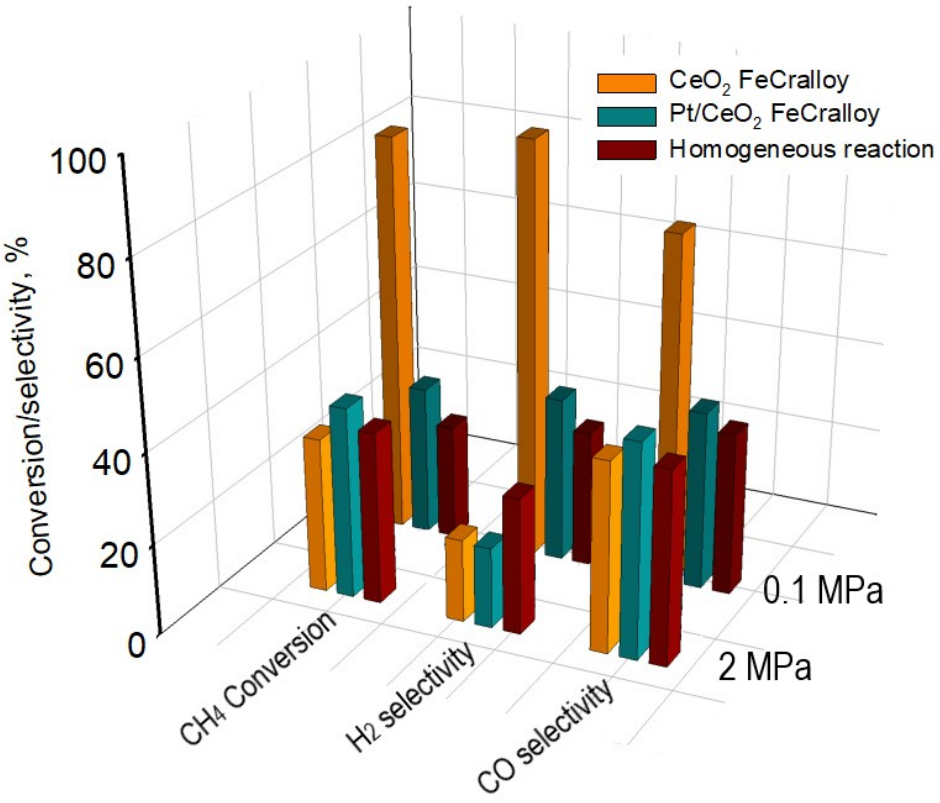

Figure 8.8 Methane conversion, H_2 selectivity and CO selectivity of CeO_2 FeCralloy and Pt/CeO_2 FeCralloy in CPOX at 900 °C under pressure of 0.1 MPa and 2 MPa. As a comparison, the homogeneous reaction was without active components but inert glasswool fillings.

to 87 %. The CO selectivity increased concurrently to 76 %. It was superb in H_2 production with a selectivity of 91 %. CO_2 selectivity was 13 % with coke selectivity was 10 % according to carbon balance.

Pt/CeO_2 FeCralloy catalyst (Figure 8.8, pine, second row) were poorly reactive in CPOX and only 7 % more methane converted to mainly complete oxidation products compared to the homogeneous gas reaction.

At high pressure of 2 MPa, more methane reacted in the homogeneous reaction (Figure 8.8, apricot, first row) while methane conversion increased to 38 %.

CeO_2 FeCralloy highly converted methane to syngas at ambient pressure, however at 2 MPa (Figure 8.8, apricot, first row), H_2 and CO selectivity decreased to 18 % and 43 % with 34 % methane conversion. At higher pressure, while keeping the contact time constant, the weight

hourly space velocity is higher (same amount of catalysts treated more mole of gas), the conversion was lower. However, methane conversion was even lower than the homogeneous reaction. Less methane reacts on the CeO_2 FeCralloy surface also its homogeneous reaction was interfered.

We calculated the O mass balance (Equation 8.6) based on 7 GC results in a 65 min test. As methane conversion and H_2 selectivity were stable during 65 min, an average H_2O formation rate calculated by weighting the water adsorbent before and after test is reasonable. At ambient pressure, the first measurement (GC analysis taken at 5 min) shows the oxygen content of the effluent gases was 43 % higher than the feed oxygen. It may because cerium oxide release oxygen and reduced to Ce^{3+} from Ce^{4+} which contributed to methane combustion [179]. From 35 min (the fourth measurement), CeO_2 FeCralloy reached an oxygen balance within ±10 %. However, at 2 MPa, the oxygen balance displayed opposite consequence. Effluent gases was deficient of oxygen by 26 % during 65 min of reaction : this phenomenon suggested that it stores lattice oxygen [21, 49] . Less oxygen in the gas phase probably causes the lower methane conversion than gas phase reaction. Thus the cerium oxidation state rose during the whole period. Fathi et al. [179] postulated that with relatively fresh and near fully oxidized catalyst, hydroxyl groups accumulated on cerium surfaces. This also explained the dominant complete oxidative product of H_2O with respect to low H_2 selectivity. From Figure 8.4 (b), whisker coke grew on CeO_2 particles and covered its surface ; according to carbon balance, twice as much coke formed at high pressure than at 0.1 MPa. Coke most likely comes from methane decomposition rather than the Boudouard reaction [5]. Higher coke indicated that methane reacted through decomposition in an oxygen deficient environment thus lower conversion occured.

The oxygen balance also correlated with the low Pt/CeO_2 reactivity (Figure 8.8, pine, first row). At 0.1 MPa and 2 MPa, 20 % less oxygen leaves as carbon monoxide, carbon oxides and water versus the feed — similar to the cerium oxide FeCralloy catalyst at 2 MPa. Pt/CeO_2 over γ-Al_2O_3 [179] performed well in methane partial oxidation since Pt exists as independent crystallites on top of the cerium oxide via a separate impregnation procedure. Pino [180] worked with Pt/CeO_2 catalyst in CPOX reaction in a fuel cell and received 96 % methane conversion and 99 % H_2 selectivity. The one-pot synthesis by SCS in this paper delivered partially encapsulated Pt over CeO_2 layer. Fan et al. [185] indicated that the status of metal/oxides interface is particularly relevant to the reducibility and oxygen release behavior of the low surface area oxides. The encapsulation of Pt led to a disorder of the cationic sublattice, which facilitated the formation of Ce^{3+} or oxygen vacancies thus increased the dynamic oxygen storage capacity.

We therefore assume that oxygen and methane in the gas phase is competitive in adsorbing on the catalyst surface. Under this reaction condition, oxygen preferably adsorbed and supplemented the oxygen vacancies in CeO_2 based catalysts.

Separate feeding of methane and oxygen

Ceria based materials store and release oxygen thus is widely adopted in Chemical Looping technology (CL). In CL process, oxygen carriers fully or partially oxidize fuels like methane in the reducer reactor ; then the reduced oxygen carrier is exposed to air to recover its original oxidation state. Inspired by CL process, at 900 °C and ambient pressure, we separately fed methane and oxygen to the reactor equipped with CeO_2 or Pt/CeO_2 FeCralloy catalysts .

When only feeding methane (30 % in Ar), suprisingly, Pt/CeO_2 converted methane completely (Figure 8.9 (a)). At the beginning of the methane reduction, more CO_2 formed than CO due to the preferable complete oxidation with sufficient surface oxygen. As the surface oxygen consumed fast, CO_2 formation rate declined sharply meantime H_2 formation rate boomed. Bulk oxygen replenished lattice oxygen to form partial oxidation product, so CO continuously formed and decreased slowly.

After methane reduction, we fed 21 % oxygen in Ar to oxidize the catalyst (Figure 8.9 (b)). Only pure CO formed during the beginning 50 min. Oxygen swept the surface carbon and no oxygen left the outlet. Then CO formation almost linearly decreased while amount of CO_2 increased in the end of the carbon burning. Also we noticed a release of H_2 stream after 50 min which may be ascribed to the oxidation of cerium hydride species [187].

CeO_2 presented a similar syngas production ability (Figure 8.10 (a)). Moreover, in the oxidation step (Figure 8.10 (b)), it burned surface carbon more efficiently within 60 min (30 min more methane reduction reaction than P/CeO_2). CO finished immedietly while a sharp peak of CO_2 announced all surface carbon burned out. Meantime in the gas phase there was mainly oxygen.

Separate feeding of methane and oxygen to produce H_2 and CO proved the high activity of Pt/CeO_2 FeCralloy. Also it proved our assumption that methane is less competitive in adsorbing then reacting on the catalyst surface with the presence of gas phase oxygen. CeO_2 based FeCralloy catalysts are suitable candidates to produce pure CO and H_2 in a chemical looping methane partial oxidation process.

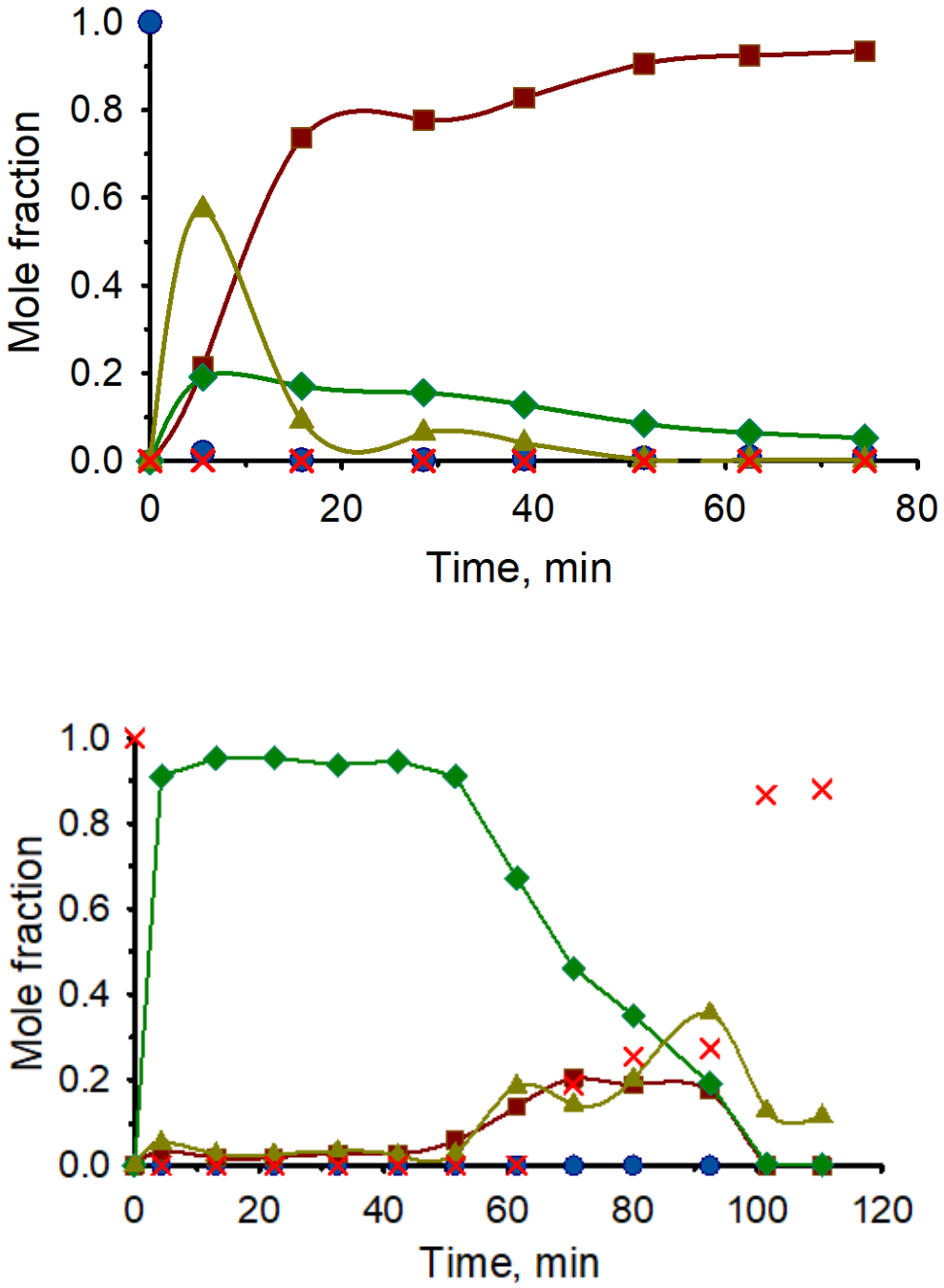

Figure 8.9 Seperately feeding (a) methane and (b) oxygen to Pt/CeO_2 FeCralloy at 900 °C and ambient pressure, the outlet gas composition (exempt inert gas Ar, analyzed by GC) of methane : blue circle ; O_2 : red cross ; H_2 : scarlet square ; CO : green diamond ; CO_2 : ginger triangle.

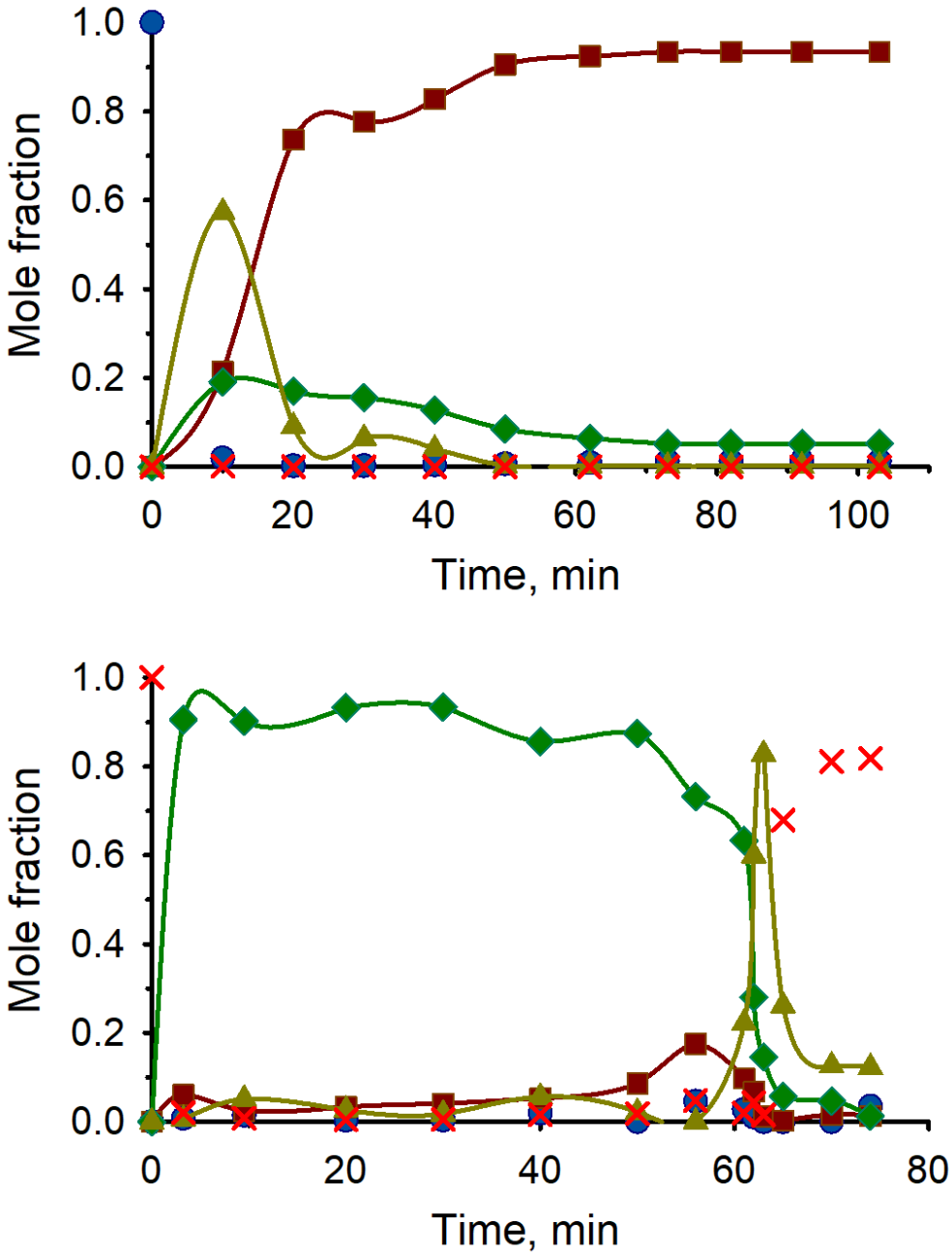

Figure 8.10 Seperately feeding (a) methane and (b) oxygen to CeO_2 FeCralloy at 900 °C and ambient pressure, the outlet gas composition (exempt inert gas Ar, analyzed by GC) of methane : blue circle ; O_2 : red cross ; H_2 : scarlet square ; CO : green diamond ; CO_2 : ginger triangle.

8.4.3 Kinetics on CeO_2 FeCralloy

Methane activation

CeO_2 based FeCralloy catalysts revealed diverse reactivity according to different reaction conditions. The adsorption between methane and oxygen is quite competitive. Separate feeding methane and oxygen to the catalytic system provides an alternative view to understand the methane activation on the catalyst surface.

A non-dissociative adsorption mechanism of methane proposed by Snoeck et al [188] is as following :

$$CH_4 + S \leftrightarrow CH_4{\cdot}S \tag{8.7}$$

$$CH_4{\cdot}S + S \leftrightarrow CH_3{\cdot}S + H{\cdot}S \tag{8.8}$$

$$CH_3{\cdot}S + S \leftrightarrow CH_2{\cdot}S + H{\cdot}S \tag{8.9}$$

$$CH_2{\cdot}S + S \leftrightarrow CH{\cdot}S + H{\cdot}S \tag{8.10}$$

$$CH{\cdot}S + S \leftrightarrow C{\cdot}S + H{\cdot}S \tag{8.11}$$

$$2H{\cdot}S \leftrightarrow H_2 + 2S \tag{8.12}$$

We placed a layer of CeO_2 FeCralloy weighing 0.08 g on inert glass wool and fed methane and oxygen separately to reduce and oxidize the catalyst. Methane conversion decreased as carbon accumulated on the surface. Between 650 – 1050 °C, and a linear velocity between 4 to 11Ncm s^{-1}, the outlet gas composition of methane and hydrogen was stable during the first 10 min. The GC detected neither CO nor CO_2. (So for all other GC traces, we sampled the gas at 3 min and the GC analyzed the composition.) The main factors in the experimental design were temperature (850 °C to 1050 °C), methane concentration (10 % to 30 %), and contact time on CeO_2 FeCralloy (Table 8.2). At these conditions, the methane conversion is quite low ($\leqslant$ 10 %, except at 1040 °C), so we considered the reactor to be operating under differential conditions. We calculated the reaction rate, r, by :

$$r = \frac{P_{0,CH_4}/P_{0,\text{total}} - P_{CH_4}/P_{\text{total}}}{W/F} \tag{8.13}$$

P_{0,CH_4} is the initial partial pressure of methane in inlet flow, while P_{CH_4} is the partial pressure of methane in outlet flow. $P_{0,\text{total}}$ is equal to P_{total} which was the local atmospheric pressure (101.11 kPa). W is the mass of catalyst and F is the total molar flow rate at the inlet. We

adopted a power law model to correlate experimental data. We proposed the reaction rate equation as :

$$r = k_0 \exp\left[-\frac{E_\mathrm{a}}{R}\left(\frac{1}{T}-\frac{1}{T_0}\right)\right] P_{\mathrm{CH_4}}^{a} P_{\mathrm{H_2}}^{b} \tag{8.14}$$

T_0 is the reference temperature which we took 827 K. By non-linear solver, the reaction rate is first order with respect to methane and zero order with respect to hydrogen. k_0 is $0.5\mu\mathrm{mol\,g^{-1}\,s^{-1}}$. The activation energy is $46\,\mathrm{kJ\,mol^{-1}}$. Activation energy for methane decomposition without catalysts ranges from $360\,\mathrm{kJ\,mol^{-1}}$ to $400\,\mathrm{kJ\,mol^{-1}}$[189, 190] while with catalyst it ranges from $60\,\mathrm{kJ\,mol^{-1}}$ to $240\,\mathrm{kJ\,mol^{-1}}$[191]. The activation energy in this study is lower than reported.

Alstrup [192] proposed a mechanism in which the chemisorption of methane is dissociative. According to Alstrup's mechanism, the reaction order of H_2 is non-zero. In this study, methane activated over the CeO_2 FeCralloy catalyst surface : the reaction rate is independent of hydrogen partial pressure. The non-dissociative adsorption of methane on the catalyst surface as the rate-limiting step is consistent with our experimental observations (R^2=0.92).

Oxidation

Gas transient step response techniques measure the residence time distribution that assess potential non-uniformities. The tanks–in–series model is an good first approximation to characterize the gas-phase hydrodynamics and it agrees well with the axial–dispersion model for Peclet numbers above 5 (i.e. moderate deviation from plug flow). All tanks have the same volume and then we have :

$$\frac{Q}{V_\mathrm{i}} = \frac{n}{t_\mathrm{m}} \tag{8.15}$$

where Q is the volumetric flow rate, $\mathrm{m^3\,s^{-1}}$; V_i the volume of tank i, $\mathrm{m^3}$; n is the number of tanks and t_m is the mean residence time, s. The residence time distribution for the whole system is from a mass balance for n tanks [193] :

$$F(t) = 1 - e^{-nt/t_\mathrm{m}}[1 + \frac{nt}{t_\mathrm{m}} + \frac{1}{2!}(\frac{nt}{t_\mathrm{m}})^2 + ... + \frac{1}{(n-1)!}(\frac{nt}{t_\mathrm{m}})^{(n-1)}] \tag{8.16}$$

The MS monitored the oxygen concentration online at a frequencey of 1 Hz. We oxidized the CeO_2 FeCralloy catalyst after methane reduction at 850 °C, 900 °C, 950 °C and 1000 °C with

Table 8.2 Experiment results of CH_4 activation on CeO_2

Temperature °C	$P_{0,CH_4}/P_{0,total}$ %	W/F $g\,s\,mol^{-1}$	X_{CH4} %	r $\mu mol\,s^{-1}\,g^{-1}$	P_{CH_4}/P_{total} %	P_{H_2}/P_{total} %
	13	345	0.9	8.1	12	0.2
	20	355	1.0	16	19	0.4
	34	375	1.2	2.5	34	0.8
	12	532	1.3	2.9	12	0.3
850	19	532	1.3	3.8	19	0.5
	33	545	1.6	7.5	33	1.1
	11	945	2.1	5.7	11	0.5
	18	965	2.0	5.2	18	0.7
	32	1037	2.3	17	30	1.4
	12	345	1.7	4.9	12	0.4
	19	360	1.8	5.2	19	0.7
	35	374	2.0	14	34	1.4
	12	491	1.9	5.6	12	0.5
900	19	532	2.3	2.6	19	0.9
	34	545	2.4	15	33	1.6
	11	945	3.1	2.1	11	0.7
	18	965	3.3	4.0	18	1.2
	32	1037	3.0	6.7	31	2.0
	12	345	2.6	7.7	12	0.6
	19	360	2.9	8.9	19	1.1
	35	374	3.1	26	34	2.2
	12	532	3.5	5.1	12	0.9
950	19	532	3.7	6.5	19	1.4
	34	545	3.6	17	33	2.4
	11	945	4.6	3.9	11	1.0
	18	965	4.7	6.2	18	1.7
	32	1037	4.7	12	31	3.0
	12	345	4.5	8.5	12	1.1
	19	355	4.5	17	19	1.8
	35	374	5.0	44	33	3.5
	12	532	5.1	7.5	12	1.3
1000	19	532	5.4	13	18	2.1
	34	545	5.8	29	32	3.9
	11	945	6.6	3.7	11	1.5
	18	965	7.0	8.0	17	2.6
	32	1037	7.5	24	29	4.8
	12	345	7.3	22	11	1.8
	19	355	8.2	48	17	3.1
	35	374	9.4	104	31	6.4
	12	532	8.1	15	11	2.0
1040	19	532	9.1	29	18	3.5
	34	545	11	55	31	7.5
	11	945	11	9.9	10	2.3
	18	965	12	19	16	4.2

21 % oxygen in Ar flow at linear velocity of $4\,\mathrm{cm\,s^{-1}}$ (normal). We fed a same flow of argon and oxygen to the fully oxidized catalyst, the oxygen concentration increases gradually to its steady–state value which we consider it as the tracer signal.

The partial differential equations was discretized in terms of the transport terms leaving the rate of change of concentration with respect to time in differential form :

$$V_{\mathrm{cat,i}}\frac{dC_{\mathrm{j,i}}}{dt} = Q(C_{\mathrm{j,i-1}} - C_{\mathrm{j,i}}) + \sum r_{\mathrm{j,i}} V_{\mathrm{cat,i}} \tag{8.17}$$

where $V_{\mathrm{cat,i}}$ is the volume of catalyst in volume elemet i, m^3 ; $C_{\mathrm{j,i}}$ is the concentration of gas species j in volume element i, $\mathrm{mol\,m^{-3}}$; $\sum r_{\mathrm{j,i}}$ is the total reaction rate of gas species j in volume element i.

For solid phase CeOx and surface coke we referred as C_s, we have

$$V_{\mathrm{cat,i}}\frac{dC_{\mathrm{j,i}}}{dt} = M_{\mathrm{s}}(2C_{\mathrm{j,i}} - C_{\mathrm{j,i-1}} - C_{\mathrm{j,i+1}}) + \sum r_{\mathrm{j,i}} V_{\mathrm{cat,i}} \tag{8.18}$$

where M_{s} is a hypotherical solid circulation rate, in a fixed bed, we take a value of zero for M_{s}.

In the oxidation step, oxygen not only reacts with the surface coke to produce CO and CO_2, also oxidizes the catalyst. We proposed a hybrid Eley-Rideal power law model to characterize the interaction between solid phase and gaseous oxygen : gas phase oxygen oxidizes the reduced catalyst (Ce_2O_3) to CeO_2, and reacts directly with adsorbed carbon to form gas phase CO and CO_2.

$$O_{2,\mathrm{g}} + 2Ce_2O_{3,\mathrm{s}} = 4CeO_{2,\mathrm{s}} \tag{8.19}$$

$$O_{2,\mathrm{g}} + C_{\mathrm{s}} = CO_{2,\mathrm{g}} \tag{8.20}$$

$$O_{2,\mathrm{g}} + 2C_{\mathrm{s}} = 2CO_{\mathrm{g}} \tag{8.21}$$

The reaction rates are expressed as a power law :

$$r_1 = k_1 C_{\mathrm{O_2}} C^2_{\mathrm{Ce_2O_3}} \tag{8.22}$$

$$r_2 = k_2 C_{\mathrm{O_2}} C_{\mathrm{C_s}} \tag{8.23}$$

$$r_3 = k_3 C_{\mathrm{O_2}} C^2_{\mathrm{C_s}} \tag{8.24}$$

We minimize the following objective function (ϕ) to estimate the kinetic parameters that R^2

based on the mole fractions of O_2, CO_2 and CO measured by the MS :

$$\phi = 3 - R^2_{O_2} - R^2_{CO_2} - R^2_{CO} \tag{8.25}$$

$$R^2_{O_2} = 1 - \frac{\sum (y_{O_2,calc} - y_{O_2,exp})^2}{\sum (y_{O_2,exp} - \bar{y}_{O_2,exp})^2} \tag{8.26}$$

$$R^2_{CO_2} = 1 - \frac{\sum (y_{CO_2,calc} - y_{CO_2,exp})^2}{\sum (y_{CO_2,exp} - \bar{y}_{CO_2,exp})^2} \tag{8.27}$$

$$R^2_{CO} = 1 - \frac{\sum (y_{CO,calc} - y_{CO,exp})^2}{\sum (y_{CO,exp} - \bar{y}_{CO,exp})^2} \tag{8.28}$$

We also fit the data based on the sum of the square of the errors, but the fit was poor.

The variance attributed to the hydrodynamics in the gas space in the reactor, the inlet and outlet line to the reactor and the MS was approximately 12 CSTRs in series. The reactor system was divided into three volume elements. We fitted the hydrodynamics parameters, particularly the breakthrough time, independently for each temperature. The far left set of data points labeled blank in Figure 8.11 is the expected response to a step change in the oxygen mole at the inlet from 0 % to 21 %. The agreement between the model predictions and experimental data was good for O_2 and CO_2 at 850 °C to 1000 °C. The oxygen consumed equals that necessary to react the carbon on the surface and to oxidize the catalyst surface. The surface carbon preferentially reacts to form CO_2 than CO. At 850 °C and 900 °C, no visible CO forms ; while at 950 °C and 1000 °C, less than 1 % CO forms challenging the detection limit of MS which could explain the poorer fit.

Table 8.3 summarizes the rate constant for each reaction together with the amount of coke deposited expressed as mole of oxygen required to conbust the carbon on 1 m^3 CeO_2 FeCralloy catalyst.

Table 8.3 Fitted oxidation reaction rate constants, carbon deposits and R values

Temperature °C	k_1	k_2 $cm^3 mol^{-1} s^{-1}$	k_3	C_s mole O_2 per m^3 CeO_2	$R^2_{O_2}$	$R^2_{CO_2}$	R^2_{CO}	ϕ
850	7.4	2.3	0	7.9	0.97	0.93	-1.6	2.7
906	7.2	2.6	0	6.5	0.94	0.90	-1.5	2.7
950	2.5	1.7	0.09	5.3	0.79	0.68	-0.49	2.0
990	0.6	2.4	0.20	7.2	0.43	0.83	-0.20	1.9

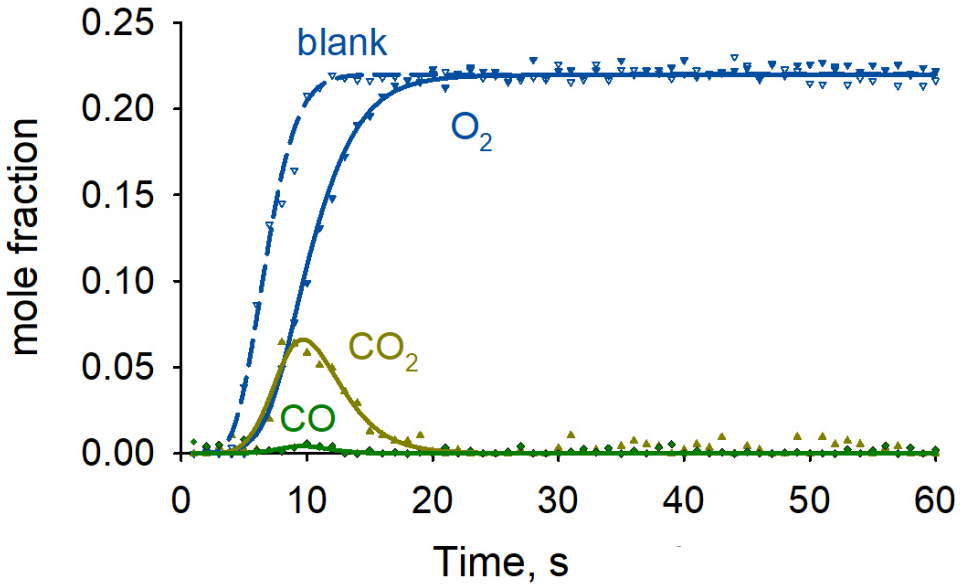

Figure 8.11 Oxidation model predictions (solid lines) versus experimental data (symbols) for test at 950 °C.

Separate feeding at 2 MPa

At 2 MPa, 900 °C, and a contact time of 150 ms, the catalyst operated for 180 min while the feed gas alternated between methane and oxygen over Pt/CeO_2 FeCralloy. The composition in the feed during the first cycle was 30 % methane in Ar (Figure 8.12 1a,). Ar swept the catalyst during the first 6 min and all the methane reacted from minute 6 to minute 9. Methane completely converted to hydrogen and CO and CO_2. The effluent concentration of CO was more than double that of CO_2 but the H_2 concentration was more than double the sum of the carbon oxides, which indicates carbon chemisorbed to the surface. As the methane concentration rose (after 9 min, the carbon oxides dropped towards zero). The H_2 concentration dropped from a maximum of about 30 % but continued to react and reached 15 % at 18 min. Although, the catalyst no longer formed carbon oxides, it was still capable of reacting methane to hydrogen.

In the first oxidation-reduction cycle (Figure 8.12 1b), air oxidized/regenerated the carbon/catalyst for 10 min. All the oxygen reacted for 2 min to form carbon oxides : CO breakthrough preceded CO_2 by 1 min. Presumably, as the oxidation state of the catalyst rises, it is sufficient to form CO_2. Oxygen continues to react with carbon species during the whole dosing period—neither the CO concentration no the CO_2 concentration returned to baseline.

In the second methane dosing period (Figure 8.12 1c), carbon oxide concentrations were

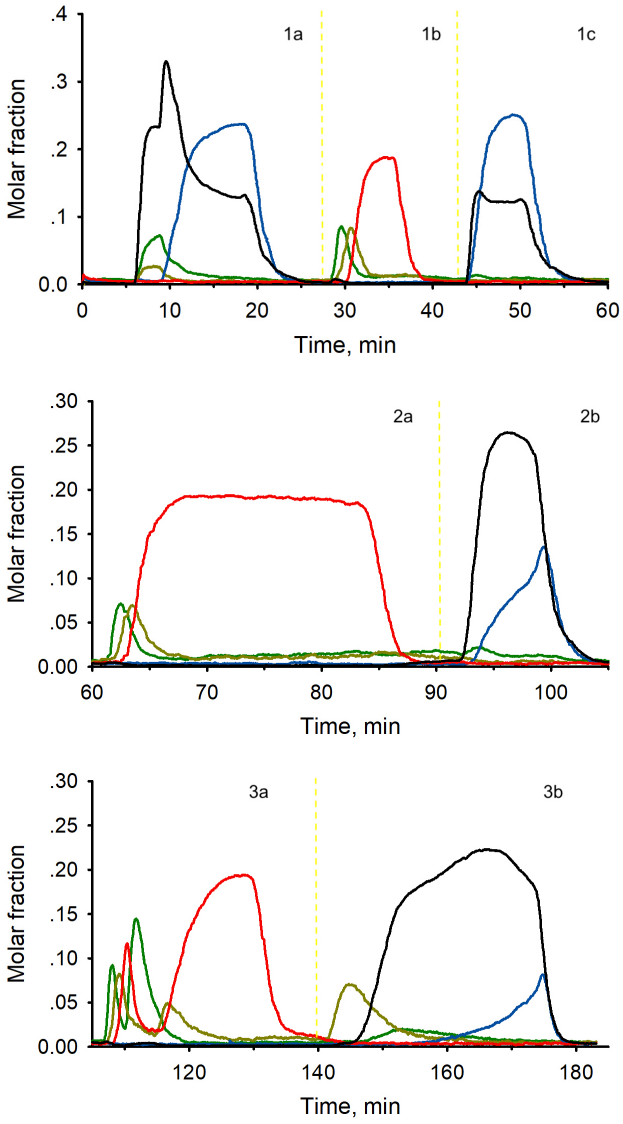

Figure 8.12 At 2 MPa, 900 °C, in a continuous 180 min reaction, (1a) methane firstly reduced the fresh Pt/CeO_2 FeCralloy ; then 3 oxidation-reduction cycles (1st : (1b) and (1c) ; 2ed : (2a) and (2b) ; 3rd : (3a) and (3b)) revealed the change of its surface state. The outlet gas composition (analyzed by online MS) of methane : blue ; O_2 : red ; H_2 : black ; CO : green ; CO_2 : ginger.

negligibly small while the hydrogen and methane concentrations resembled those at the end of the first cycle. Clearly, the oxygen contact time was insufficient to return the catalyst to its oxidized state.

Therefore, we increased the second oxidation (Figure 8.12 2a) to 30 min. As in Figure 8.12 2a, neither CO nor CO_2 returned to baseline. At ambient pressure, all the coke reacts after

2 min, while at 2 MPa even after 30 min coke remains on the surface.

Surprisingly, in the next methane reduction step (Figure 8.12 2b), all the methane reacted in the first minute and formed H_2. The hydrogen concentration is double after the longer oxygen dosing cycle and remains constant even as the methane concentration begins to rise. CO_2 concentrations are negligible.

In the third oxidation-reduction cycle (Figure 8.12 3a), we regenerated the catalyst in 30 min again. The concentration profiles of CO, CO_2, and O_2 have never been reported previously : The first 5 min dosing period was the same as Figure 8.12 1b and 2a : CO breakthrough preceded CO_2 and when O_2 appears the carbon oxide concentrations drop. Then, unexpectedly, the CO concentration rises again as the oxygen reacts with the rest carbon on the surface (while the CO_2 concentration remains low). The O_2 concentration begins to rise again when the CO concentration approaches the baseline.

The next methane dosing cycle (Figure 8.12 3b), unlike the other tests, CO_2 evolves from the catalyst, even before H_2. When CO_2 concentration began to drop, H_2 appeared.

Figure 8.12 1a, 1b, 2a and 3a indicate that on the catalyst surface, CO forms under direct mechanism. As long as there are carbon and oxygen source on the catalyst, CO formed simutaneously with CO_2. The formation of CO_2 depends on the extent of oxygen storage. When there are sufficient oxygen on the catalyst, carbon is completely oxidized to CO_2.

8.5 Conclusions

Wasted flared gas calls for alternative solution. Combining CPOX with FT in a Micro-Refinery Unit to produce synthetic fuel has advantages over standard technologies with respect to operation and investment. The challenge is to operate catalytic partial oxidation of methane at high pressure. A qualified catalyst not only resists both high temperature and high pressure stresses also is highly selective to produce CO and H_2.

FeCralloy knitted fibres reveal distribute tempeature well over high temperature and have negligible pressure drop that allows high flow output. We prepared 2 CeO_2 based FeCralloy catalyst : 5 % CeO_2 and 1 % Pt/5 % CeO_2 supported on oxidized FeCralloy knitted fibres. High pressure limits the activity of 5 % CeO_2 FeCralloy catalyst. Encapsulated Pt by CeO_2 offered it a stronger ability of oxygen storage. Our solution, inspired by chemical looping, is to separately feed methane and oxygen to the catalytic system. Mainly H_2 produced in the methane reduction step while mainly CO produced in the oxidation step. kinetic models of reduction and oxidation reactions on the CeO_2 surface proved a direct mechanism, which was confirmed by 3 reduction and oxidation cycles at 2 MPa. CeO_2 based catalysts are potential

candidates in high pressure chemical looping partial oxidation of methane process.

8.6 Acknowledgement

The authors acknowledge the financial support from the Natural Sciences and Engineering Research Council of Canada (NSERC).

CHAPTER 9 GENERAL DISCUSSION

9.1 General discussion

High pressure disfavors methane partial oxidation step with respect to thermodynamic equilibrium. We recalculated the thermodynamic equilibrium by FactSage, which gives all species composition at equilibrium state by minimizing the Gibbs energy. Methane conversion and CO and H_2 selectivity rise with temperature, while selectivity of CO_2 first increases due to complete oxidation then drops as CO selectivity rises. The selectivity of coke decreases with temperature. High pressure restrains CPOX reaction and lowers methane conversion and syngas selectivity, on the other hand, more coke and CO_2 are expected.

High pressure CPOX calls for suitable catalyst candidates. FeCralloy fibres are promising supports because they resist high temperatures and are highly conductive. By an infrard camera, we saw a uniform temperature distribution over FeCralloy. Also its flexible struture makes it possible to fit any reactors and allow high space velocities. The pressure drop of FeCralloy is negligible compared to common inert fillings (glasswool and sand).

We initially employed virgin FeCralloy (untreated FeCralloy) and oxidized FeCralloy as supports. We found that they are reactive to converting methane, however, the selectivity to syngas is poor. As the surface structure of the oxidized FeCralloy is stable under severe operation conditions, we applied oxidized FeCralloy as support.

Solution combustion synthesis, compared to spray pyrolysis, generates fine particles and dispersed active phases on the surface of fibres uniformly. So far we successfully dispersed Pt and Rh and/or CeO_2 and coated MgO over the surface of FeCralloy fibres.

On the surface of Pt/Rh/MgO FeCralloy catalyst, Pt particles were crystalline with particle size of 54 nm (calculated by Scherrer equation). At a constant weight hourly space velocity of 15 $g_{CH_4} g_{cat}^{-1} h^{-1}$, pressure of 2 MPa increased methane conversion to 80 % from 45 % at 0.1 MPa. CO selectivity increased to 55 % at 0.5 MPa from 45 % at 0.1 MPa. The highest H_2 selectivitiy of 60 % was at 2 MPa. Higher pressure produced more coke and less CO_2. The average H_2/CO ratio at 2 MPa was 2, ideal for FT reaction. At a constant contact time of 0.1 s, methane conversion dropped to 75 % at 2 MPa from 90 % at 0.1 MPa while CO and H_2 selectivity decreased to 44 % and 34 % at 2 MPa from 90 % and 99 % at 0.1 MPa. The average H_2/CO ratio at 2 MPa was 1.6. We compared equlibrium coke yield with experimental data. The coke formed in CPOX was above the equilibrium value. High pressure promoted the reverse Boudouard reaction and thus produced more coke and CO_2. At lower pressure of 0.1

MPa and 0.5 MPa, coke formation was close to the equilibrium value. Increasing residence time decreased the amount of metastable coke.

To further reduce the cost of the catalyst, we deposited Pt/Rh (9 :1) directly on the oxidized FeCralloy by SCS method. The characteristic peaks of FeCr, Al_2O_3 and Pt were with low intensity in the XRD pattern. By SEM analysis, we discovered that the surface of the Pt/Rh FeCralloy was fluffy and the particle size of Pt was around 100 nm. From 350 °C to 900 °C at ambient pressure, methane conversion and selectivity of CO, H_2, CO_2 and carbon followed the trend of thermodynamic predictions. After a 65 min reaction at 2 MPa at 900 °C, the top layer of virgin FeCralloy coked severely, however, no coke formed on the surface of Pt/Rh FeCralloy. The methane conversion was 47 % and CO and H_2 selectivity were 62 % and 67 %, respectively. Increasing O_2/CH_4 ratio to 0.7, methane conversion increased to 82 % with H_2 selectivity of 72 %. Regenerated Pt/Rh FeCralloy catalyst could repeat similar results for the 65 min tests at both 0.1 MPa and 2 MPa.

CeO_2 based FeCralloy catalyst could release and store oxygen. Ceria particles agglomerated on the surface of oxidized FeCralloy and whisker coke accumulated over these agglomerates. The regeneration led to more uniform rod–like ceria particles which have higher oxygen storage capacity [181, 182, 183]. The extent of encapsulation of Pt by CeO_2 increased after high temperature reaction and regeneration. At 0.1 MPa, the turnover zone was narrow (around 700 °C). Pt/CeO_2 FeCralloy was inert at this condition with a maximum methane conversion of 54 % at 800 °C. At 2 MPa, with CeO_2 FeCralloy catalyst, methane conversion dropped to 34 % (87 % at 0.1 MPa) and CO and H_2 selectivity decreased to 43 % and 18 % from 76 % and 91 % at 0.1 MPa. With the absence of oxygen, ceria based catalyst converted methane completely to H_2 and some CO and CO_2 and produced high purity of CO when feeding oxygen. To understand the methane activation on the catalyst surface without oxygen, we investigated the effects of temperature, methane concentration and contact time on CeO_2 FeCralloy catalyst and derived a first–order model for methane reduction. The activation energy for methane activation was 46 $kJ\,mol^{-1}$. The adsorption of methane on the catalyst surface was non–dissociative. We derived a hybrid Eley-Rideal model for oxidation. By separate feeding methane and oxygen to Pt/CeO_2 FeCralloy catalyst at 2 MPa, we observed that high pressure restrained the oxidation of the catalyst, which required much longer time than at 0.1 MPa. CO and CO_2 formed simutaneously with deficient oxygen and more CO_2 formed with sufficient surface oxygen. Therefore we proposed that CO formed under direct mechanism rather than CO_2 reforming.

9.2 Limitation and problems

9.2.1 Catalyst charaterization

Structured catalysts are very compact and easy to handle, but they are more difficult to characterize with commonly available non-destructive techniques, such as volumetric adsorption, chemisorption or XRD. Their low surface to volume ratio and the 3D structure may hinder X-ray scans. We sucessfully analyzed FeCralloy catalysts with extra coating (Al_2O_3 or MgO) via XRD analysis. For FeCralloy catalysts without extra coating (oxidized FeCralloy as supports), we noticed huge noise signal from the stainless steel substrate of the instrument. With a silicon substrate, we were able to detect signals of FeCr and Pt. However, the intensities were quite low.

The surface of FeCralloy is non–porous. After catalyst preparation, the surface area of FeCralloy catalysts deposited with Pt or CeO_2 is hard to analyze. Autosorb determines the BET surface with an error within $4m^2g^{-1}$. With the current sample cells, the maximum sample loading of FeCralloy catalysts is around 2g –3 g, which is far from enough for an accurate analysis.

We had difficulty in the thermogravimetric analysis (TGA) of our FeCralloy catalysts. The weight of coked catalysts flucatuated at high temperature under air (Figure 9.1), probably due to the competition of the oxidation of the FeCralloy and the surface coke. Therefore, no pattern fitted the gained weight and consumed oxygen.

Although FeCralloy fibre resists high temperature over long period of time, its surface (elements composition) is heterogenous due to its manufacture procedure. The performance of FeCralloy is different with different production date. After high temperature calcination or reaction, sometimes the surface of FeCralloy was covered by iron oxides solids (brown red color) or chromium oxides (blue color).

9.2.2 Gas phase reaction

As we used air as the oxidant, the feed gas ratio for CH_4, O_2 and Ar is around 30 :15 :55. We found that without catalyst, more than 30 % methane reacted at ambient pressure. Conversion was higher at elevated pressure. Lane and Wolf [194] studied the gas phase reaction of co-feeding methane and oxygen, and also reported up to 32 % methane conversion and 29 % C_2 selectivity. Gas phase reaction is important, when reaction temperature is over 650 °C, reactant partial pressure $(P_{CH4}+P_{O2})/P_{tot}$ exceeds 0.4 and residence time is longer than 0.1 min. Our experimental data corrsponds to their study as well.

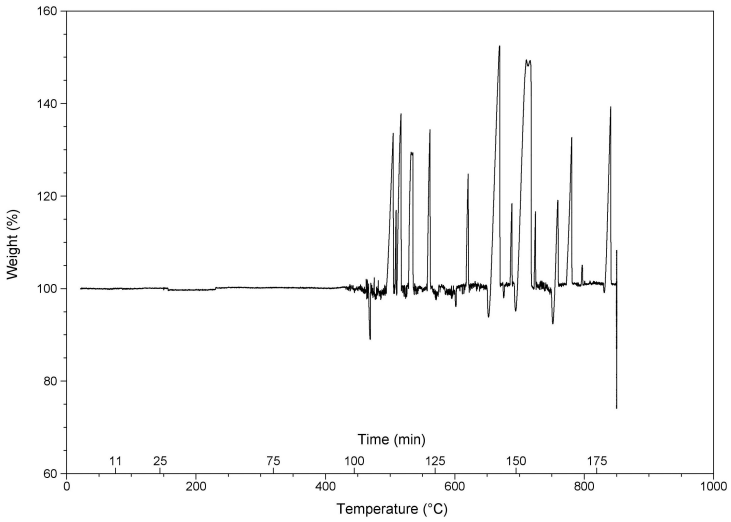

Figure 9.1 A typical TGA pattern of the oxidation of coked Pt FeCralloy catalyst. 50 mm of N_2 flow swept the sample and temperature increased from room temperature to 150 °C at a heating rate of 5 °C min^{-1}. Kept isothermal for 15 min. Then 50 mm of O_2 flow swept the sample and temperature increased from 150 °C to 850 °C at a heating rate of 5 °C min^{-1}. Kept isothermal for 60 min.

We also found that the methane conversion of gas phase reaction or CPOX reaction is different with a new reactor or a used reactor. In a used stainless steel tubular reactor, over 50 % of the methane reacted. Hatano et al [195] showed that an inert material such as quartz chips inhibits methane oxidation. Martin et al. [196] found that quartz reactors contaminated with active materials introduced considerable errors.

Therefore, in order to understand the kinetics of the FeCralloy catalyst under industrial conditions (CH_4, O_2 and inert gas ratio of 30 :15 :55, temperature of 900 °C, pressure of 2 MPa), the interuption of gas phase reaction would be problematic. Researchers employed diluted methane feed (below 5 %) in order to avoid the gas phase reaction. However, it is questionable to employ it for real industrial conditions. By separate feeding methane and oxygen to the catalytic system, we were able to study the kinetics over ceria based FeCralloy catalysts (Chapter 7, article 4).

9.2.3 Reactor coking

Pt FeCralloy catalysts largely prevent coke formation. However, coke accumulates on the tube wall and pipelines, which is more severe after high pressure test. Coke also forms on type K thermocouples. Quartz (as interior) reactor cokes the least, however, coke forms near the exit of quartz reactor and between quartz and stainless steel tubes. We heated the quartz

reactor and stainless steel reactor up to 900 °C under air for 3–4 h, some coke still remained. This pyrolytic coke affects carbon mass balance. A better choice of the reactor is necessary.

CHAPTER 10 CONCLUSION

10.1 Conclusion

Gas-to-Liquids technology is uneconomic at a scale of 10 bbl/day with conventional technology. Integrating the partial oxidation step with Fischer-Tropsch synthesis at high pressure reduces investment costs, processes equipment and operating complexity. Several challenges remain to develop a dual reactor vessel that operates at a temperature difference of 600 °C and at a pressure of 2 MPa.

• We firstly carried on CPOX at pressure up to 2 MPa in labtory micro reactor, and produced suitable syngas (H_2/CO ratior of 2) for further processes. • We are the first to employ noble catalysts supported on FeCralloy knitted fibres in CPOX reaction.

Overall, FeCralloy supported catalysts are good candidates for high pressure syngas production. Their high thermal conductivity helps to distribute the excess heat through the catalyst bed, reducing the presence of small local hot spot. Knitted structure offers the benefit of a reduced pressure drop over the bed, which allows higher linear gas velocities and increases the overall throughput, which is important when scaling up the process.

We prepared several FeCralloy catalysts that perform well in converting methane to syngas selectively. By solution combustion synthesis, we were able to coat MgO and CeO_2 uniformly and deposited fine and stable Pt particles over the catalyst surface. To reduce the cost of catalyst, oxidized FeCralloy was preferred as supports and a mass fraction of 1 % Pt was adopted for all the Pt FeCralloy catalysts.

The thermodynamic calculations demonstrated that the coke over Pt/MgO FeCralloy was metastable. Coke conversion to CO through the Boudouard reaction is the limiting factor to eliminate metastable coke. Increasing residence time should reduce metastable coke formation. At 2 MPa, a residence time of 0.3 s reduced 33 % coke formation compared to a residence time of 0.1 s.

Adding precious metals of Pt/Rh highly increased the methane conversion and syngas selectivity, and also resisted coke formation. Whisker coke formed on FeCralloy catalysts was easy to remove by oxygen and recovery of their reactivity was straightforward. Pt FeCralloy catalysts with good ability of regeneration, are suitable for high pressure continuous syngas production with interval regenerations.

By solution combustion synthesis, CeO_2 particles were rod–like and gradually encapsulated

Pt particles, which implied a potential high oxygen storage capacity and high oxygen transfer rate. A separate feeding of methane and oxygen demonstrated the high activity of CeO_2 based FeCralloy catalysts. They are potential candidates for high pressure chemical looping partial oxidation of methane process.

Based on the current study, Pt FeCralloy catalysts are suggested for syngas production due to their high reactivity, regenerative abilities and coke resistances. However, more work should be continued in order to meet the requirements of micro-refinery units for industrial purposes.

10.2 Recommendation for future work

A better understaning of gas phase reaction would be beneficial for CPOX reactor modelling. In our unpublished work, we studied the gas phase reaction and investigated the effects of temperature and methane concentration. We also attempted to feed a non-mixing stream of methane and oxygen and investigated the influence of the distance between the source gas (methane or oxygen) and the distributor, all greatly affecting the methane conversion. A thorough work is still required in order to study the kinetics of FeCralloy catalysts.

Due to the special composition and structure of FeCralloy, non-conventional heating system, such as induction heating or electric current heating, is suggested.

The surface area of FeCralloy is low, which limits the metal loading on it. With imperfect FeCralloy fibres, extra coating or active phases are necessary. The price of noble metals is expensive for industrial purpose, the combination of noble metal catalysts supported on FeCralloy and cheap catalysts (Ni, Co) is recommended.

Even though FeCralloy sometimes has flaws from its manufacture (hard to tell from its appearance), the virgin FeCralloy once worked very well in CPOX reaction . But we failed to repeat the results with other FeCralloy with different manufactures. Cheap metal alloy as catalysts for high pressure CPOX would be another interesting topic.

REFERENCES

[1] M. D. Argyle and C. H. Bartholomew, "Heterogeneous catalyst deactivation and regeneration : A review," *Catalysts*, vol. 5, pp. 145–269, 2015.

[2] Z. Zhao, "Nano-oxides fabricated in-situ spray pyrolysis technique as anode materials for lithium secondary batteries," Master's thesis, University of Wollongong, 2004.

[3] A. Alves, C. Bergmann, and F. A. Berutti, *Novel synthesis and characterization of nanostructured materials*, C. Synthesis, Ed. New York : Springer-Verlag Berlin Heidelberg, 2013.

[4] B. C. Enger, R. Lodeng, and A. Holmen, "A review of catalytic partial oxidation of methane to synthesis gas with emphasis on reaction mechanisms over transition metal catalysts," *Applied Catalysis A : General*, vol. 346, no. 1-2, pp. 1–27, 2008.

[5] J. B. Claridge, M. L. H. Green, S. C. Tsang, A. P. E. York, A. T. Ashcroft, and P. D. Battle, "A study of carbon deposition on catalysts during the partial oxidation of methane to synthesis gas," *Catalysis Letters*, vol. 22, no. 4, pp. 299–305, 1993.

[6] R. Horn, K. Williams, N. Degenstein, and L. Schmidt, "Syngas by catalytic partial oxidation of methane on rhodium : Mechanistic conclusions from spatially resolved measurements and numerical simulations," *Journal of Catalysis*, vol. 242, pp. 92–102, 2004.

[7] R. Horn, K. A. Williams, N. J. Degenstein, A. Bitsch-Larsen, D. D. Nogare, S. A. Tupy, and L. D. Schmidt, "Methane catalytic partial oxidation on autothermal rh and pt foam catalysts : Oxidation and reforming zones, transport effects, and approach to thermodynamic equilibrium," *Journal of Catalysis*, vol. 249, no. 2, pp. 380–393, 2007.

[8] AER, "Alberta Energy Regulator," 2013, ST60B-2013 : Upstream Petroleum Industry Flaring and Venting Report, 2013.

[9] S. K. Gibb, "Benefits for both health and climate shape debate over cuts in methane emissions," *Chemical and Engineering News*, vol. 93, pp. 21–22, 2015.

[10] D. A. Wood, C. Nwaoha, and B. F. Towler, "Gas-to-liquids (gtl) : A review of an industry offering several routes for monetizing natural gas," *Journal of Natural Gas Science and Engineering*, vol. 9, pp. 196–208, 2012.

[11] D. A. Wood, S. Mokhatab, and M. J. Economides, "Technology options for securing markets for remote gas." Proceedings of 87th Annual Convention of the Gas Processors Association (GPA), 2008, grapevine, Texas. USA.

[12] J. R. Nielsen and L. J. Christiansen, *Concepts in Syngas Manufacture*. Denmark : Imperial College Press, 2011.

[13] BP, "Bp statistical review of world energy, www.bp.com/statisticalreview2009," 2009.

[14] K. Chew, "Fundamentals of gas to liquids," *Petroleum Economist*, p. 11, 2003.

[15] J. R. Nielsen, *Sustainable strategies for the upgrading of natural gas : fundaments, challenges and oppotunities*. Dortrecht : Springer, 2005.

[16] J. R. R. Nielsen, "Fuels and energy for the future : The role of catalysis," *Catalysis Reviews*, vol. 46, pp. 247–270, 2004.

[17] V. Subramani, P. Sharma, L. Zhang, and K. Liu, *Hydrogen and Syngas Production and Purifi cation Technologies*. American Institute of Chemical Engineers, 2010, ch. Catalytic Steam Reforming Technology for the Production of Hydrogen and Syngas, pp. 14–126.

[18] K. Liu, G. D. Deluga, A. B. Larsen, L. D. Schmidt, and L. Zhang, *Hydrogen and Syngas Production and Purifi cation Technologies*. American Institute of Chemical Engineers, 2010, ch. Catalytic Partial Oxidation and Autothermal Reforming, pp. 14–126.

[19] T. S. Christensen and I. I. Primdahl, *Hydrocarbon process*, L. K. Wang, N. C. Pereira, and Y. T. Hung, Eds. USA : Gulf, 2004.

[20] T. S. Christensen, P. S. Christensen, I. Dybkjoer, J. H. B. Hansen, and I. I. Primdahl, "Developments in autothermal reforming," *Studies in Surface Science and Catalysis*, vol. 119, pp. 883–888, 1998.

[21] A. P. E. York, T. Xiao, and M. L. H. . Green, "Brief overview of the partial oxidation of methane to synthesis gas," *Topics in Catalysis*, vol. 22, pp. 345–358, 2003.

[22] D. A. Hickman and L. D. Schmidt, "Synthesis gas formation by direct oxidation of methane over pt monoliths," *Journal of Catalysis*, vol. 138, no. 1, pp. 267–282, 1992.

[23] ——, "Production of syngas by direct catalytic oxidation of methane," *Science*, vol. 259, pp. 343–346, 1993.

[24] ——, "Steps in CH_4 oxidation on pt and steps in CH_4 oxidation on pt and rh surfaces : high-temperature reactor simulations." *AIChE Journal*, vol. 39, pp. 1164–1177, 1993.

[25] "Us 5648582 a," (1997), L. D. Schmidt, D. A. Hickman.

[26] K. H. Hofstad, T. S., O. A. Rokstad, and A. Holmen, "Partial oxidation of methane to synthesis gas over a pt/10% rh gauze," *Catalysis Letters*, vol. 45, no. 1-2, pp. 97–105, 1997.

[27] M. Fathi, K. H. Hofstad, T. S., O. Rokstad, and A. Holmen, "Partial oxidation of methane to synthesis gas at very short contact times," *Catalysis Today*, vol. 42, no. 3, pp. 205–209, 1998.

[28] J. M. Australia, ""Catalyst gauze" *Johnson Matthey Australia*, accessed on 15 january 2015, http ://www.matthey.com.au/products/catalyst-gauze," 2015.

[29] "US 0126628," (2015), G. S. Patience, D. C. Boffito.

[30] A. L. Tarasov and L. M. Kustov, "Partial methane oxidation into synthesis gas over catalysts supported on meshed metallic materials," *Catalysis in Industry*, vol. 5, no. 1, pp. 14–20, 2013.

[31] T. Leonidovich and K. Modestovich, "Method of making catalyst for production of synthesis gas," *Patent RU2491118*, 2012.

[32] C. Bjorn, R. Lodeng, and A. Holmen, "A review of catalytic partial oxidation of methane to synthesis gas with emphasis on reaction mechanisms over transition metals." *Aplied Catalysis A : General*, vol. 346, pp. 61–27, 2008.

[33] J. R. R. Nielsen and M. Boudart, *Catalysis, Science and Technology.* Berlin : Verlag, 1984.

[34] A. Basile, Handbook of Membrane Reactors : Reactor Types and Industrial Applications. Sawston, Cambridge : Woodhead Publishing, 2013.

[35] J. R. Nielsen, J. Shested, and J. Norskov, "Hydrogen and synthesis gas by steam- and C_{02} reforming," *Advances in Catalysis*, vol. 47, pp. 65–139, 2002.

[36] D. Goetsch and L. Schmidt, "Microsecond catalytic partial oxidation of alkanes," *Science*, vol. 271, pp. 1560–1562, 1996.

[37] S. Rabe, T. B. Truong, and F. Vogel, "Low temperature catalytic partial oxidation of methane for gas-to-liquids applications," *Applied Catalysis A : General*, vol. 292, pp. 177–188, 2005.

[38] G. Jones, J. G. Jakobsen, S. S. Shim, J. Kleis, M. P. Andersson, J. Rossmeisl, F. A. Pedersen, T. Bligaard, S. Helveg, B. Hinnemann, J. R. R. Nielsen, I. Chorkendorff, J. Sehested, and J. K.Norskov, "First principles calculations and experimental insight into methane steam reforming over transition metal catalysts," *Journal of Catalysis*, vol. 259, pp. 147–160, 2008.

[39] J. R. R. Nielsen, "Coking on nickel catalysts for steam reforming of hydrocarbons," *Journal of Catalysis*, vol. 33, pp. 184–201, 1974.

[40] J. Wei and E. Iglesia, "Mechanism and site requirements for activation and chemical conversion of methane on supported pt clusters and turnover rate comparisons among noble metals," *J. Phys. Chem. B*, vol. 108, pp. 4094—-4103, 2004.

[41] J. B. Claridge, A. P. E. York, A. J. Brungs, C. M. Alvarez, J. Sloan, S. ChiTsang, and M. L. H. Green, "New catalysts for the conversion of methane to synthesis gas : Molybdenum and tungsten carbide," *Journal of Catalysis*, vol. 180, no. 1, pp. 85–100, 1998.

[42] J. Sehested, C. Jacobsen, S. Rokni, and J. R. Nielsen, "New catalysts for the conversion of methane to synthesis gas : Molybdenum and tungsten carbide," *Journal of Catalysis*, vol. 201, no. 2, pp. 206–212, 2001.

[43] B. Mosqueda, J. Toyir, A. Kaddouri, and P. Gelin, "Steam reforming of methane under water deficient conditions over gadolinium-doped ceria," *Applied Catalysis B : Environmental*, vol. 88, no. 3–4, pp. 361–367, 2009.

[44] E. Ruckenstein and Y. H. Wang, "Partial oxidation of methane to synthesis gas over mgo - supported rh catalysts : The effect of precursor of mgo," *Applied Catalysis A : General*, vol. 198, pp. 33–41, 2000.

[45] J. R. R. Nielsen, *Steam reforming catalysts*. Copenhagen : Danish Technical Press, 1975.

[46] X. Hong, "Partial oxidation of methane to synthesis gas catalyzed by metallic ni catalysts," Master's thesis, Tianjin University, 2007.

[47] J. Y. Mehr, K. J. Jozani, A. N. Pour, and Y. Zamani, "Influence of mgo in the CO_2-steam reforming of methane to syngas by nio/mgo/α-Al_2O_3 catalyst," *Reaction Kinetics and Catalysis Letters*, vol. 75, pp. 267–273, 2002.

[48] W. Dong, K. Jun, H. Roh, Z. Liu, and S. Park, "Comparative study on partial oxidation of methane over ni/ZrO_2, ni/CeO_2 and ni/ce-ZrO_2 catalysts," *Catalysis Letters*, vol. 78, pp. 215–222, 2002.

[49] V. Botu, R. Ramprasad, and A. Mhadeshwar, "Ceria in an oxigen environment : Surface phase equilibria and its descriptors," *Surface Science*, vol. 619, pp. 49–58, 2014.

[50] S. Specchia, C. Galletti, and V. Specchia, "Solution combustion synthesis as intriguing technique to quickly produce performing catalysts for specific applications," *Studies in Surface Science and Catalysis*, vol. 175, pp. 59–67, 2010.

[51] H. T. Wang, Z. H. Li, and S. X. Tian, "Effect of promoters on the catalytic performance of ni/Al_2O_3 catalyst for partial oxidation of methane to syngas," *Reaction Kinetics and Catalysis Letters*, vol. 83, pp. 245–252, 2004.

[52] T. K. Das, G. Jacobs, P. M. Patterson, W. A. Conner, J. Li, and B. H. Davis, "Fischer–tropsch synthesis : characterization and catalytic properties of rhenium promoted cobalt alumina catalysts," *Fuel*, vol. 82, no. 7, pp. 805–815, 2003.

[53] A. Wongkaew and P. Limsuvan, "Removal of carbon monoxide from hydrogen-rich fuels over CeO_2- promoted pt/Al_2O_3 catalysts," *ACES*, vol. 3, pp. 7–14, 2013.

[54] K. Heitnes, S. Lindber, O. A. Rokstad, and A. Holmen, "Catalytic partial oxidation of methane to synthesis gas," *Catalysis Today*, vol. 24, pp. 211–216, 1995.

[55] C. de Smet, M. de Croon, R. Berger1, G. Marin, and J. Schouten, "An experimental reactor to study the intrinsic kinetics of catalytic partial oxidation of methane in the presence of heat-transport limitations," *Applied Catalysis A : General*, vol. 187, pp. 33–48, 1999.

[56] M. Fathi, F. Monnet, Y. Schuurman, A. Holmen, and C. Mirodatos, "Reactive oxygen species on platinum gauzes during partial oxidation of methane into synthesis gas," *Journal of Catalysis*, vol. 190, pp. 439–445, 2000.

[57] "Us 6746658 b2," (2004), H. Dindi, W. H. Manogue, J. J. Barnes.

[58] A. Vita, G. Cristiano, C. Italiano, S. Specchia, F. Cipiti, and V. Specchia, "Methane oxy-steam reforming reaction : Performances of Ru/γ–Al_2O_3 catalysts loaded on structured cordierite monoliths," *International Journal of Hydrogen Energy*, vol. 39, no. 32, pp. 18 592–18 603, 2014.

[59] J. Oudar and H. Wise, *Deactivation and Poisoning of Catalysts*. New York : Marcel Dekker, 1985.

[60] L. L. Hegedus and R. W. McCabe, *Studies in Surface Science and Catalysis*. Amsterdam : Elsevier, 1980.

[61] J. R. R. Nielsen, *Progress in Catalyst Deactivation*, J. L. Figueiredo, Ed. Dordrecht : Springer, 1982.

[62] P. G. Menon, "Coke on catalysts—harmful, harmless, invisible and beneficial types," *J. Mol. Catal.*, vol. 59, pp. 207–220, 1990.

[63]

[64] R. T. Baker, C. H. Bartholomew, and D. B. Dadyburjor, *Stability of Supported Catalysts : Sintering and Redispersion*. Mountain View, 1991.

[65] J. B. Hansen and F. Joensen, "High conversion of synthesis gas into oxygenates," *Studies in Surface Science and Catalysis*, vol. 61, pp. 457–467, 1991.

[66] L. S. Lobo and D. L. Trimm, "Carbon formation from light hydrocarbons on nickel," *Journal of Catalysis*, vol. 29, pp. 15–19, 1973.

[67] F. A. Pedersen, J. Greeley, F. Studt, J. Rossmeisl, T. R. Munter, P. G. Moses, E. Skulason, T. Bligaard, and J. K. Norskov, "Scaling properties of adsorption energies for

hydrogen-containing molecules on transition-metal surfaces," *PHYSICAL REVIEW LETTERS*, vol. 99, p. 016105, 2007.

[68] D. L. Trimm, "Catalysts for the control of coking during steam reforming," *Catalysis Today*, vol. 49, pp. 3–10, 1999.

[69] L. L. Ross, *Pyrolysis : Theory and Industrial Practice.* New York : Academic Press, 1983.

[70] H. H. Gierlich, M. Fremery, A. Skov, and J. R. R. Nielsen, "Deactivation phenomena of a ni-based catalyst for high temperature methanation," *Studies in Surface Science and Catalysis*, vol. 6, pp. 459–469, 1980.

[71] Y. Li, "Partial oxidation of methane into syngas catalyzed by metallic nickel–based monolithic catalysts," Master's thesis, Tianjin University, 2006.

[72] Z. Pan, C. Dong, and S. Shen, *Journal of fuel chemistry and technology*, vol. 28, p. 348, 2000.

[73] P. Trambouze and J. P. Euzen, *Chemical reactors : from design to operation.* Paris : Technip, 2004.

[74] Q. Jing and X. Zheng, "Combined catalytic partial oxidation and co2 reforming of methane over zro2–modified ni/sio2 catalysts using fluidized–bed reactor," *Energy*, vol. 31, pp. 2184–2192, 2006.

[75] S. S. Bharadwaj and L. D. Schmidt, "Catalytic partial oxidation of natural gas to syngas," *Fuel Processing Technology*, vol. 42, pp. 109–127, 1995.

[76] A. Santos, M. Menendez, and J. Santamaria, "Partial oxidation of methane to carbon monoxide and hydrogen in a fluidized bed reactor," *Catalysis Today*, vol. 21, pp. 481–488, 1994.

[77] J. Llorca, *Monolithic Reactor.* Berlin : Springer, 2015.

[78] "Production of methanol from hydrocarbonaceous feedstock, WO1990006282A1," (2015), Joseph D. Korchnak and Michael Dunster and Alan English.

[79] P. M. Torniainen, X. Chu, and L. D. Schmidt, "Comparison of monolith–supported metals for the direct oxidation of methane to syngas," *Catalysis Today*, vol. 146, pp. 1–10, 1994.

[80] T. Kikas, I. Bardenshteyn, C. Williamson, C. Ejimofor, P. Puri, and A. G. Fedorov, "Hydrogen production in a reverse–flow autothermal catalytic microreactor : from evidence of performance enhancement to innovative reactor design," *Ind. Eng. Chem. Res.*, vol. 42, pp. 6273–6279, 2003.

[81] T. R. Schwiedernoch, S. Tischer, C. Correa, and O. Deutschmann, "Experimental and numerical study on the transient behavior of partial oxidation of methane in a catalytic monolith," *Chem. Eng. Sci*, vol. 58, pp. 633–642, 2003.

[82] S. Uemiya, N. Sato, H. Ando, T. Matsuda, and E. Kikuchi, "Steam reforming of methane in a hydrogen–permeable membrane reactor," *Applied Catalysis*, vol. 67, pp. 223–230, 1991.

[83] W. Liang, Z. Cao, G. He, J. Caro, and H. Jiang, "Oxygen transport membrane for thermochemical conversion of water and carbon dioxide into synthesis gas," *ACS Sustainable Chem. Eng.*, vol. 5, pp. 8657–8662, 2017.

[84] O. Deutschmann and L. D. Schmidt, "Modeling the partial oxidation of methane in a short-contact-time reactor," *American Institute of Chemical Engineers Journal*, vol. 44, pp. 2465–2477, 1998.

[85] C. G. Jr., R. O'Connor, and L. D. Schmidt, "Modeling homogeneous and heterogeneous chemistry in the production of syngas from methane," *Chemical Engineering Science*, vol. 55, p. 1357–1370, 2000.

[86] G. Veser, J. Frauhammer, and U. Friedle, "Syngas formation by direct oxidation of methane : Reaction mechanisms and new reactor concepts," *Catalysis Today*, vol. 61, pp. 55–64, 2000.

[87] I. Tavazzi, A. Beretta, G. Groppi, and P. Forzatti, "Development of a molecular kinetic scheme for methane partial oxidation over a rh/α–al2o3 catalyst," *Journal of Catalysis*, vol. 241, pp. 1–13, 2006.

[88] D. Wang, O. Dewaele, A. M. D. Groote, and G. F. Froment, "Reaction mechanism and role of the support in the partial oxidation of methane on rh/al2o3," *Journal of Catalysis*, vol. 159, pp. 418–426, 1996.

[89] E. P. J. Mallens, J. H. B. J. Hoebink, and G. B. Marin, "The reaction mechanism of the partial oxidation of methane to synthesis gas : A transient kinetic study over rhodium and a comparison with platinum," *Journal of Catalysis*, vol. 167, pp. 43–56, 1997.

[90] J.Slaa, R. Berger, and G. Marin, "Partial oxidation of methane to synthesis gas over rh/α–al2o3 at high temperatures," *Catalysis Letters*, vol. 43, pp. 63–70, 1997.

[91] M. Souza and M. Schmal, "Autothermal reforming of methane over pt/zro2/al2o3 catalysts," *Applied Catalysis A : General*, vol. 281, pp. 19–24, 2005.

[92] W. Z. Weng, M. S. Chen, Q. G. Yan, T. H. Wu, Z. S. Chao, Y. Y. Liao, and H. L. Wan, "Mechanistic study of partial oxidation of methane to synthesis gas over supported rhodium and ruthenium catalysts using in situ time-resolved ftir spectroscopy," *Catalysis Today*, vol. 63, pp. 317–326, 2000.

[93] O. Deutschmann, T. R. Schwiedernoch, L. I. Maier, and D. Chatterjee, "Natural gas conversion in monolithic catalysts : Interaction of chemical reactions and transport phenomena," *Stud. Surf. Sci. Catal.*, vol. 136, p. 251, 2001.

[94] M. Lyubovsky, S. Roychoudhury, and R. LaPierre, "Catalytic partial "oxidation of methane to syngas" at elevated pressures," *Catalysis Letters*, vol. 99, pp. 113–117, 2005.

[95] N.Burke and D. Trimm, "Co-generation of energy and synthesis gas by partial oxidation of methane," *Catalysis Today*, vol. 117, pp. 248–252, 2006.

[96] A. Bitsch-Larsen, R. Horn, and L. Schmidt, "Catalytic partial oxidation of methane on rhodium and platinum : spatial profiles at elevated pressures," *Applied Catalysis A : General*, vol. 348, pp. 165–172, 2008.

[97] L. Basini, K. Aasberg-petersen, and A. Guarinoni, "Catalytic partial oxidation of natural gas at elevated pressure and low residence time," *Cataysis Today*, vol. 64, pp. 9–20, 2001.

[98] M. Fichtner, J. Mayer, D. Wolf, , and K. Schubert, "Microstructured rhodium catalysts for the partial oxidation of methane to syngas under pressure," *Ind. Eng. Chem. Res.*, vol. 40, pp. 3475–3483, 2001.

[99] S. M. Ibrahim, A. A. Badawy, G. A. El-Shobaky, and H. A. Mohamed, "Structural, surface and catalytic properties of pure and ZrO_2-doped nanosized cobalt-manganese mixed oxides," *Canadian Journal of Chemical Engineering*, vol. 92, no. 4, pp. 676–684, 2014.

[100] C. Grant, "7th world congress of chemical engineering : A review," *Chemical Engineering Research and Design*, vol. 93, pp. 1345–1360, 2005.

[101] A. Acocella, E. Lim, K. Cedrone, L. Bromberg, S. Seethamraju, D. Cohn, and W. Green, "System and market analysis of methanol production using compact engine reformers." ASME 2014 8th International Conference on Energy Sustainability, 2014, boston, Massachusetts, USA.

[102] Z. Bamji, "New Data Reveals Uptick in Global Gas Flaring, *The World Bank*, accessed on 01 april 2017, http ://http ://www.worldbank.org/en/news/press-release/2016/12/12/new-data-reveals-uptick-in-global-gas-flaring," 2016.

[103] E.I.A., ""EIA projects world energy consumption will increase 56% by 2040", *U. S. Energy Information Admistration*, accessed on 12 january 2015, http ://www.eia.gov/todayinenergy/detail.cfm ?id=12251," 2013.

[104] ——, ""International Energy Outlook 2014", *U. S. Energy Information Admistration*, accessed on 12 january 2015, http ://www.eia.gov/forecasts/ieo/," 2014.

[105] I. Dybkjaer and K. Aasberg-Petersen, "Synthesis gas technology large-scale applications," *Canadian Journal of Chemical Engineering*, vol. 94, pp. 607—612, 2016.

[106] E. G. Lim, E. E. Dames, K. D. Cedrone, A. J. Acocella, T. R. Needham, A. Arce, D. R. Cohn, L. Bromberg, W. K. Cheng, and W. H. Green, "The engine reformer : Syngas production in an engine for compact gas-to-liquids synthesis," *Canadian Journal of Chemical Engineering*, vol. 94, no. 4, pp. 623–635, 2016.

[107] C. Trevisanut, S. M. Jazayeri, S. Bonkane, C. Neagoe, A. Mohamadalizadeh, D. C. Boffito, C. L. Bianchi, C. Pirola, C. G. Visconti, L. Lietti, N. Abatzoglou, L. Frost, J. Lerou, W. Green, and G. S. Patience, "Micro-syngas technology options for gtl," *Canadian Journal of Chemical Engineering*, vol. 94, no. 4, pp. 613–622, 2016.

[108] L. Frost, E. Elangovan, and J. Hartvigsen, "Production of synthetic fuels by high-temperature co-electrolysis of carbon dioxide and steam with fischer-tropsch synthesis," *Canadian Journal of Chemical Engineering*, vol. 94, pp. 636—-641, 2016.

[109] V. R. R. Pendyala, W. D. Shafer, G. Jacobs, and B. H. Davis, "Fischer-tropsch synthesis : Effect of solvent on the h2-d2 isotopic exchange rate over an activated cobalt catalyst," *Canadian Journal of Chemical Engineering*, vol. 94, pp. 678–684, 2016.

[110] F. Fischer and H. Tropsch, "Phe preparation of synthetic oil mixtures (synthol) from carbon monoxide and hydrogen," *Brennst. Chem.*, vol. 4, pp. 276–285, 1923.

[111] G. P. V. D. Laan and A. A. C. M. Beenackers, "Kinetics and selectivity of the fischer–tropsch synthesis : A literature review," *Catalysis Reviews*, vol. 41, no. 3-4, pp. 255–318, 1999.

[112] M. E. Dry, "The fischer-tropsch process 1950-2000," *Catalysis Today*, vol. 71, pp. 227–243, 2002.

[113] D. R. Lide, *CRC Handbook of Chemistry and Physics*. CRC Press, 2005.

[114] "A compact catalytic reactor. WO2013108011 A1," (2013), M. J. Bowe and I. K. Baxter and I. Chanis.

[115] Velocys, "Retrieved 28 december 2014, from http ://www.velocys.com." 2014.

[116] Q. Zhu, X. Zhao, and Y. Deng, "Advances in the partial oxidation of methane to synthesis gas," *Journal of Natural Gas Chemistry*, vol. 13, pp. 191–203, 2004.

[117] Gas-2, "Retrieved 24 december 2014, from http ://www.gas-2.com," 2014.

[118] J. K. Dunleavy, "Sulfur as a catalyst poison," *Platinum Metals Review*, vol. 50, p. 110, 2004.

[119] J. Blanchard, I. Achouri, and N. Abatzoglou, "H2s poisoning of nial2o4/al2o3-ysz catalyst during methane dry reforming," *Canadian Journal of Chemical Engineering*, vol. 94, pp. 650–654, 2016.

[120] L. K. Wang, C. Williford, and W. Y. Chen, *HANDBOOK OF ENVIRONMENTAL ENGINEERING, vol 2, Advanced Air and Noise Pollution Control.*, L. K. Wang, N. C. Pereira, and Y. T. Hung, Eds. New Jersey : Humana Press, 2005.

[121] U. E. P. Agency, "Wet scrubber for gaseous control, retrieved 12 april 2016, from https ://cfpub.epa.gov/oarweb/mkb/contechnique.cfm ?controlid=29," 2016.

[122] M. Thundyil, D. Seeger, R. G. Vazquez, and S. Pallavkar, "An alternative approach to sulpur recovery, retrieved 12 april 2016, from http ://www.gtctech.com/wp-content/uploads/nov-13.pdf," 2013.

[123] U. department of Energy, "More economical sulfur removal for fuel processing plants, retrieved 12 april 2016, from http ://energy.gov/sites/prod/files/2013/11/f5/tda-sbir-case-study-2010.pdf," 2013.

[124] D. Hoang, L., and S. H. Chan, "Modeling of a catalytic autothermal methane reformer for fuel cell applications," *Applied Catalysis A : General*, vol. 268, pp. 207–216, 2004.

[125] M. E. E. Abashar, "Steam reforming of n-heptane for production of hydrogen and syngas," *International Journal of Hydrogen Energy*, vol. 38, pp. 861–869, 2013.

[126] F.-X. Chiron, G. S. Patience, and S. Rifflart, "Steam carbon gasification of a nickel based oxygen carrier," *Fuel*, vol. 90, no. 7, pp. 2461–2466, 2011.

[127] "Us 20090026420 a1," (2009), B. Xu.

[128] "US 5 405 260," (1995), R. A. Della Betta, K. Tsurumi, T. Shoji.

[129] F. Basile, P. Benito, G. Fornasari, V. Rosetti, E. Scavetta, D. Tonelli, and A. Vaccari, "Electrochemical synthesis of novel structured catalysts for H_2 production," *Applied Catalysis B : Enviromental*, vol. 91, no. 1-2, pp. 563–572, 2009.

[130] P. Benito, M. Monti, W. D. Nolf, G. Nuyts, G. Janssen, G. Fornasari, E. Scavetta, F. Basile, K. Janssens, F. Ospitali, D. Tonelli, and A. Vaccari, "Improvement in the coating homogeneity in electrosynthesized rh structured catalysts for the partial oxidation of methane," *Catalysis Today*, vol. 246, pp. 154–164, 2015.

[131] P. Benito, M. Monti, I. Bersani, F. Basile, G. Fornasari, E. Scavetta, D. Tonelli, and A. Vaccari, "Coating of fecralloy foam with rh catalysts : Optimization of electrosynthesis parameters and catalyst composition," *Catalysis Today*, vol. 197, no. 1, pp. 162–169, 2012.

[132] E. Verlato, S. Barison, S. Cimino, F. Dergal, L. Lisi, G. Mancino, M. Musiani, and L. Vazquez-Gomez, "Catalytic partial oxidation of methane over nanosized rh supported on fecralloy foams," *International Journal of Hydrogen Energy*, vol. 39, no. 22, pp. 11 473–11 485, 2015.

[133] C. Neagoe, D. C. Boffito, Z. Ma, C. Trevisanut, and G. S. Patience, "Pt on fecralloy catalyses methane partial oxidation to syngas at high pressure," *Catalysis Today*, vol. 270, pp. 43–50, 2016.

[134] C. Trevisanut, S. M. Jazayeri, S. Bonkane, C. Neagoe, A. Mohamadalizadeh, D. C. Boffito, C. L. Bianchi, C. Pirola, C. G. Visconti, L. Lietti, N. Abatzoglou, L. Frost, J. Lerou, W. Green, and G. S. Patience, "Micro-syngas technology options for gtl," *Canadian Journal of Chemical Engineering*, vol. 94, p. 613, 2016.

[135] S. Tang, J. Lin, and K. L. Tan, "Partial oxidation of methane to syngas over ni/mgo, ni/cao and ni/CeO_2," *Catalysis Letters*, vol. 51, no. 3-4, pp. 169–175, 1998.

[136] M. Soick, O. Buyevskaya, M. Hohenberger, and D. Wolf, "Partial oxidation of methane to synthesis gas over pt/mgo kinetics of surface processes," *Catalysis Today*, vol. 32, no. 1-4, pp. 163–169, 1995.

[137] I. H. Son, S. J. Lee, I. Y. Song, W. S. Jeon, I. Jung, D. J. Yun, D. W. Jeong, J. O. Shim, W. J. Jang, and H. S. Roh, "Study on coke formation over ni/γ-Al_2O_3, co-ni/γ-Al_2O_3, and mg-co-ni/γ-Al_2O_3 catalysts for carbon dioxide reforming of methane," *Fuel*, vol. 136, pp. 194–200, 2014.

[138] B. I. Imasogie, A. A. Afonja, and J. A. Ali, "Properties of ductile cast iron nodularised with multiple calcium–magnesium based master alloy," *Materials Science and Technology*, vol. 16, no. 2, pp. 194–201, 2000.

[139] N. J. Degenstein, R. Subramanian, and L. D. Schmidt, "Partial oxidation of n-hexadecane at short contact times : Catalyst and washcoat loading and catalyst morphology," *Applied Catalysis A : General*, vol. 305, no. 2, pp. 146–159, 2006.

[140] R. Abbasi, G. Huang, G. M. Istratescu, L. Wu, and R. E. Hayes, "Methane oxidation over pt, pt :pd, and pd based catalysts : Effects of pretreatment," *Canadian Journal of Chemical Engineering*, vol. 93, no. 8, pp. 1474–1482, 2015.

[141] P. Rofouie, M. Moshkelani, M. Perrier, and J. Paris, "A modified thermodynamic equilibrium model for woody biomass gasification," *Canadian Journal of Chemical Engineering*, vol. 92, no. 4, pp. 593–602, 2014.

[142] S. Ayabe, H. Omoto, T. Utaka, R. Kikuchi, K. Sasaki, Y. Teraoka, and K. Eguchi, "Catalytic autothermal reforming of methane and propane over supported metal catalysts," *Applied Catalysis A : General*, vol. 241, no. 1-2, pp. 261–269, 2003.

[143] E. Newson and T. B. Truong, "Low-temperature catalytic partial oxidation of hydrocarbons (C_1–C_{10}) for hydrogen production," *International Journal of Hydrogen Energy*, vol. 28, no. 12, pp. 1379–1386, 2003.

[144] C. W. Bale, P. Chartrand, S. A. Degterov, G. Eriksson, K. Hack, R. B. Mahfoud, J. Melancon, A. D. Pelton, and S. Petersen, "Factsage thermochemical software and databases," *Calphad*, vol. 26, no. 2, pp. 189–228, 2002.

[145] P. Ouzilleau, A. E. Gheribi, G. Eriksson, D. K. Lindberg, and P. Chartrand, "A size-dependent thermodynamic model for coke crystallites : The carbon–hydrogen system up to 2500 k," *Carbon*, vol. 85, pp. 99–118, 2015.

[146] R. C. Oliver, S. E. Stephanou, and R. W. Baier, "Calculating free energy minimization," *Chem. Eng.*, vol. 69, no. 4, pp. 121–128, 1962.

[147] G. Eriksson and E. Rosen, "Thermodynamic studies of high temperature equilibria. viii. general equations for the calculation of equilibria in multiphase systems," *Chemica Scripta*, vol. 4, pp. 193–194, 1973.

[148] J. Tollefson, "Flaring wastes 3.5 % of world's natural gas," *Nature News & Comment*, vol. 11, 2016, january.

[149] Z. Ma, C. Trevisanut, C. Neagoe, D. C. Boffito, S. M. Jazayeri, C. Jagpal, and G. S. Patience, "A micro-refinery to reduce associated natural gas flaring," *Sustainable Cities and Society*, vol. 27, pp. 116–121, 2016.

[150] "Zero routine flaring by 2030, *The World Bank*, accessed on 11 march 2016, http ://www.worldbank.org/en/programs/zero-routine-flaring-by-2030," 2015.

[151] L. C. Buelens, V. V. Galvita, H. Poelman, C. Detavernier, and G. B. Marin, "Super–dry reforming of methane intensifies co2 utilization via le chatelier's principle," *Science*, vol. 354, pp. 449–452, 2016.

[152] R. B. Anderson, A. Krieg, and R. A. Friedei, "Fischer-tropsch synthesis differential reaction rate studies with cobalt catalysts," *Industrial and Engineering Chemistry*, vol. 41, pp. 2189–2197, 1949.

[153] J. Horiguchi, Y. Kobayashi, S. Kobayashi, Y. Yamazaki, K. Omata, D. Nagao, M. Konno, and M. Yamada, "Mesoporous nio–al2o3 catalyst for high pressure partial oxidation of methane to syngas," *Applied Catalysis A : General*, vol. 392, pp. 86–92, 2011.

[154] L. Chen, Q. Hong, J. Lin, and F. M. Dautzenberg, "Hydrogen production by coupled catalytic partial oxidation and steam methane reforming at elevated pressure and temperature," *Journal of Power Sources*, vol. 164, pp. 803–808, 2007.

[155] N.Burke and D. Trimm, "Coke formation during high pressure catalytic partial oxidation of methane to syngas," *React. Kinet. Catal. Lett.*, vol. 84, pp. 137–142, 2004.

[156] Z. Ma, P. Ouzilleau, C. Trevisanut, C. Neagoe, S. Lotfi, D. C. Boffito, and G. S. Patience, "Partial oxidation of methane to syngas over pt/rh/mgo catalyst supported on fecralloy woven fibre," *Canadian Journal of Chemical Engineering*, vol. 94, pp. 642–649, 2016.

[157] C. Neagoe, D. C. Boffito, Z. Ma, C. Trevisanut, and G. S. Patience, "Pt on fecralloy catalyses methane partial oxidation to syngas at high pressure," *Catalysis Today*, vol. 270, no. 15, pp. 43–50, 2016.

[158] X. Wu, D. Weng, S. Zhao, and W. Chen, "Influence of an aluminized intermediate layer on the adhesion of a g-al2o3 washcoat on fecral," *Surface and Coatings Technology*, vol. 190, pp. 434–439, 2005.

[159] M. Fathi, F. Monnet, Y. Schuurman, A. Holmen, and C. Mirodatos, "The effect of Rh addition on $Pd/g{-}Al_2O_3$ catalysts deposited on fecralloy fibers for total combustion of methane," *Applied Catalysis A : General*, vol. 333, pp. 1–10, 2007.

[160] R. T. A. Al-Rubaye and A. A. Garforth, "Generation of catalytic films of zeolite y and zsm-5 on fecralloy metal," *International Journal of Chemical, Nuclear, Materials and Metallurgical Engineering*, vol. 8, pp. 548–556, 2014.

[161] J. A. H. Lalinde, J. Jiang, G. Jai, and J. Kopyscinski, "Preparation and characterization of ni/al2o3 catalyst coatings on fecral – loy plates used in a catalytic channel reactor with in-situ spatial profiling to study co2 methanation," *Chemical Engineering Journal*, vol. 357, pp. 435–446, 2019.

[162] D. Naumenko, B. A. Pint, and W. J. Quadakkers, "Current thoughts on reactive element effects in alumina-forming systems : in memory of john stringer," *Oxidation of Metals*, vol. 86, pp. 1–43, 2016.

[163] D. Ugues, S. Specchia, and G. Saracco, "Optimal microstructura design of a catalytic premixed fecralloy fiber burner for methane combustion," *Industrial & Engineering Chemistry Research*, vol. 43, pp. 1990–1998, 2004.

[164] Y. Matatov-Meytal and M. Sheintuch, "Catalytic fibers and cloths," *Applied Catalysis A : General*, vol. 231, pp. 1–16, 2002.

[165] E. Reichelt, M. P. Heddrich, M. Jahn, and A. Michaelis, "Fiber based structured materials for catalytic applications," *Applied Catalysis A : General*, vol. 476, pp. 78–90, 2014.

[166] Y. A. Chang and W. A. Oates, *Materials thermodynamics*. New York : Wiley, 2010.

[167] G. Berthome, E. N'Dah, Y. Wouters, and A. Galerie, "Temperature ependence of metastable alumina formation during thermal oxidation of fecral foils," *Oxidation of Metals*, vol. 56, pp. 389–392, 2005.

[168] S. Helveg, J. Sehested, and J. R. Nielsen, "Whisker carbon in perspective," *Catalysis Today*, vol. 178, pp. 42–46, 2011.

[169] C. O. Tuck, E. Perez, I. T. Horvath, R. A. Sheldon, and M. Poliakoff, "Valorization of biomass : deriving more value from waste," *Science*, vol. 337, pp. 695–699, 2012.

[170] M. Mogensen, N. M. Sammes, and G. A. Tompsett, "Physical, chemical and electrochemical properties of pure and doped ceria," *Solid State Ionics*, vol. 129, pp. 63–94, 2000.

[171] A. Trovarelli, "Catalytic properties of ceria and ceo2-containing materials," *Catalysis Reviews*, vol. 38, pp. 439–520, 1996.

[172] T. Masui, T. Ozaki, K. Machida, and G. Adachi, "Preparation of ceria-zirconia subcatalysts for automotive exhaust cleaning," *J. Alloy Compd.*, vol. 303, pp. 49–55, 2000.

[173] C. Leitenburg, A. Trovarelli, J. Llorca, F. Cavani, and G. Bini, "The effect of doping ceo2 with zirconium in the oxidation of isobutane," *Appl. Catal. A : Gen.*, vol. 139, pp. 161–173, 1996.

[174] Q. Dong, S. Yin, C. Guo, X. Wu, T. Kimura, and T. Sato, "Aluminium doped ceria-zirconia supported palladium-alumina catalyst with high oxygen storage capacity and co oxidation activity," *Mater. Res. Bull.*, vol. 48, pp. 4989–4992, 2013.

[175] T. Bunluesin, R. J. Gorte, and G. W. Graham, "Studies of the water-gas-shift reaction on ceria-supported pt, pd, and rh : implications for oxygen-storage properties," *Catal. B : Environ.*, vol. 15, pp. 107–114, 1998.

[176] L. P. Perez, R. Buitrago-Sierra, and A. Sepulveda-Escribano, "Ceo2-promoted ni/activated carbon catalysts for the water–gas shift (wgs) reaction," *Int. J. Hydrogen Energ.*, vol. 39, pp. 17 589–17 599, 2014.

[177] T. R. Reina, S. Ivanova, M. A. Centeno, and J. A. Odriozola, "Boosting the activity of a au/ceo2/al2o3 catalyst for the wgs reaction," *Catal. Today*, vol. 253, pp. 149–154, 2015.

[178] P. Li, X. Chen, Y. Li, and J. W. Schwank, "A review on oxygen storage capacity of ceo2-based materials : Influence factors, measurement techniques, and applications in reactions related to catalytic automotive emissions control," *Catalysis Today*, 2018, https ://doi.org/10.1016/j.cattod.2018.05.059.

[179] M. Fathi, E. Bjorgum, T.Viig, and O. A. Rokstad, "Partial oxidation of methane to synthesis gas : Elimination of gas phase oxygen," *Catalysis Today*, vol. 63, pp. 489–497, 2000.

[180] L. Pino, A. Vita, M. Cordaro, V. Recupero, and M. S. Hegde, "A comparative study of pt/ceo2 catalysts for catalytic partial oxidation of methane to syngas for application in fuel cell electric vehicles," *Applied Catalysis A : General*, vol. 243, pp. 135–146, 2003.

[181] H. Mai, L. Sun, Y. Zhang, R. Si, W. Feng, H. Zhang, H. Liu, and C. Yan, "Shape-selective synthesis and oxygen storage behavior of ceria nanopolyhedra, nanorods, and nanocubes," *J. Phys. Chem. B*, vol. 109, pp. 24 380–24 385, 2005.

[182] K. Zhou, X. Wang, X. Sun, Q. Peng, and Y. Li, "Enhanced catalytic activity of ceria nanorods from well-defined reactive crystal planes," *J. Catal.*, vol. 229, pp. 206–212, 2005.

[183] T. S. Sreeremya, A. Krishnan, K. C. Remani, K. R. Patil, D. F. Brougham, and S. Ghosh, "Shape-selective oriented cerium oxide nanocrystals permit assessment of the effect of the exposed facets on catalytic activity and oxygen storage capacity," *ACS Appl. Mater. Interfaces*, vol. 7, pp. 8545–8555, 2015.

[184] E. Aneggi, D. Wiater, C. de Leitenburg, and A. T. J. Llorca, "Shape-dependent activity of ceria in soot combustion," *Acs Catal.*, vol. 4, pp. 172–181, 2013.

[185] J. Fan, X. Wu, X. Wu, Q. Liang, R. Ran, and D. Weng, "Pt on low surface area ceo2-zro2-la2o3 mixed oxides : effect on the osc performance," *Catal. B : Environ.*, vol. 81, pp. 38–48, 2008.

[186] Z. Liu, J. P. H. Li, E. Vovk, Y. Zhu, S. Li, S. Wang, A. P. van Bavel, and Y. Yang*, "Online kinetics study of oxidative coupling of methane over la2o3 for methane activation : What is behind the distinguished light-off temperatures," *ACS Catalysis*, vol. 8, pp. 11 761–11 772, 2018.

[187] Z. Wu, Y. Cheng, F. Tao, L. Daemen, G. S. Foo, L. Nguyen, X. Zhang, A. Beste, and A. J. Ramirez-Cuesta, "Direct neutron spectroscopy observation of cerium hydride species on a cerium oxide catalyst," *Journal of the American Chemical Society*, vol. 139, pp. 9721–9727, 2017.

[188] J. W. Snoeck, G. F. Froment, and M. Fowles, "Kinetic study of the carbon filament formation by methane cracking on a nickel catalyst," *Journal of Catalysis*, vol. 169, pp. 250–262, 1997.

[189] A. Holmen, O. A. Rokstad, and A. Solbakken, "High-temperature pyrolysis of hydrocarbons. 1. methane to acetylene," *Industrial & Engineering Chemistry Process Design and Development*, vol. 15, pp. 439–444, 1976.

[190] J. K. Dahl, V. H. Barocas, D. E. Clough, and A. W. Weimer, "Intrinsic kinetics for rapid decomposition of methane in an aerosol flow reactor," *International Journal of Hydrogen Energy*, vol. 27, pp. 377–386, 2002.

[191] S. H. S. Zein, A. R. Mohamed, and P. S. T. Sai, "Kinetic studies on catalytic decomposition of methane to hydrogen and carbon over ni/tio2 catalyst," *Industrial & Engineering Chemistry Research*, vol. 43, pp. 4864–4870, 2004.

[192] I. Alstrup and M. Tavares, "Kinetics of carbon formation from ch4 + h2 on silica-supported nickel and ni-cu catalysts," *Journal of Catalysis*, vol. 139, pp. 513–524, 1993.

[193] M. J. Lorences, J.-P. Laviolette, G. S. Patience, M. Alonso, and F. V. Diez, "Fluid bed gas RTD : Effect of fines and internals," *Powder Technol.*, vol. 168, no. 1, pp. 1–9, 2006.

[194] G. S. Lane and E. E. Wolf, "Methane utilization by oxidative coupling : I. a study of reactions in the gas phase during the cofeeding of methane and oxygen," *Journal of Catalysis*, vol. 113, pp. 144–163, 1988.

[195] M. Hatano, P. G. Hinson, K. S. Vines, and J. H. Lunsford, "Comments on "blank reactor corrections in studies of the oxidative dehydrogenation of methane" by d. j. c. yates and n. e. zlotin," *Journal of Catalysis*, vol. 124, pp. 557–561, 1990.

[196] G. A. Martin, A. Bates, V. Ducarme, and C. Mirodatos, "Methane utilization by oxidative coupling : I. a study of reactions in the gas phase during the cofeeding of methane and oxygen," *Applied Catalysis*, vol. 47, pp. 287–297, 1989.